Targeted Proteomics Studies:

Design, Development and Translation of Mass Spectrometric Immunoassays

for Diabetes and Kidney Disease

by

Paul Oran

A Dissertation Presented in Partial Fulfillment
of the Requirements for the Degree
Doctor of Philosophy

Approved November 2011 by the
Graduate Supervisory Committee:

Mark Hayes, Co-Chair
Randall Nelson, Co-Chair
Alexandra Ros
Peter Williams

ARIZONA STATE UNIVERSITY

December 2011

ABSTRACT

In an effort to begin validating the large number of discovered candidate biomarkers, proteomics is beginning to shift from shotgun proteomic experiments towards targeted proteomic approaches that provide solutions to automation and economic concerns. Such approaches to validate biomarkers necessitate the mass spectrometric analysis of hundreds to thousands of human samples. As this takes place, a serendipitous opportunity has become evident. By the virtue that as one narrows the focus towards "single" protein targets (instead of entire proteomes) using pan-antibody-based enrichment techniques, a discovery science has emerged, so to speak. This is due to the largely unknown context in which "single" proteins exist in blood (i.e. polymorphisms, transcript variants, and posttranslational modifications) and hence, targeted proteomics has applications for established biomarkers. Furthermore, besides protein heterogeneity accounting for interferences with conventional immunometric platforms, it is becoming evident that this formerly hidden dimension of structural information also contains rich-pathobiological information. Consequently, targeted proteomics studies that aim to ascertain a protein's genuine presentation within disease-stratified populations and serve as a stepping-stone within a biomarker translational pipeline are of clinical interest.

Roughly 128 million Americans are pre-diabetic, diabetic, and/or have kidney disease and public and private spending for treating these diseases is in the hundreds of billions of dollars. In an effort to create new solutions for the early detection and management of these conditions, described herein is the design,

development, and translation of mass spectrometric immunoassays targeted towards diabetes and kidney disease. Population proteomics experiments were performed for the following clinically relevant proteins: insulin, C-peptide, RANTES, and parathyroid hormone. At least thirty-eight protein isoforms were detected. Besides the numerous disease correlations confronted within the disease-stratified cohorts, certain isoforms also appeared to be causally related to the underlying pathophysiology and/or have therapeutic implications. Technical advancements include multiplexed isoform quantification as well a "dual-extraction" methodology for eliminating non-specific proteins while simultaneously validating isoforms. Industrial efforts towards widespread clinical adoption are also described. Consequently, this work lays a foundation for the translation of mass spectrometric immunoassays into the clinical arena and simultaneously presents the most recent advancements concerning the mass spectrometric immunoassay approach.

DEDICATION

I would like to dedicate this to my parents Haluk and Suzan Oran. They have been a living example of integrity and love and have supported me at every single step in my life. I am grateful.

ACKNOWLEDGMENTS

I would like to acknowledge my advisor, Dr. Randy Nelson. Thank you for all of your valuable insights and teachings. I truly appreciate your “out-side-of-the-box” perspectives, entrepreneurial spirit, and encouragement to change the world. I hope this is just the beginning of our friendship.

I would like to acknowledge Dr. Chad Borges. Thank you for all of your selfless support and assistance with teaching me essentials of analytical chemistry, troubleshooting with experiments gone-bad, and support with manuscripts.

I would like to thank Jason Jarvis for all of his assistance with experiments. It was a pleasure to work with you in the laboratory.

Thank you Biomarkers Research Initiatives in Mass Spectrometry (BRIMS) Center at Thermo Fisher Scientific (expressly Dr. Mary Lopez and Bryan Krastins). I honored my time spent working with the BRIMS team and hope the PTH assay ends up serving millions of individuals afflicted with kidney disease and related complications.

And lastly, I would like to thank my girlfriend Heidi Adams for all the support and assistance she provided me (e.g. manuscript proof-reading).

TABLE OF CONTENTS

Page

LIST OF TABLES viii

LIST OF FIGURES ix

CHAPTER

1 INTRODUCTION 1

The Dawn of Proteomics 1

Mass Spectrometric Detection of Large Biomolecules Come of Age 2

Enter Discovery Proteomics 4

Targeted Proteomics 5

The Need for Full-Length Protein Population Studies 10

2 MASS SPECTROMETRIC IMMUNOASSAYS FOR DIABETES 12

3 C-PEPTIDE MICROHETEROGENEITY IN TYPE 2 DIABETES POPULATIONS 15

Experimental 18

Results and Discussion 20

4 MASS SPECTROMETRIC IMMUNOASSAY OF INTACT INSULIN AND RELATED VARIANTS FOR POPULATION PROTEOMICS STUDIES 29

Experimental 31

Results and Discussion 35

CHAPTER Page

5 INSULIN AND C-PEPTIDE MASS SPECTROMETRIC IMMUNOASSAY DEVELOPMENTS 47

Experimental 48

Results and Discussion 52

6 INTRAPERSONAL AND POPULATIONAL HETEROGENEITY OF THE CHEMOKINE RANTES 62

Experimental 65

Results and Discussion 68

7 A MASS SPECTROMETRIC IMMUNOASSAY FOR KIDNEY DISEASE AND RELATED DISORDERS 83

Parathyroid hormone microheterogeneity in renal failure populations ... 87

Experimental 89

Results and Discussion 91

8 SELECTED REACTION MONITORING–MASS SPECTROMETRIC IMMUNOASSAY RESPONSIVE TO PARATHYROID HORMONE AND RELATED VARIANTS 98

Experimental 100

Results and Discussion 105

9 PERFORMANCE CHARACTERISTICS OF INTACT (I)-PTH ASSAYS RELATIVE TO A MASS SPECTROMETRIC IMMUNOASSAY FOR PARATHYROID HORMONE 117

Experimental 118

CHAPTER Page

Results and Discussion 119

10 CONCLUSION 127

REFERENCES 129

APPENDIX

A APROVAL DOCUMENTATION AND LIST OF PUBLICATIONS. 146

Copywrite approval documentation 147

Previously Published 149

Co-author authorization 149

IRB documentation 149

List of publications 150

LIST OF TABLES

Table Page

1. Average relative percent abundance (RPA) and RPA range of C-peptide (1-31) and C-peptide (3-31) for the T2D and healthy cohorts. 25
2. Intra/inter-assay insulin precision experiments 43
3. List of all insulin heterogenity encountered within this study 44
4. RANTES variants evident in human plasma..... 70
5. PTH variant frequencies as measured by MALDI-TOF-MS..... 95
6. PTH variant frequencies as measured by MALDI-TOF-MS..... 107
7. Cobas and PTH MSIA quantification values for the first ten patients assayed. 125
8. An overview of the two studies within the context of bioactive PTH quantification 126

LIST OF FIGURES

Figure Page

1. C-peptide MSIA spectrum qualitatively representative of the subjects in this study 21
2. Variant II frequencies 25
3. MS/MS of C-peptide (1-31) and C-peptide (3-31) 26
4. Development of the insulin MSIA 38
5. MS/MS of insulin β-chain 39
6. Representative insulin MSIA working curve 42
7. Insulin MSIA spectra from diabetic samples 43
8. Comparison of healthy versus T2D insulin MSIA spectra 45
9. Multiplexed C-peptide and insulin spectrum 53
10. Dual-capture of light and heavy C-peptide variant standards 55
11. C-peptide (3-31) quantification 56
12. Oral glucose tolerance test results for two healthy individuals 58
13. MALDI-TOF/TOF (MS/MS) quantitative working curves 59
14. Mass spectrum resulting from the targeted top-down analysis of RANTES 69
15. Dual extraction methodolgy 72
16. Mass spectra from a T2D individual and a non-T2D indiviudal 75
17. Stacked bar plot population data for mixed cohort of about 250 individuals: [1-68] and [3-68] 78

Figure Page

18. Stacked bar plot population data for mixed cohort of about 250 individuals: oxidized RANTES 79

19. Stacked bar plot population data for mixed cohort of about 250 individuals: glycated RANTES 80

20. Stacked bar plot population data for mixed cohort of about 250 individuals: low level isoforms 81

21. PTH variant map 93

22. ROC curve for PTH (34-84) 96

23. PTH variant map with SRM fragments 106

24. Pinpoint workflow for development of multiplexed SRM assays 109

25. SRM calibration curves for PTH peptides 111

26. Chromatograms for peptides SVSEIQLM HNLGK (aa1-13), LQDVHNFVALGAPLAPR (aa28-44), and LMHNLGK (aa7-13) 112

27. Pinpoint SRM data from clinical samples of normal and renal failure patients 113

28. SRM quantitative ratios and sample variances of PTH peptides in samples from renal failure patients (Renal) and healhy controls . 114

29. Commercial (I)-PTH assays versus PTH MSIA assay 121

Chapter 1

INTRODUCTION

THE DAWN OF PROTEOMICS

During the 1980's peak in biological reductionist research, which was centered on the philosophy that one should begin by correlating an observed phenotype followed by an investigation of the genes and proteins responsible, i.e. *forward genetics*, a would be emerging field, *proteomics*, was being formulated out of a complimentary field: *protein chemistry*. Underneath the umbrella of *protein chemistry*, efforts geared towards the development of more sensitive and reliable sequencing technologies for protein characterization were underway. One such method, despite being slow and having poor sensitivity relative to modern methods, Edman sequencing of two-dimensional gel electrophoretically separated (2DE) proteins provided crucial information regarding the N-terminal portion of an intact protein or tryptic fragment, thus providing link between understanding the activity of a protein and it's corresponding gene. From derived sequence information, one could now synthesize degenerate oligonucleotide primers and the respective gene could be cloned using PCR (1). These technological breakthroughs fueled the growth and development of evermore detailed and sophisticated sequence databases. Eventually a collective paradigm shift began to take root, a *reverse* approach, wherein one studies and/or manipulates genes and proteins a priori, followed by phenotype observation, i.e. *bottom up*. High-resolution 2DE coupled to computer software programs built for the interpretation of resulting large quantities quantitative protein profile data provided researchers

with the tools necessary begin this journey (1980s) (2, 3). Indeed, ideas such building protein databases from resulting 2DE protein profiles began to emerge, as was the case with *the human protein index* (4). It was within this framework of large-scale *discovery science* that technologies such as 2DE would pave the road for the development of a field of research that would eventually yield the discovery of thousands (if not tens of thousands) of putative disease-correlated biomarkers.

MASS SPECTROMETRIC DETECTION OF LARGE BIOMOLECULES COME OF AGE

The realization of *proteomics* would not have been possible without the advent of mass spectrometry (MS) towards protein characterization via the development of matrix-assisted laser desorption ionization (MALDI) and electrospray ionization (ESI) in the late 1980's (3, 5, 6). MS could now allow protein chemists the possibility to identify and examine the proteins resolvable by 2DE. This dramatically increased the possibilities of large-scale protein studies where the intent is to not only separate and quantify complex protein mixtures, but to also provide unambiguous protein identification per resolvable 2DE spot. The strength of MS lies in its ability to detect the mass-to-charge (m/z) of an analyte, and as such, the analyte must become ionized for it to be detected. Before ESI and MALDI, MS instruments failed to successfully volatize proteins and/or involved excessive fragmentation (3). The 2002 Nobel Prize winner John Fenn described it as "*it's like making elephant's fly*". Regarding the mass analyzer component of

typical MS scheme, time-of-flight (TOF) for MALDI and triple-quadruple MS/MS or ion-trap for ESI proved to be powerful instruments in this emerging field of *discovery proteomics*. Due to issues including the lack of specificity for typical proteomic experiments, the overlapping nature of eukaryotic proteins in general over a typical m/z window when using MALDI, and intrinsic instrument limitations wherein high-resolution data is only achievable for low m/z, the use of trypsin was employed to offer a means for a high-degree of protein identification due to unique peptide masses, aka "fingerprints." The paradigm of digest first then analyze (i.e. *bottom-up proteomics*) would take deep root within the collective mindset of the *proteomics* field. While effective for certain applications, the pervasive use of trypsin would later become questionable due to the unknown landscape of intact proteins.

Besides being labor intensive, expensive, and the inherent lack of automation, the discovery of a high degree of co-migrating proteins in a typical 2DE analysis via MS detection fueled the desire for a new separation technology to emerge for large-scale protein studies (3, 7). Furthermore, limitations in proteome coverage where proteins have extreme pI values (isoelectric point), and/or molecular weights, as well as the sub-standard level of membrane protein detection, supported the idea that 2DE might be fundamentally restricted (8). Thus, the groundwork was laid for gel-independent methodologies to take the stage for proteomic studies.

ENTER DISCOVERY PROTEOMICS

In 1994, the word proteome was coined and was defined as the protein complement of the genome (9). In 2003, Patterson (3) defined *proteomics* as "…the systematic study of the many and diverse properties of proteins in a parallel manner with the aim of providing detailed descriptions of the structure, function, and control of biological systems in health and disease." As a collective group, *proteomics* up until this point in time was primarily focused on the discovery of diagnostic and prognostic biomarkers and novel drug targets. In the mid nineties and up until modern times, LC-MS/MS (liquid chromatography tandem mass spectrometry) coupled with sequence database searches of digested (e.g. Trypsin) complex samples emerged as the mainstream approach for *discovery proteomic* studies, aka *shotgun proteomics* (3). Such methods employ one or more dimensions of separation before MS detection, which enables a more effective protein analysis (e.g. an improved qualitative dynamic range). One such method called multidimensional protein identification technology (aka MudPIT) utilizes a first dimension of separation via strong cation exchange chromatography wherein discrete additions of salt concentration are added to the column followed by a C_{18} reverse phase (RP) chromatography separation step. Eluted peptides are then detected via tandem MS (commonly via an ion-trap) (8). Such technologies are powerful in that a single experiment may yield thousands of identifiable proteins. Despite *shotgun proteomic* technologies revealing thousands (possibly hundreds of thousands) of *candidate* biomarkers from the human proteome, *validation* of such proteomic data (i.e. *targeted proteomics*)

requires the use of hundreds to thousands of samples. A refined, yet complimentary, methodology to conventional discovery proteomic techniques is required as a single "discovery" experiment can take weeks to analyze a relatively small sample set (n < 10) (10). Indeed, Parker et al. states "only a small number of the reported 'candidate' biomarkers have been qualified or verified, and even fewer have been validated, which requires measuring the proposed biomarker in even larger groups of patients" (10). Astonishingly, only 7 markers were FDA approved between 2003 and 2008 (11), stressing the necessity for translational proteomic technologies to enter into mainstream workflows.

TARGETED PROTEOMICS

Automation of sample processing, time and cost per analysis, and finally robust data processing methods are some of the motivating forces driving *targeted proteomics* and the respective competing methods (as outlined below) towards the realization of *1000+* sample cohort studies (10). Furthermore, due to the reality that only a few abundant proteins comprise upwards of 90% of the entire plasma-protein mass (12), plasma proteins exist within a dynamic range of 10^{10} (13), and that MS instruments suffer from suppression effects when multiple analytes are in the ion-source at the same time (10), antibody-based enrichment techniques have taken the center stage in *targeted proteomics* when the intent is to quantify the mid-range to low abundant proteins (i.e. the target is already known, as opposed to *discovery proteomics*). Additionally, despite enzyme-linked immunosorbent assays (ELISA) still holding the throne for conventional biomarker quantification, assay development costs tend to be extremely high (14), multiplexing potential is

not as great as with proteomic approaches, and substantial assay interferences from non-specific proteins and/or non-bioactive protein variants are becoming well-acknowledged as pervasive (15-18). Thus the need for a biomarker translational pipeline exists if the large quantity of candidate biomarkers are to be translated into the real world. Two modern and well-acknowledged *targeted proteomic* methods include SISCAPA (Stable Isotope Standards and Capture by Anti-Peptide Antibodies) and MSIA (Mass Spectrometric Immunoassay).

The SISCAPA workflow starts with sample digest (i.e. an entire plasma sample is denatured and digested at a ratio of 1:80 trypsin/plasma mass), followed by addition of heavy labeled internal standards, enrichment of peptides using anti-peptide antibodies immobilized to a bead-based support which are specific for a known tryptic sequence, and concludes with peptide elution followed by detection via single reaction monitoring (SRM) or multiple reaction monitoring (MRM) LC-MS/MS (19). With it's recent debut in 2003, SISCAPA has "taken off", so to speak. An August 2011 *Google Scholar* search of "SISCAPA" yielded 333 hits, indicating a very strong presence of this emerging proteomics technology. In 2010, Whiteaker et al. demonstrated an automated iteration of SISCAPA that was also multiplexed wherein nine protein targets (via respective surrogate tryptic fragments) were quantified at relatively low plasma concentrations (~nM) and with adequate precision (a *median* coefficient of variation of 12.5% was reported) (14). Despite the early success of SISCAPA, there are a few notable deficiencies that need to be addressed. Due to varying tryptic digest efficiencies, which are protein specific, a significant amount of variance is introduced into an assays

performance (not to mention the excessive amount of trypsin required per analysis). The assay is also not quite yet suitable for large-scale studies due to throughput limitations. Sample studies comprised of small cohorts typically take days, although advancements in higher capillary flow-rates could accelerate sample processing (10). Furthermore, a large reservoir of clinically relevant proteins exist at sub-nM concentrations in plasma (e.g. Insulin exists in the low pM range (20)), and thus, SISCAPA as it currently stands, does not provide adequate performance to quantify proteins of interest within an essential clinical range of human biomarkers. Perhaps SISCAPA's most questionable attribute is found within the first step of the protocol: sample digestion prior to peptide capture.

Recent studies have shown that there appears to be a pervasive backdrop of protein diversity within plasma comprised of structurally alike but functionally distinct proteins (18, 21-24), and as such, this large pool of putative clinical data is forfeited when a sample is digested prior to peptide or protein capture for MS detection (variants become merged into a single signal). Thus, *targeted proteomic* technologies that can provide the clinical metrics necessary for widespread adoption including pM and lower sensitivity, CVs $\leq$ 10%, multiplex mode, automation, are cost efficient, *and* can detect potential and known protein heterogeneity distinct from one another may provide *target proteomics* the approach necessary for wide-spread adoption into clinical diagnostics.

Notwithstanding, such a technology may open up a new and unexpected progression yielding the unification of *discovery and targeted proteomics* into a single scientific field.

MSIA technology debuted in 1995 (25) and could be considered ahead of it's time considering the recent (mid 00's) large-scale movement within *proteomics* towards the validation of candidate biomarkers using antibody-based enrichment techniques. Although the method was originally presented using MALDI-TOF MS detection, the method can be translated to most MS instruments (26, 27). Conceptually, MSIA can be considered a micro-affinity column whereby analytes from complex protein mixtures (e.g. serum, plasma, urine, etc.) are rinsed repeatedly through the column and retained due to antibody-protein coulombic forces, Van der Waals forces, hydrogen bonding, and hydrophobic interactions. Micro-columns are created using commercially available wide-bore P-200 pipettor tips fitted with a solid support frit at the base at the barrel (chemically treated with 15-kDa molecular mass carboxylated dextran) (28). The use of pipette tips allows seamless integration into modern robotic workstations, thus engendering high-throughput capabilities. The frits are subsequently treated with varying customized antibody immobilization chemistries, which allow for optimized singleplex or multiplex MSIA functionality (i.e. multiple covalently linked antibodies per tip). Assuming the antibody binds to the tip with an average orientation supportive of antigen binding (which can be modified using alternative binding chemistries), and practical thermodynamic considerations are acknowledged including the antibody's dissociation constant (K_d), the total

amount of concentration of antigen (free and bound), the volume of the sample, the total amount of antibody (free and bound), and finally the total amount of theoretically bound antigen for MS analysis (i.e. it must be within the detection range of the mass spectrometer) (29), the next stage of assay development may commence.

Strategic application of buffers, salts, and detergents to biological samples prior to antigen extraction enhances MSIA performance via improved antigen-antibody binding, the release of antigen from pre-existing biological protein-complexes, and minimal non-specific binding the MSIA pipette tip (16, 30). Furthermore, the use of a chemically modified protein or heavy isotope labeled peptide/protein may be introduced into the sample to serve as an internal standard for MS quantification. After antigen extraction, MSIA tips are rinsed using various combinations of buffers and detergents that simultaneously respect the antigen-antibody complex and remove non-specifically bound species. Prior to MS detection, antigen-antibody complexes are disrupted typically by the use of an acidic solution (e.g. sinapic matrix for MALDI or formic acid for ESI). Finally, proteins are qualitatively and/or quantitatively detected as intact proteins, or alternatively, as proteotypic fragments resulting from a post-elution enzymatic digestion via MS (i.e. a high-degree of protein variant information is still embedded within the sample). An additional level of specificity can also be achieved, although is not always mandatory, via the use of tandem MS. As one might expect, the MSIA technology has matured in the past 2 decades and has displayed an aptitude to rival conventional ELISA-based technologies (as well as

SISCAPA) via the successful execution of high-throughput cohort studies comprised of patient populations in the thousands (31), detection of analytes in volumes containing sub-fmol quantities of analyte (see chapter 4) (32), and perhaps most interestingly, simultaneous quantification of both native and post-transnationally modified proteins (see chapter 5) (26, 29).

THE NEED FOR FULL-LENGTH PROTEIN POPULATION STUDIES

Despite the human genome being comprised of an estimated 22,333 genes (33), the human body likely encompasses millions of gene products, which arise out of genetic transcript variants, polymorphisms, and posttranslational modifications. This resulting protein diversity paints a very different picture from what traditional *discovery proteomics* might lead one to believe. This can be observed by recognizing a reoccurring theme in *proteomics* wherein genetic products tend to be correlated to a *single* native-protein or tryptic "fingerprint." Regardless, within the human body there is an underlying sea of protein diversity that flows from the interior of human cells into the blood stream, and is even further diversified from the host of chemical reactions that occur within blood. As such, this provides at least two significant implications for diagnostic technologies: 1) there is a high probability for negative assay interferences arising from interactions with modified forms of proteins that have altered functionality, ultimately compromising the efficacy of an assay (15) and 2) the possibility of acquiring determinant data linked to specific disease via technologies that can detect protein isoforms (21). Mass spectrometers empower the pursuit of this new

form of data, as they can, with ease, discriminate between highly similar forms of proteins from their unique parent m/z and/or resulting daughter-ions from tandem MS. Ironically, the past two decades of *proteomics* has largely ignored this opportunity. By approaching bloodborne protein characterization from a "we don't know what we don't know" paradigm in tandem with mass spectrometric analysis, researchers have an opportunity to potentially redefine the underlying assumptions surrounding protein-based diagnostics. As such, studies that aim to explore the underlying depth of bloodborne protein diversity within human disease-stratified populations may simultaneously enable a high-throughput pipeline for candidate biomarker validation (e.g. *RANTES*), and may also provide the means for classical biomarkers, such as *Insulin, C-peptide and Parathyroid Hormone*, to be reevaluated and potentially redefined within this exciting new framework of *population proteomics*. *Proteomics*, as with most scientific fields of research, exemplifies the characteristic of an ever-evolving field of thought, and despite the slow translation of candidate biomarkers and the under-appreciated reality of protein diversity, *proteomics* may be experiencing a renaissance as it ascends into the real world of clinical diagnostics.

Chapter 2

MASS SPECTROMETRIC IMMUNOASSAYS FOR DIABETES

At the turn of the century, it was estimated that 2.8% of the world population had diabetes (accounting for 171 million individuals) (34). According to the Center for Disease Control and Prevention (CDC), it was estimated that 26 million Americans had diabetes and 79 million Americans had pre-diabetes in the year 2010. Even more striking, 1 in 3 individuals in United States that were born in the year 2000 are estimated to develop diabetes within their lifetimes, indicating the prevalence the disease is expected to increase profoundly (35). Consequently, the burden on the American economy is weighty, with a conservative estimate placing total costs incurred in 2002 alone at 132 billion dollars (36). This worldwide epidemic has motivated extensive research into the biological underpinnings of this devastating disease.

Diabetes, a multifaceted metabolic disease, results primarily from defects in pancreatic β-cell insulin secretion and/or defects in insulin action on target tissues. Diabetes is currently monitored and diagnosed primarily by the downstream physiological aftermath of resulting hyperglycemia found in blood. Long-term hyperglycemia has been shown to result in the damage, dysfunction, and failure of organs including nerves, eyes, kidneys, heart, and blood vessels (37, 38). Diabetes is currently classified within two etiopathogenetic categories: type 1 diabetes (T1D) and type 2 diabetes (T2D). T1D simply involves a total insulin secretion deficiency via autoimmune processes resulting on the destruction of β-cells. T2D is a much broader disease encompassing hosts of distinct molecular pathways, but

in its most broad sense, causes insulin resistance and/or inadequate insulin secretory response. As such, the resulting inaction of insulin towards carbohydrate metabolism results in above average basal glucose levels in diabetics (defined by a fasting plasma glucose (FPG) $\geq$ 126 mg/dL or via an oral glucose tolerance test $\geq$ 200 mg/dL). Over time, this results in the non-enzymatic glycation of proteins such is the case with hemoglobin A1C, a clinically used biomarker ($\geq$ 6.5% total hemoglobin A1C is indicative of diabetes). This marker is interesting in that it provides a longitudinal assessment of a patient's history via the extended half-life of A1C, with A1C levels representing average blood glucose levels over a 2-3 month period (37, 39). Although current gold standard assays (e.g. glucose and A1C) are indisputably helpful in the broad classification of this disease, new diagnostic tests and panels have the potential to dramatically improve the diagnosis and treatment on an individual level.

In addition to monitoring the time-sensitive posttranslationally modified protein marker A1C, investigating more in-depth biomarker panels that address native forms *and* variant forms within the context of diabetes via mass spectrometric immunoassays may enable a more precise diagnosis of diabetes within specific groups of individuals. As a consequence, this may yield the necessary findings for the development of next-generation antidiabetes medications. Similarly, new insights into the pathobiology of diabetes and related comorbidities (e.g. coronary artery disease) via detection of oxidized proteins induced by systemic oxidative stress and/or protein truncation produced by enzymes involved in disrupted hormone pathways (40) have the opportunity to

expand the definition and classification of diabetes and related comorbidities. Consequently, such “isoform-aware” assays have the potential to provide a never-before-seen level of detail within an individual and might support the realization of personalized medicine for the treatment and management of diabetes and related comorbidities. Within this framework, population proteomics studies were undertaken to investigate the classical biomarkers C-peptide and insulin and the more contemporary, candidate biomarker, RANTES (i.e., Regulated on Activation, Normal T cell Expressed and Secreted).

Chapter 3

C-PEPTIDE MICROHETEROGENEITY IN TYPE 2 DIABETES POPULATIONS

In response to elevated blood glucose levels within the beta cells of the pancreatic islets of Langerhans, preproinsulin is produced in the endoplasmic reticulum and is cleaved by microsomal enzymes to generate proinsulin. Proinsulin is subsequently transported to the Golgi apparatus and packaged into clathrin-coated secretory granules, where it is processed by a cascade of proconvertases and carboxypeptidases, resulting in the portal circulation of equimolar amounts of C-peptide and insulin (41-43). The reported half-life of C-peptide in plasma is between 20-30 minutes and its concentration is 3-5 times that of insulin (42, 44-46).

Conventionally, C-peptide functions as a mediator/connector in the protein folding of the proinsulin precursor molecule to facilitate two disulfide bridges between the α- and β-chains of the insulin molecule. Excluding this well-established role in the insulin biosynthesis pathway, the physiological functions of C-peptide have remained largely undefined. Recently, however, C-peptide has been shown to have alleviating physiological effects towards diabetes. Diabetic rats with pharmacological doses of C-peptide demonstrated a restoration toward normal of the diabetes-induced decrease in cellular sodium-potassium adenosine triphosphatase (ATPase) activity and impaired nerve conduction, and a decrease in the diabetes-induced increase in vascular permeability and blood flow (47). Moreover, structural studies indicate the C-terminal pentapeptide segment (27-31

residues, particularly Glu27) as the site of receptor-ligand binding which is thought to be responsible for increasing intracellular Ca^{2+} concentrations, stimulation of MAP kinase signaling pathways, and the stimulation of Na^{+},K^{+}-ATPase and endothelial eNOS. However, it is possible that there are other signaling pathways involved (42, 48-51).

In clinical application, C-peptide is a useful indicator for differentiating between type 1 and type 2 diabetes (42, 44, 52-54). Low fasting levels of C-peptide are used in combination with other biomarkers to classify diabetics as having idiopathic type 1 diabetes of nonautoimmune or autoimmune origin. C-peptide concentrations are generally measured using immuno-based assays such as enzyme-linked immunosorbent assays (55) and radioimmunoassay (56), or fluorescence (57, 58). However, a recent study investigating the inter-assay and inter-laboratory reproducibility of these industry-standard assays has reached the conclusions that results generated by different methods and laboratories do not always agree, and that calibrating C-peptide measurement to a reference method can increase comparability between laboratories (57). The reference method indicated in this recent study is isotope-dilution mass spectrometry (ID-MS), which is a natural extension of a significant body of work using mass spectrometry for the accurate quantification of C-peptide (59-65). In particular, two methodologies, – either 2D-LC/MS operating in select ion monitoring mode (59), or LC-MS/MS operating in a multiple reaction monitoring mode (60) – have demonstrated excellent analytical metrics (e.g., in accuracy (94.6 – 104.1% (60)), precision (CV < 1.5% (59); CV < 4% (60)), LOD 10 pM (60) and LOQ ~ 50 pM

(59, 60)) for the quantification of intact C-peptide. Accordingly, these approaches are likely to become “gold standard” assays for C-peptide (57, 63).

One caveat of the ID-MS approaches (as they are described, e.g., (59, 60) without full-scan data), as well as the conventional immunometric assays, is the inability to differentiate between wild-type and variant forms of C-peptide that might be encountered in plasma. Formally, the consideration of such microheterogeneity may help to explain measurement discrepancies found between ID-MS and conventional assays. Alternatively, from a biological perspective the study of microheterogeneity is important when considering that genetic and posttranslational variants of proteins contain additional information regarding the personal makeup of an individual, which in turn may have significant implications towards personalized medicine. For example, inactivation of peptide hormones by N-terminal dipeptide truncation via Dipeptidyl Peptidase IV (DPP-IV), such as glucagon-like peptide-1 (GLP-1), result in multiple endogenous isoforms which can begin to describe an individual’s state of enzymatic activity (e.g. DPP-IV activity) and peptide signaling activity (e.g. the relative abundance of the agonist form of GLP-1) (66). In addition, in acknowledging that increased activity levels of protein regulatory enzymes have been in many cases disease correlated, such as with T2D and DPP-IV (67), it is essential to take an in-depth look at the breadth of protein microheterogeneity.

Thus, future studies stand to benefit from a more complete survey of qualitatively different variants of C-peptide as they exist in healthy and diseased populations. To this end, this report focuses on the use of mass spectrometric

immunoassay (MSIA) (25) to map structural differences in C-peptide found in healthy and type 2 diabetes (T2D) populations.

EXPERIMENTAL

STUDY SUBJECTS, SAMPLE COLLECTION AND PREPARATION

CDI (1,1'-Carbonyldiimidazole)-activated affinity pipette tips were prepared and derivatized with mouse anti-human C-peptide antibody (AbD Serotec), as previously described for other antibodies (23). For the development of the assay, healthy human female plasma was purchased from ProMedDx (Norton, MA). Ninety six additional human plasma samples (equaling 48 healthy individuals, 12 insulin dependent type 2 diabetics, and 36 non-insulin dependent type 2 diabetics) were purchased from ProMedDx. Five hundred microliters of human plasma was pre-treated with 250 µL of a solution containing: 4.5 % Tween 20, 150mM Octyl-β-glucopyranoside, 1.5M Ammonium Acetate, and Concentrated PBS (0.67M sodium phosphate, 1M sodium chloride), for a total analytical volume of 0.75 mL.

PLASMA MASS SPECTROMETRIC IMMUNOASSAYS

C-peptide was extracted with the aid of a Beckman Multimek 96 pipetting robot by repeatedly (250 repetitions) drawing and expelling (back into the analytical volume) 125 µL aliquots of the analytical volume through an anti-C-peptide affinity pipette. After extraction, the pipettes were rinsed using PBS (0.1M sodium phosphate, 0.15M sodium chloride, pH 7.2), HBS-P (0.01M HEPES, 0.15M NaCl, 0.05% v/v Surfactant P20, pH 7.4), H_2O, 100mM

Tris(hydroxymethyl)aminomethane hydrochloride (pH 4.6), and H_2O (in this order, each rinse = 10 repetitions of 150 µL), after which C-peptide was eluted and prepared for MALDI-TOF MS by drawing 4 µL of MALDI matrix solution (saturated aqueous solution of α-cyano-4-hydroxycinnamic acid, in 33% (v/v) acetonitrile, 0.45% (v/v) trifluoroacetic acid, TFA) into the pipette and depositing onto a MALDI target.

MASS SPECTROMETRY

MALDI-TOF MS was performed using a Bruker Ultraflex MALDI-TOF instrument operating in the negative ion, delayed-extraction mode; reflector engaged with 'ion source 1' at 20.00 kV, 'ion source 2' at 17.45 kV, lens at 7.50 kV, 'reflector' at 21.00 kV, 'reflector 2' at 10.95, 60 ns delayed extraction, deflection signal suppression up to *m/z* 1500, and 2 GS/s sample rate. Two hundred laser-shots were signal averaged for each mass spectrum. Single stage MALDI-TOF mass spectra were externally calibrated with a mixture of 6 peptides supplied by Bruker (Cat. No. 208241) ranging in monoisotopic *m/z* from 1044.53 (Angiotensin II $[M-H]^-$) to 3145.46 (Somatostatin $[M-H]^-$)

DATA ANALYSIS

Individual mass spectra were baseline subtracted and smoothed prior to peak integration. Peaks representing the five most abundant C-peptide and C-peptide-variant isotopes were integrated and tabulated in a spreadsheet for determination of percent relative abundances.

TANDEM MASS SPECTROMETRY

LIFT-TOF/TOF mass spectra of C-peptide were acquired on a Bruker Ultraflex MALDI-TOF/TOF instrument in positive ion mode using sinapic acid as a matrix. Precursor ions were selected within a 30 Da mass window. The LIFT-TOF/TOF instrument control method was calibrated according to the instrument manufacturer's protocol and was run without CID gas.

RESULTS AND DISCUSSION

Figure 1 shows a MSIA spectrum qualitatively representative of those obtained for the individuals investigated in this study. In addition to intact C-peptide (observed monoisotopic *m/z* 3017.50), signals registering at *m/z* 2888.49, 2817.45, and 2688.41 (labeled I, II and III, respectively) were observed at varying relative intensity in many but not all samples throughout both the healthy and T2D cohorts (n = 48 each). The sequence of human C-peptide is:

H_2N—EAEDLQVGQVELGGGPGAGSLQPLALEGSLQ—*COOH*

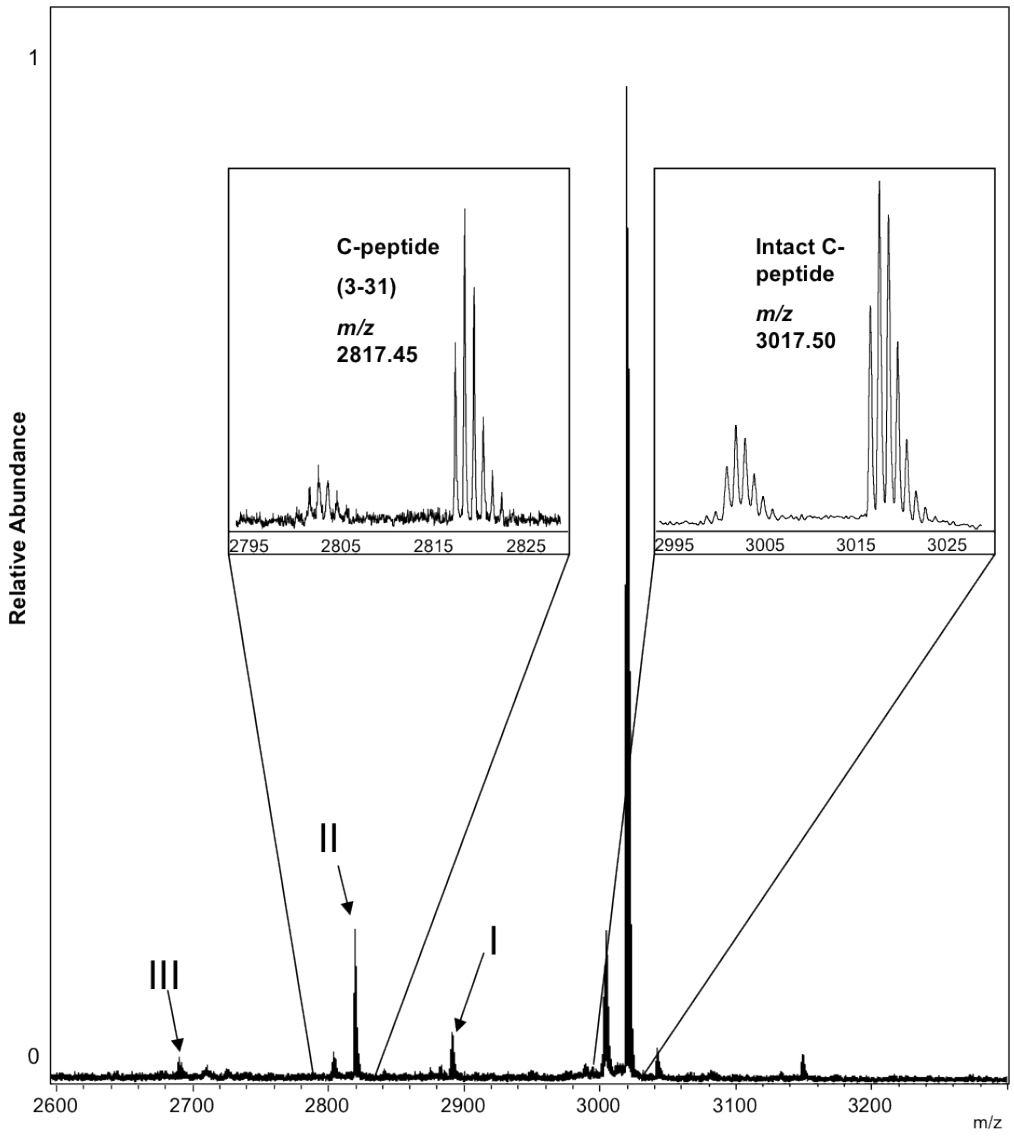

Figure 1: C-peptide MSIA spectrum qualitatively representative of the subjects in this study. The mass spectrum contains the intact form of C-peptide as well as C-peptide (2-31) (calc. monoisotopic *m/z* 2888.47), C-peptide (3-31) (calc. monoisotopic *m/z* 2817.44), and C-peptide(4-31) (calc. monoisotopic *m/z* 2688.39). These N-terminally truncated variants had signals registering at *m/z* = 2888.49, 2817.45, and 2688.41 (labeled as I, II and III, respectively). The loss of ammonia from the N-terminus is observed on all native and variant forms and is frequently observed under reflector-TOF-MS conditions.

Two major considerations arise from protein surveys such as this one that are conducted across human populations. First, the concept of populational frequency addresses the question of the number of samples (out of the total) in which a particular protein variant was observed with signal to noise ratio greater than three: Out of the forty eight type 2 diabetics, isoform I was observed in 1 subject, isoform II in 44 subjects, and isoform III in 1 subject. In the healthy cohort, isoform I was observed in 9 subjects, isoform II in 43 subjects, and isoform III was not observed.

Second, the relative percent abundance (RPA) of each unique variant may be obtained (without the use of an internal standard) by integrating all mass spectral peak areas corresponding to variant forms of the target protein, then dividing the peak area of each variant form by the summed areas of all forms and multiplying by one hundred. The use of affinity capture ensures that spurious peaks unrelated to the target protein do not arise in the mass range of interest. Using this form of relative quantification, the RPA for C-peptide variant II was evaluated with respect to the presence of T2D by grouping data from individuals into their respective cohorts. **Table 1** presents the average RPA with standard deviation as well as RPA range of intact C-peptide and variant II within the T2D and healthy cohorts. (Variants I and III were not tabulated in analogous manner because they were infrequently detected throughout both cohorts.)

Variant	T2D		Healthy	
	Average Relative Percent Abundance (RPA)	RPA Range	Average Relative Percent Abundance (RPA)	RPA Range
C-peptide (1-31)	90 ± 12%	20-100%	95 ± 4%	68-99%
C-peptide (3-31)[a]	10 ± 12 %[b]	0-80%	5 ± 4 %	1-32%

Table 1: Average relative percent abundance (RPA) and RPA range of C-peptide (1-31) and C-peptide (3-31) for the T2D and healthy cohorts.

RPA is obtained following peak area integration by dividing each individual peak area by the sum of all peak areas representing C-peptide and multiplying by 100. RPA range provides the low and high values observed for each variant in the two 48 sample cohorts described here.

a) The population distribution of C-peptide(3-31) for the RPA ranges of healthy and diabetic individuals are given in Figure 2.
b) Statistically significant from the healthy cohort at $p < 0.01$

Interestingly, the relative contribution of variant II was found to be comparatively different between the T2D and healthy cohorts. **Figure 2** shows histograms comparing the frequency of occurrence between the two cohorts for the RPA of variant II. A broad distribution averaging 10% RPA (average of all individuals in the cohort) was observed for the T2D cohort, as compared to a narrow distribution averaging 5% RPA observed for the healthy cohort. Taking these differing variances into account, the average RPA for variant II in the T2D cohort was found by t-test to be significantly different from the healthy cohort at $p < 0.01$.

To verify repeatability of the assay, plasma from a single donor was divided into 96 aliquots and analyzed as described above. The average RPA value for unmodified C-peptide was 93% ± 1.0% SD and the average RPA for variant II was 7.4% ± 1.0% SD.

Given accurate mass determination (within 10 ppm), variants I, II and III can be can be tentatively identified as truncated forms of C-peptide respectively lacking one, two or three N-terminal amino acids (i.e., C-peptide (2-31), C-peptide (3-31) and C-peptide (4-31)). Because of its observed greater contribution in the diabetic population, tandem mass spectrometry was used to confirm the identity of variant II via partial sequencing. For reference, **Figure 3A** shows a MALDI-TOF/TOF-MS spectrum obtained from intact C-peptide (positive mode m/z = 3019.50). Signals are observed to align predominantly with y-ions (with ~0.2 Da mass accuracy) yielding a fragmentation signature for intact C-peptide.

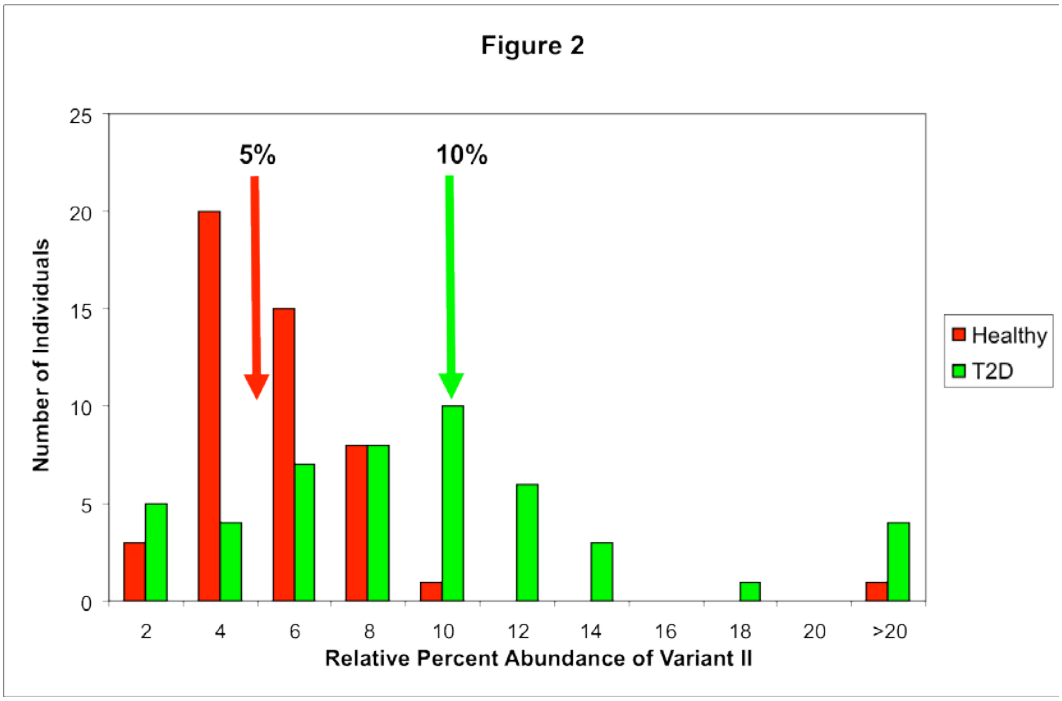

Figure 2: Variant II frequencies. Expanding upon the last row of Table 1, these histograms provide the frequency of occurrence within the Healthy and T2D populations for the relative percent abundance of variant II. A broad distribution averaging 10% RPA (average of all individuals in the cohort) was observed for the T2D cohort, as compared to a narrow distribution averaging 5% observed for the healthy cohort.

Figure 3B shows a tandem mass spectrum obtained for variant II aligned to the sequence of C-peptide (3-31). Although of lower signal intensity, the y-ion fragmentation series registers the same pattern and mass as the intact C-peptide series (note the three overlaid enlarged glycine registers) which is expected for N-terminally truncated peptide forms. Notably, the signal for the b-ion of C-peptide(1-31) terminating at Q22 is observed at m/z 2093.1, but the b-ion of the putatively truncated C-peptide terminating at the same glutamine residue is shifted in mass by -200.2 Da, which corresponds to the mass difference associated with the loss of the N-terminal Glu-Ala dipeptide.

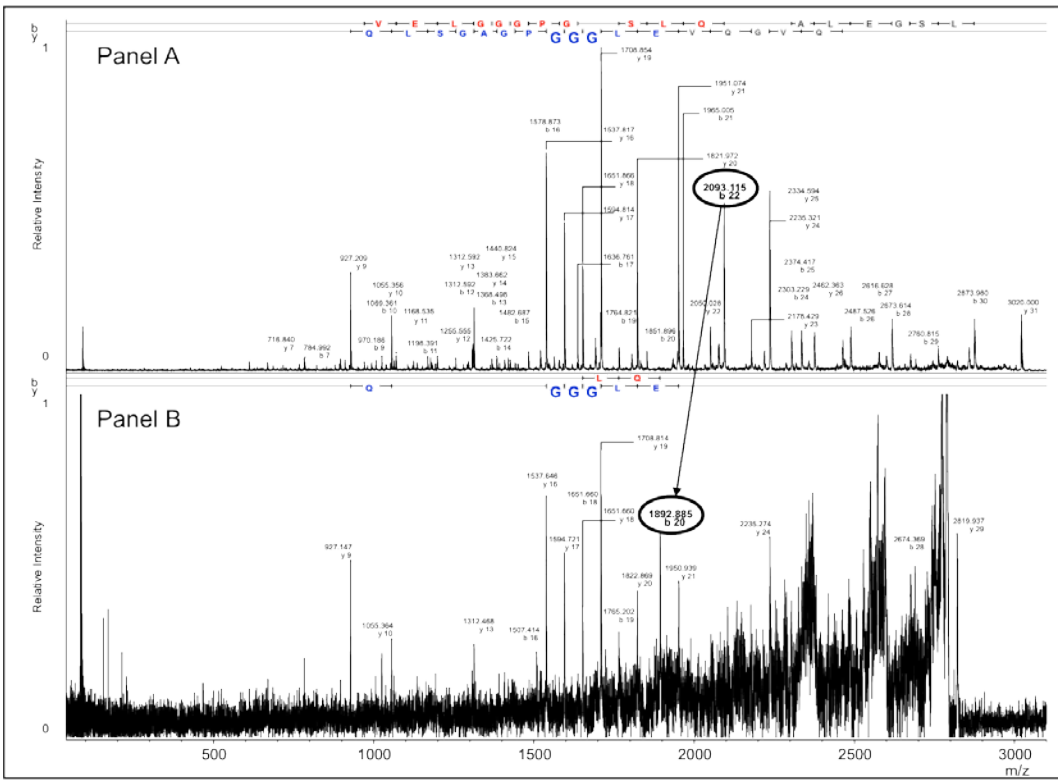

Figure 3: MS/MS of C-peptide (1-31) and C-peptide (3-31). (A) MALDI-TOF/TOF-MS spectrum of intact C-peptide (positive mode *m/z* = 3019.50; calc. monoisotopic *m/z* = 3019.52). (B) MALDI-TOF/TOF-MS spectrum of variant II aligned to the sequence of C-peptide (3-31). The y-ion fragmentation series registers as the same pattern and mass as the intact series (note the three overlaid blue glycine registers), which is expected for N-terminally truncated peptide forms. The signal for the b-ion of C-peptide (1-31) terminating at Q22 is observed at m/z 2093.1, but the b-ion of the putatively truncated C-peptide terminating at the same glutamine residue is shifted in mass by -200.2 Da, which corresponds to the mass difference associated with the loss of the N-terminal Glu-Ala dipeptide.

Together, the affinity extraction, mass mapping, and MS/MS data firmly support the conclusion that variant II is C-peptide(3-31).

Previous to this study, another C-peptide variant – in the form of C-peptide (1-26) – had been reported in the literature. This variant form was first discovered in

rats but was later found to exist at very low relative abundance in humans. Furthermore, it was not observed to increase in individuals with T2D or insulinoma (68, 69). To our knowledge, however, N-terminally truncated forms have yet to be reported or studied. The consequences and utility of the truncated variants are thus not understood, but are intriguing; in particular, the observation of elevated levels of C-peptide (3-31) in the diabetic population. Structural and biophysical characterization of dipeptidyl peptidase IV (DPP-IV; EC 3.4.14.5) (70), a multifunctional type II transmembrane serine peptidase, reveals a preferred enzyme specificity of Xaa-Pro or Xaa-Ala from the amino termini of peptide hormones. Moreover, DPP-IV is a critical enzyme in regulating physiological glucose homeostasis via N-terminal cleavage of peptide hormones such as glucagon-like peptide-1 (GLP-1) and glucose-dependent insulinotropic polypeptide (GIP) (66). As such, control of DPP-IV activity via drug formulations is a major focus of new T2D drug development (71-73). Observation of C-peptide (3-31) is thus consistent with DPP-IV cleavage at the N-terminal GluAla- of C-peptide, and the elevated levels observed in the diabetic population may be explained by abnormal DPP-IV activity in the diabetic population. If C-peptide is indeed an *in vivo* substrate for DPP-IV, these results are in alignment with previous work that showed an increase in DPP-IV activity in T2D individuals with moderate to severe hyperglycaemia relative to newly diagnosed diabetics, impaired glucose tolerance subjects, and normal glucose tolerance subjects (67). Consequently, the measurement of C-peptide (3-31) as a companion marker to C-

peptide is a potential avenue to improve the already gold-standard ID-MS assays, and, moreover, the measurement of both C-peptide forms may offer an assay simultaneously reflective of insulin production and modulation of DPP-IV activity during therapy. Further investigations in larger clinically well defined healthy and diabetic cohorts are necessary to gauge the relative behavior of C-peptide and C-peptide (3-31) and their individual implications in assay improvement and disease stratification.

Chapter 4

MASS SPECTROMETRIC IMMUNOASSAY OF INTACT INSULIN AND RELATED VARIANTS FOR POPULATION PROTEOMICS STUDIES

Numerous genetic polymorphisms and splice variants of human insulin have been characterized (74-77) [UniProtKB AC P01308]. Yet there remains a need for systematic methods to monitor polymorphisms, splice variants, and particularly, posttranslational modifications (e.g. degradation products) *that are not pre-defined*, in the population at large. Data arising from the application of such methods will take us one step closer to making personalized medicine in the context of diabetes a reality.

An essential and differentiating characteristic of mass spectrometric-based assays that are designed from a *top-down* perspective is that immunoreactive forms are clearly and immediately evident in the sample and can be independently quantified. Likewise, protein variants that are distinctly monitored in this way are in many circumstances the same variants that interfere with classical analytical techniques such ELISAs and radioimmunoassays (RIA) (i.e. the variants cross-reacts with the antibody) or, conceivably, with recent *bottom-up* quantitative mass spectrometric approaches such as LC-MRM, e.g., SISCAPA (Stable Isotope Standards and Capture by Anti-Peptide Antibodies) (19). As in the case of the latter example, it is the unmodified portions of variants and native protein (in the presentation of tryptic fragments) which equally bind to the antibody and cause diminished assay specificity. These techniques (e.g. LC-MRM) result in the

summation of protein variants, which may or may not have modified biological activity. Consequently, an erroneous read on the concentration of the native, bio-active form a protein may result. Indeed, this was shown with insulin twenty years ago where immunoassays where shown to cross-react with proinsulin related molecules (78). (The same phenomenon has been documented recently with regard to human brain natriuretic peptide (BNP) (79).) Moreover, a more contemporary study showed 11 commercially available insulin assays (one RIA and 10 enzyme/chemiluminescent based) to vary by a factor of 2 indicating assay-specific cross-reactivity (80). Consequently, several groups have responded to this challenge with the development of quantitative mass spectrometric insulin assays. With the mass spectrometer serving as the detection component of the assay, it is now possible to unambiguously quantify intact insulin out of plasma and urine distinct from preproinsulin byproducts, insulin degradation products, and synthetic insulin analogs (81-85). While there are some relative advantages to previously reported MS techniques including the ability to monitor for unique MS^2 diagnostic product ion signatures resulting from insulin isoforms (85), assays such as these are not suited for large population screenings when the goal is to monitor for unanticipated forms of insulin. Herein we report a high-throughput, *full-scan mode* mass spectrometric assay for quantifying insulin which simultaneously provides accurate-mass detection of insulin-related protein variants that have not been pre-defined.

EXPERIMENTAL

STUDY SUBJECTS, SAMPLE COLLECTION AND PREPARATION

CDI (1,1'-Carbonyldiimidazole)-activated affinity pipette tips were prepared and derivatized with mouse anti-human insulin antibody (AbD Serotec, Cat No. 5329-3806), as previously described for other antibodies (23, 86). For development of the assay, a bulk quantity (> 100 mL) of healthy human EDTA plasma from an individual female donor was used. Sixteen additional human EDTA plasma samples from patients including 8 healthy individuals and 8 type 2 diabetics (6 ID T2D (insulin dependent type 2 diabetics), and 2 non-ID T2D (non-insulin dependent type 2 diabetics)) were acquired under IRB approval. Cohorts were matched by gender. The diabetic cohort had an average age of 57 and the healthy cohort had an average age of 51. Sheep plasma was used as the matrix to generate standard curves and was acquired from Bioreclamation, Inc. All samples were stored at -80˚ C prior to use. Upon use, samples were centrifuged for 5 minutes at 10,500 x g and subsequently re-aliquoted into a 96 well sample tray. Porcine insulin, human insulin, and bovine serum albumin were purchased from Sigma-Aldrich. As qualitative negative controls, anti-resistin and anti-osteocalcin were purchased from R&D Systems and Novus Biological, respectively.

PLASMA MASS SPECTROMETRIC IMMUNOASSAYS

Five hundred microliters of human plasma was pre-treated with 250 µL of a solution containing: 4.5 % Tween 20, 150mM Octyl-β-glucopyranoside, 1.5M Ammonium Acetate, and Concentrated PBS (0.67M sodium phosphate, 1M sodium chloride), for a total analytical volume of 750 µL. Insulin and related variants were extracted with the aid of a Beckman Multimek 96 pipetting robot by repeatedly (250 repetitions) drawing and expelling (back into the sample volume) 125-µL aliquots of the sample volume through an anti-insulin affinity pipette. After extraction, the pipettes were rinsed using PBS (0.1 M sodium phosphate, 0.15 M sodium chloride, pH 7.2), HBS-P (0.01 M HEPES, 0.15 M NaCl, 0.05% v/v Tween Surfactant P20, pH 7.4), H_2O, 100mM Tris HCl (Tris(hydroxymethyl)aminomethane hydrochloride pH 4.6), and H_2O (in this order, each rinse = 10 repetitions of 150 µL), after which insulin was eluted and prepared for MALDI-TOF MS by drawing 4 µL of MALDI matrix solution (saturated aqueous solution of sinapic acid, in 33% (v/v) acetonitrile, 0.45% (v/v) trifluoroacetic acid, TFA) into the pipette and depositing onto a MALDI target.

MASS SPECTROMETRY

MALDI-TOF MS was performed using a Bruker Ultraflex III MALDI-TOF-MS instrument. The instrument was used in both linear mode (for precision experiments as explained below) and with reflector engaged. In the former, positive ion, delayed-extraction mode was used with ‘ionsource 1’ at 25.00 kV,

'ion source 2' at 23.50 kV, lens at 6.00 kV, 50 ns delayed extraction, deflection signal suppression up to *m/z* 2500, and 1 GS/s sample rate. When the reflector was engaged, the instrument operated in the positive ion, delayed-extraction mode with 'ion source 1' at 25.00 kV, 'ion source 2' at 21.90 kV, lens at 9.50 kV, 'reflector' at 26.30 kV, 'reflector 2' at 13.80, 190 ns delayed extraction, deflection signal suppression up to *m/z* 2000, and 2 GHz sampling rate. At least 10 thousand laser-shots were signal averaged for each mass spectrum to ensure good ion counting statistics. In linear mode, spectra were externally calibrated with a mixture of 4 proteins, supplied by Bruker (Cat. No. 208241), ranging from *m/z* 5734.52 (Insulin $[M+H]^+$ to *m/z* 12,360.97 (Cytochrome C $[M+H]^+$. When in reflector mode, MALDI-TOF-MS mass spectra were externally calibrated with a mixture of peptides and proteins supplied by Bruker including: *m/z* 2093.086 (ACTH_clip(1-17) $[M+H]^+$; monoisotopic), *m/z* 3147.471 (Somatostatin $[M+H]^+$; monoisotopic), *m/z* 5730.609 (Bovine Insulin $[M+H]^+$; monoisotopic), and *m/z* 6179.67 (Cytochrome C $[M+2H]^{2+}$; most abundant isotope).

INSULIN QUANTIFICATION

All samples used for quantification were fortified with 150 pM porcine insulin (which served as the internal standard) prior to extraction of endogenous human insulin. Samples used in the generation of insulin standard curves were prepared and assayed using sheep plasma diluted 4x in 30 g/L BSA in HBS-N (0.01M HEPES and 0.15M NaCl). The curves were prepared (via serial dilution) with a

human insulin concentration range of 15 pM to 1.92 nM. The curves had 9 concentration points in total, including the blank samples with only internal standard. For insulin quantification out of human samples, eight EDTA plasma samples from healthy volunteers and eight EDTA plasma samples from T2D volunteers were run in parallel with a standard curve. On each day of the interday/intraday precision experiment, curves were run in triplicate alongside samples with known concentrations of human insulin, at 50 pM (n=4), 100 pM (n=4), and 400 pM (n=4). Samples were prepared fresh daily.

DATA PROCESSING

Individual mass spectra were baseline subtracted (Tophat algorithm) and smoothed (SavitzkyGolay algorithm; width = 0.2 m/z; cycles = 1) prior to peak integration using Bruker Daltonics flexAnalysis 3.0. All peaks representing porcine insulin, intact insulin, and insulin variants were integrated baseline-to-baseline (using Intrinsic Bioprobes Inc. Zebra 1.0) and tabulated in a spreadsheet for quantification.

REDUCTION OF INSULIN

On-target reduction of interchain disulfide bonds was employed to verify the identification of insulin in the mass spectrum: The target (96-well format MALDI-TOF-MS gold coated plate) was placed on a 40°C heating plate followed by application of a three-microliter aliquot of 100mM dithiothreitol (DTT) in

100mM tris base (pH 8.5) to an already-dried MALDI spot previously shot from a healthy human sample. Reduction was carried out for 20 minutes, during which time the aqueous environment of the samples was maintained by the addition of a 1 µL aliquot of water at the beginning of the reduction and every 4 minutes thereafter. The reduction reaction was terminated after 20 minutes via the addition of a 3-µL aliquot of the MALDI matrix solution which lowered the pH down to ~1-2. This effectively ended the reduction process and, upon air-drying, recrystallized the matrix spot.

RESULTS AND DISCUSSION

In the development phase of the assay prior to the implementation of internal standards for quantification, various sample preparations and rinses were tested. **Figure 4(I)** shows a pre-optimized MSIA spectrum without the use of in-sample detergents, salts, and post-extraction rinses. Tween 20, Octyl-β-glucopyranoside, Ammonium Acetate, and PBS were determined, when added to the plasma sample, to minimize the non-specific binding of proteins. Next, various rinse protocols were tested. It was determined that PBS, HBS-P, H_2O, 100 mM Tris-HCl, and finally H_2O produced the best results. **Figure 4(II)** shows an optimized MSIA spectrum. Overall, the optimized protocols produced spectra largely free of non-targeted proteins, high S/N ratios, and isotopic resolution for insulin. The *open m/z window* that was created after the optimization was valuable for the potential detection of additional insulin isoforms that were cross-reactive with the

antibody. **Figure 4(III)** shows an on-target-reduction spectrum of insulin. Notably, this was generated by reducing the same MALDI matrix spot used to generate **Figure 4(II)**. Reduction of insulin breaks the two-disulfide bonds between the α-chain and β-chain and the single disulfide bond within the α-chain. Besides the specificity imparted by antibody capture and verified by the exact mass detection of intact insulin, the observation of exact masses corresponding to the α- and β-chains of insulin upon reduction confirm the qualitative specificity of the assay. Lastly, an additional measure ensuring assay specificity was achieved by generating a MALDI-TOF/TOF (MS/MS) spectrum on the insulin β-chain (**Figure 5;** methodology described elsewhere (87)). This was produced from a healthy human sample that had 50 nM recombinant human insulin spiked in pre-extraction (endogenous insulin levels did not produced adequate S/N for MS/MS).

An analog of a protein that has a different molecular weight may be used as an internal standard for quantification when using MALDI-TOF-MS (25). In this manner, the internal standard is captured with the target protein using the same antibody (the antibody must be able to cross-react). While an internal standard can be a chemically modified form of a protein (25), the use of a protein from a different species may be used provided they differ enough in *m/z* (18). Considering the monoisotopic mass of human insulin at 5804.65 Da $[M+H]^+$ and a mass resolution of 15,000 (m/Δm; FWHM), porcine insulin was determined to be an excellent internal standard which differs in mass from human insulin by -

30.01 Da (the monoisotopic molecular weight is 5774.64 Da $[M+H]^+$). This change in mass results from the presence of an alanine (rather than threonine) residue at the β-30 position of porcine insulin. The anti-human insulin antibody employed in these studies was developed with human insulin as the immunogen and is known to recognize insulin and pro-insulin, but the binding epitope has not been determined. Porcine insulin proved to be, retrospectively, well chosen due to its distinct mass relative to synthetic insulin analogs and natural insulin degradation products.

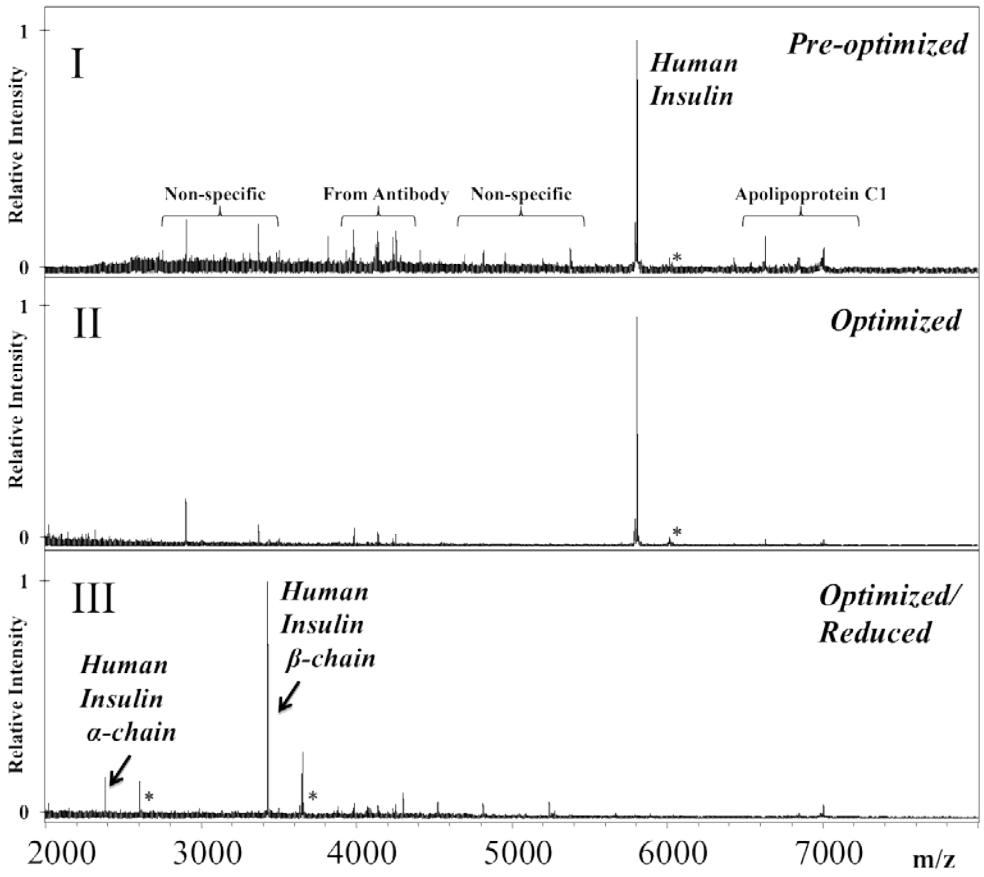

Figure 4: Development of the insulin MSIA. I) The insulin MSIA in the development phase. Plasma from a healthy individual was used (endogenous insulin extracted) to optimize protocols involved in removing non-specific proteins. Non-specific signals include Apolipoprotein C-I and residue found within the antibody solution. II) An optimized spectrum resulting from the use of in-sample detergents, salts, and post-extraction rinses. III) The MALDI-TOF-MS spot used to generate (II) was reduced on-target to verify specificity of the antibody via the appearance of the insulin α-chain and insulin β-chain. * corresponds to sinapic acid matrix adducts. The "1" label on the y-axis indicates 100% relative abundance for the spectrum shown.

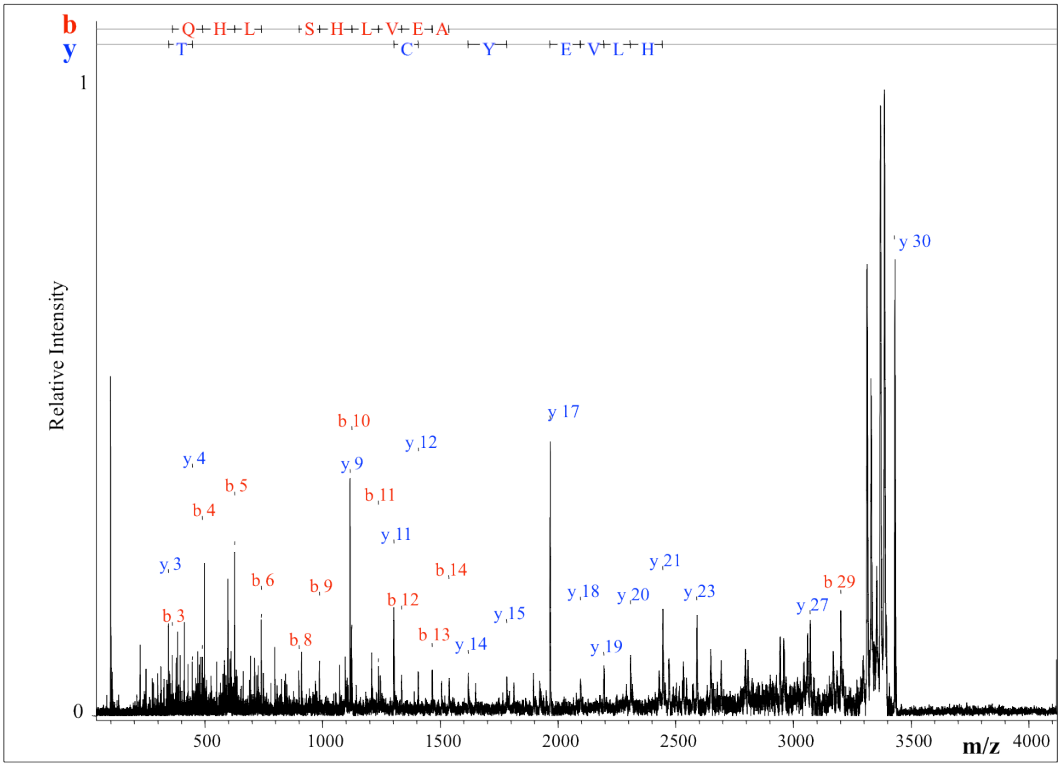

Figure 5: MALDI-TOF/TOF (MS/MS) of Insulin β-chain. A healthy human sample was spiked with human insulin at 50 nM and was subsequently immunoprecipitated with MSIA, reduced on the MALDI target, and then analyzed by MALDI-TOF/TOF (MS/MS) for assay specificity confirmation. b-ions, y-ions and their corresponding sequence tags are shown. The sequence of human insulin β-chain is: H_2N-FVNQHLCGSHLVEALYLVCGERGFFYTPKT-CO_2H.

Insulin MSIA curves demonstrated excellent linearity (the average r^2 value for all three days was 0.9983). The limit of detection (LOD) and limit of quantification (LOQ) were found to be 1 pM and 15 pM, respectively, provided that at least 500 µL of plasma were employed for the assay. Three sample sets composed of four samples each with concentrations of 50 pM, 100 pM, and 400pM were used for intra/inter-assay precision experiments conducted over three days (**Table 2)**. The intraday CVs and estimated interday CVs were < 8%. A

typical standard curve regression line was described by the equation y = 2.096x – 0.034. Using the multi-day data from the triplicate working curves run each day, the average standard error of the estimate was determined to be 24 pM. We estimate the actual captured amount of insulin to be in the range of 1 fmol at the LOQ. A typical standard curve is presented in **Figure 6**.

Figure 7 presents MALDI-TOF-MS spectra obtained in reflector mode from human samples using the insulin MSIA. In this figure, human insulin, des-thr^{30}-insulin (β-chain), des-arg$^{32\text{-}31}$-Lantus (β-chain), and porcine insulin (internal standard) are shown. Intact Lantus and intact Novolog were also detected in the T2D patient samples. With the exception of one outlier, mass accuracy of insulin variants detected was 15 ± 7 ppm (**Table 3).** With this degree of mass accuracy (< 5 ppm with internal mass calibration) and knowledge of the identity and sequence of the target protein (imparted by the specificity of the capture-antibody), mass mapping can greatly narrow a list of candidate protein modifications. Monoisotopic peak assignments were used when S/N was >3. When monoisoptic peaks did not meet this criteria (as in the case of intact Lantus), the most abundant isotope was used for assignment. Of note, we were unable to generate MS/MS information on reduced insulin isoforms due to their low concentrations. Negative control experiments were run using T2D samples known to have des-thr^{30}-insulin (β-chain), Lantus, and Novolog present using MSIA tips derivatized with anti-resistin and anti-osteocalcin. Insulin-related proteins were not detected.

Conc. (pM)	Day 1 (n = 4)	Day 2 (n = 4)	Day 3 (n = 4)	Inter-day (n = 3 days)
50	57.1 ± 2.8; 5.0%	48.8 ± 2.9; 5.9%	52.0 ± 3.2; 6.1%	52.6 ± 4.1; 7.9%
100	98.5 ± 0.9; 0.9%	86.6 ± 4.4; 5.1%	96.2 ± 4.3; 4.5%	93.8 ± 6.3; 6.7%
400	388.5 ± 5.3; 1.4%	347.5 ± 30.0; 8.6%	389.0 ± 10.0; 2.6%	375.0 ± 23.8; 6.4%

Table 2: Three samples (n = 4 ea.) with known concentrations of 50 pM, 100 pM, and 400 pM were tested using the insulin MSIA on three separate days (intra-assay precision). Using these data (n = 3 days), inter-assay precision values were calculated. Values correspond to the average concentration ± standard deviation and to the percent coefficient of variation.

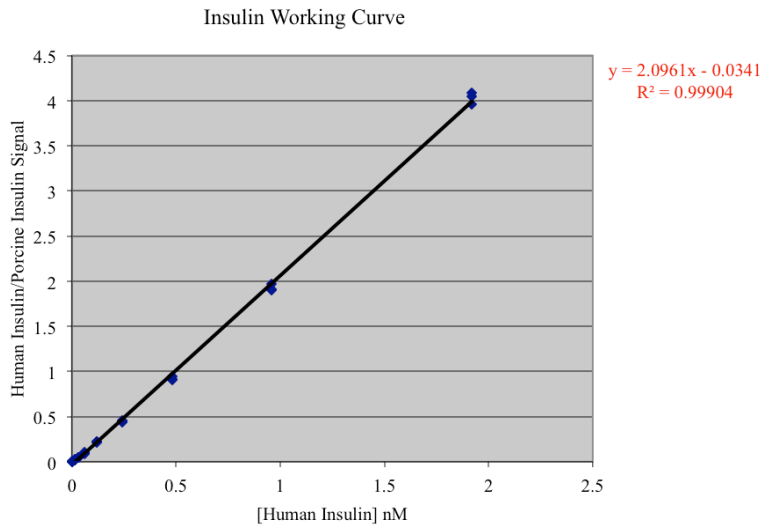

Figure 5: Representative insulin MSIA working curve.

The healthy and diabetic cohorts had an average intact insulin concentration and standard deviation (SD) of 82 ± 60 pM and 243 ± 359 pM, respectively. The range for the two cohorts were 15 – 176 pM and 32 – 1116 pM, respectively. Sample concentrations in the healthy cohort were not clustered near the LOQ and only one sample was found to have a concentration of 15 pM. Basal insulin concentrations in healthy humans are typically in the range of 30-90 pM, with a peak rise to 360-540 pM during meals (88). This is consistent with our measurements of intact insulin in healthy individuals. Outlier samples below 15 pM intact insulin concentration would have to be quantified by an alternative assay, then coupled with the qualitative assay presented here to determine the presence of molecular heterogeneity.

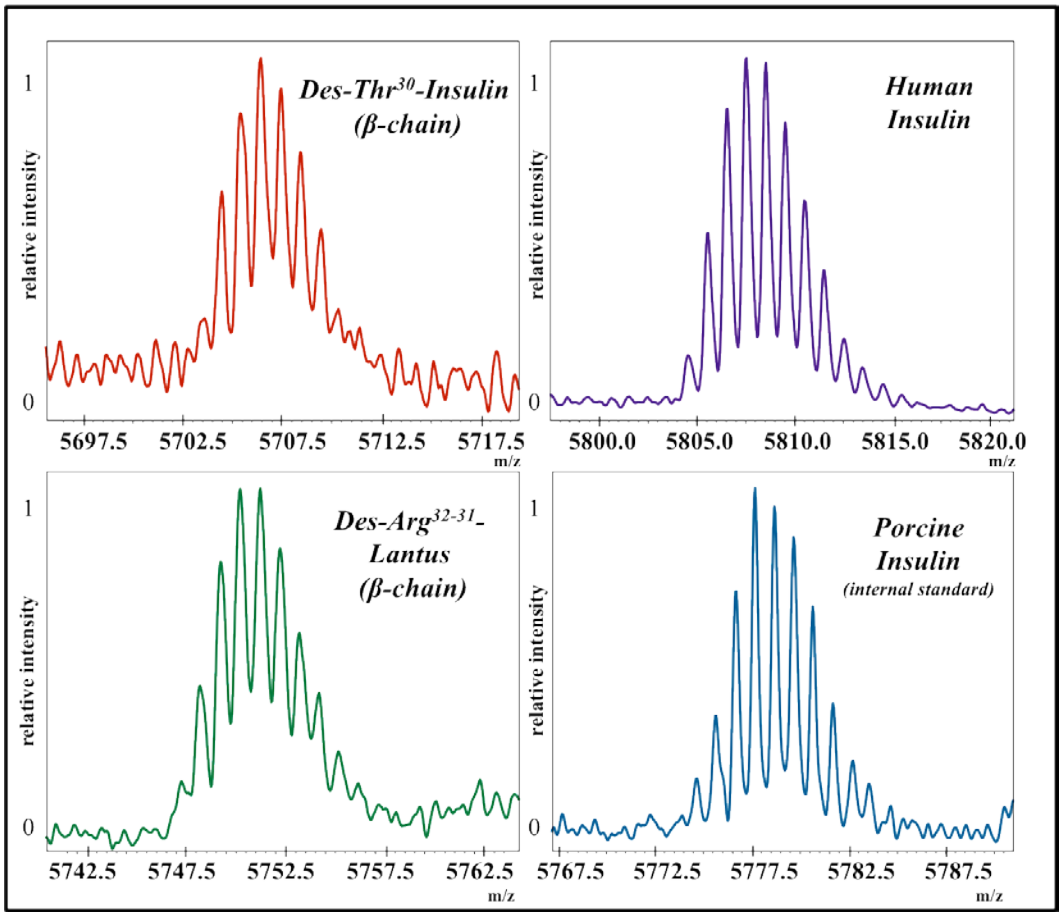

Figure 7: Insulin MSIA spectra from diabetic samples. *m/z* values refer to the monoisotopic mass $[M+H]^+$: human insulin (observed 5804.57 m/z, theoretical 5804.65); des-thr^{30}-insulin (β-chain) (observed 5703.55, theoretical 5703.60); porcine insulin (internal standard) (observed 5774.66, theoretical 5774.64); and des-arg$^{32-31}$-Lantus (β-chain) (observed 5747.50, theoretical 5747.63).

Isoform	Observed	Theoretical
Endogenous		
Intact Human Insulin	5804.57	5804.65
Des-Thr^{30}-Insulin (β-chain)	5703.55	5703.60
Exogenous		
Novalog	5822.59	5822.62
Lantus[a]	6063.13	6062.85
Des-Arg$^{32\text{-}31}$-Lantus (β-chain)	5747.50	5747.63
Intact Human Reduced		
α -chain	2382.95	2383.00
β -chain	3428.75	3428.69

Table 3: List of all insulin heterogeneity encountered within this study. *m/z* values reflect MALDI-TOF-MS monoisotopic detection. [a] denotes X + 3 isotope used for mass determination.

The known urinary metabolite of insulin, des-thr^{30}-insulin (β-chain) (89), was detected in the plasma of three diabetics and the truncated form of Lantus was detected in the plasma of one diabetic. To our knowledge, these variants have previously only been detected in urine. Sample MSIA spectra for healthy and T2D patients are presented in **Figure 8**.

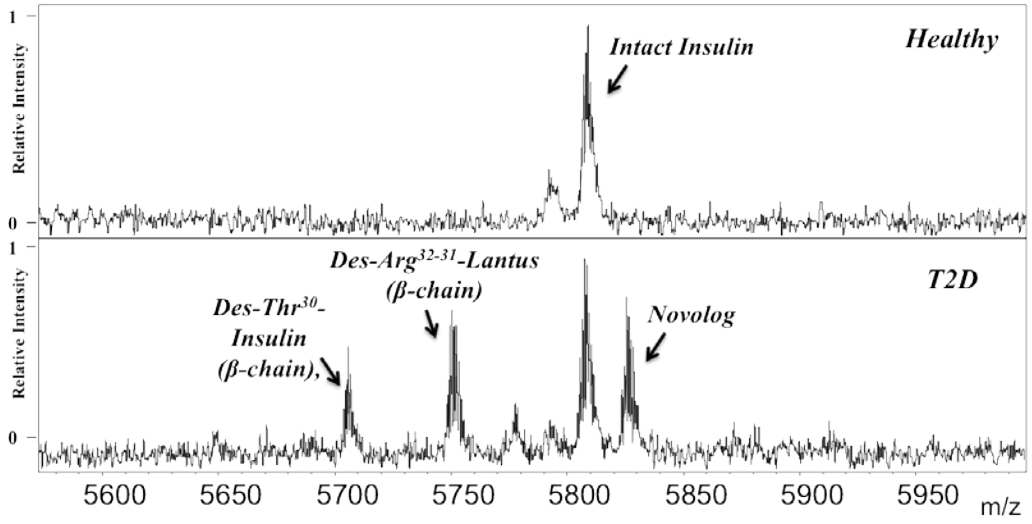

Figure 8: Comparison of representative Healthy versus T2D insulin MSIA spectra.

The research described here was designed to operate as a precursor to future, large-population based studies. In this manner, hundreds of samples (and eventually thousands) will be screened to establish the natural variation of insulin molecules in the general population. (Using the MSIA technology, a single mass spectrometer, and a single robotic pipette station, it takes 2 hours to generate data per 96-well sample plate. Accordingly, 480 data points can be acquired in each sample run resulting from the analysis of the 5 distinct insulin isoforms mentioned in this study. Using conventional methods (e.g. ELISA), five distinct assays would be required to capture the same information content and would take significantly longer.) Accordingly, due to the choice of analysis by MALDI-TOF-MS, an *open m/z window* surrounding intact insulin in every acquired spectrum may provide the opportunity for unreported variations of the molecule to reveal themselves when larger populations are scrutinized. In this framework, new

isoforms and perhaps the isoforms discussed here (e.g. metabolic products, des-thr^{30}-insulin (β-chain); proinsulin byproducts) may engender clinical utility in the form of biomarkers. Such clinically applied insulin heterogeneity would be exciting considering the preexisting scope of the molecule's history including its discovery ninety years ago (90) and well-established biology.

Chapter 5

INSULIN AND C-PEPTIDE MASS SPECTROMETRIC IMMUNOASSAY DEVELOPMENTS

In our previous mass spectrometric immunoassay (MSIA) population screenings for Insulin and separately, C-peptide (20, 91), we detected a total of nine endogenous and exogenous (i.e. therapeutic) variants found in plasma: C-peptide (1-31), C-peptide (2-31), C-peptide (3-31), C-peptide (4-31), Intact Insulin, Insulin Des (B30), Lantus, Lantus Des (B32-21), and Novalog. In particular, C-peptide (3-31) was discovered and shown be associated with diabetes. Serving to present recent assay efforts towards unifying these two assays, here we report the development of a quantitative *multiplexed* mass spectrometric immunoassay (MSIA) that offers monoisotopic MALDI-TOF-MS of all reported insulin and C-peptide variants. The assay is based on a two-antibody system that simultaneously targets C-peptide and insulin and their respective variants and internal standards, and is intrinsically capable of detecting any additional variants that may surface in future large-scale population screenings. Herein, we describe the quantification specifications of the multiplexed assay, example quantification data from human samples, and oral-glucose tolerance test (OGTT) results from two health human samples. Notably, multiple-protein and variant quantification is considered beyond what is technically feasible with conventional assay approaches (e.g. ELISA). Lastly, when the assay is applied in MS/MS mode, a novel way to quantify proteins using MALDI is achieved. Using this methodology, a higher

degree of specificity is realized by simultaneously monitoring daughter ions resulting from single intact parent molecules (e.g. daughter ions from C-peptide (1-31)) and it's respective internal standard: heavy C-peptide (1-31)). As such, this work establishes a foundation for the qualitative and quantitative analysis of intact, low-abundant, protein and/or peptide isoforms via simultaneous detection using MSIA.

EXPERIMENTAL

Of note, this experimental section closely follows the two prerequisite population studies (16, 20).

STUDY SUBJECTS, SAMPLE COLLECTION AND PREPARATION

CDI (1,1'-Carbonyldiimidazole)-activated affinity pipette tips were prepared and derivatized with mouse anti-human C-peptide and Insulin antibody (AbD Serotec), as previously described (20, 91), with the exception that both antibodies were mixed at a ratio 1:2, respectively. For the development of the assay, healthy human female plasma was purchased from ProMedDx (Norton, MA). Five hundred microliters of human plasma was pre-treated with 250 µL of a solution containing: 4.5 % Tween 20, 150mM Octyl-β-glucopyranoside, 1.5M Ammonium Acetate, and Concentrated PBS (0.67M sodium phosphate, 1M sodium chloride), for a total analytical volume of 0.75 mL.

SAMPLES

All samples used for quantification were fortified with 150 pM porcine insulin (which served as the internal standard), 100 pM heavy C-peptide (1-31), and 1 nM heavy C-peptide (3-31), prior to extraction of endogenous human insulin and C-peptide. “Heavy” refers to heavy-isotope peptides manufactured using C13 modified leucine residues (received as a gift from Thermofisher Scientific). Samples used in the generation of insulin standard curves were prepared and assayed using sheep plasma diluted 4x in 30 g/L BSA in HBS-N (0.01M HEPES and 0.15M NaCl). The curves were prepared (via serial dilution) with an insulin concentration range of 15 pM to 1.92 nM, a C-peptide concentration range from 117 pM to 15 nM, and a C-peptide (3-31) concentration range from 47 pM to 3 nM. The curves had 9 concentration points in total, including the blank samples with only internal standard. For insulin and C-peptide quantification out of human samples, six EDTA plasma samples and two OGTT sample sets from healthy volunteers were run in parallel with a standard curve. Regarding the OGTT sample sets, the two individuals were healthy males of Asian ancestry with no reported history diabetes mellitus between the ages of 25 and 60. Patients were subjected to an OGTT wherein samples were collected at different time points (0, 30, 60, 90 and 120 min) after a 75g oral glucose load (with the exception of the time point zero occurring immediately prior to ingestion).

PLASMA MASS SPECTROMETRIC IMMUNOASSAYS

C-peptide and Insulin were extracted with the aid of a Beckman Multimek 96 pipetting robot by repeatedly (250 repetitions) drawing and expelling (back into the analytical volume) 125 µL aliquots of the analytical volume through an anti-C-peptide/Insulin affinity pipette. After extraction, the pipettes were rinsed using PBS (0.1M sodium phosphate, 0.15M sodium chloride, pH 7.2), HBS-P (0.01M HEPES, 0.15M NaCl, 0.05% v/v Surfactant P20, pH 7.4), H_2O, 100mM Tris(hydroxymethyl)aminomethane hydrochloride (pH 4.6), and H_2O (in this order, each rinse = 10 repetitions of 150 µL), after which C-peptide and Insulin were eluted and prepared for MALDI-TOF MS by drawing 4 µL of MALDI matrix solution (saturated aqueous solution of sinapic acid, in 33% (v/v) acetonitrile, 0.45% (v/v) trifluoroacetic acid, TFA) into the pipette and depositing onto a MALDI target

MASS SPECTROMETRY

When exclusively analyzing C-peptide, MALDI-TOF MS was performed using a Bruker Ultraflex MALDI-TOF instrument operating in the negative ion, delayed-extraction mode; reflector engaged with ‘ion source 1’ at 20.00 kV, ‘ion source 2’ at 17.45 kV, lens at 7.50 kV, ‘reflector’ at 21.00 kV, ‘reflector 2’ at 10.95, 60 ns delayed extraction, deflection signal suppression up to *m/z* 1500, and 2 GS/s sample rate. Two hundred laser-shots were signal averaged for each mass spectrum. Single stage MALDI-TOF mass spectra were externally calibrated

with a mixture of 6 peptides supplied by Bruker (Cat. No. 208241) ranging in monoisotopic *m/z* from 1044.53 (Angiotensin II $[M-H]^-$) to 3145.46 (Somatostatin $[M-H]^-$). When analyzing both C-peptide and Insulin simultaneously, the instrument was used in both linear mode and with reflector engaged. In the former, positive ion, delayed-extraction mode was used with 'ion source 1' at 25.00 kV, 'ion source 2' at 23.50 kV, lens at 6.00 kV, 50 ns delayed extraction, deflection signal suppression up to *m/z* 2500, and 1 GS/s sample rate. When the reflector was engaged, the instrument operated in the positive ion, delayed-extraction mode with 'ion source 1' at 25.00 kV, 'ion source 2' at 21.90 kV, lens at 9.50 kV, 'reflector' at 26.30 kV, 'reflector 2' at 13.80, 190 ns delayed extraction, deflection signal suppression up to *m/z* 2000, and 2 GHz sampling rate. At least 10 thousand laser-shots were signal averaged for each mass spectrum to ensure good ion counting statistics. In linear mode, spectra were externally calibrated with a mixture of 4 proteins, supplied by Bruker (Cat. No. 208241), ranging from *m/z* 5734.52 (Insulin $[M+H]^+$ to *m/z* 12,360.97 (Cytochrome C $[M+H]^+$. When in reflector mode, MALDI-TOF-MS mass spectra were externally calibrated with a mixture of peptides and proteins supplied by Bruker including: *m/z* 2093.086 (ACTH_clip(1-17) $[M+H]^+$; monoisotopic), *m/z* 3147.471 (Somatostatin $[M+H]^+$; monoisotopic), *m/z* 5730.609 (Bovine Insulin $[M+H]^+$; monoisotopic), and *m/z* 6179.67 (Cytochrome C $[M+2H]^{2+}$; most abundant isotope).

DATA PROCESSING

Individual mass spectra were baseline subtracted and smoothed prior to peak integration. Peaks representing the five most abundant C-peptide and C-peptide-variant isotopes were integrated and tabulated in a spreadsheet for quantification. All peaks representing porcine insulin, intact insulin, and insulin variants were integrated baseline-to-baseline and tabulated in a spreadsheet for quantification. For MS/MS quantification of C-peptide, S/N values were used for quantification.

QUANTIFICATION VIA TANDEM MASS SPECTROMETRY

LIFT-TOF/TOF mass spectra of C-peptide (1-31) and heavy C-peptide (1-31) from working curve samples were acquired on a Bruker Ultraflex MALDI-TOF/TOF instrument in positive ion mode using sinapic acid as a matrix. Precursor ions were selected within a 15 Da mass window. At least 20 thousand laser-shots were signal averaged for each mass spectrum to ensure good ion counting statistics. The LIFT-TOF/TOF instrument control method was calibrated according to the instrument manufacturer's protocol and was run without CID gas.

RESULTS AND DISCUSSION

The assay is based on a two-antibody system that simultaneously targets C-peptide and insulin and their respective variants and internal standards. **Figure 9** shows the results of the multiplexed MSIA performed in order to evaluate performance when applied to human plasma (without benefit of added internal

standards). Excellent signal to noise was observed for the endogenous wild-type C-peptide and insulin. Non-specific binding was minimal, and the regions around both C-peptide and insulin were relatively clear of other species, which allowed for the detection of mass-shifted variants – i.e., both endogenous and exogenous (insulin-based therapeutics). Using the (non-internal standard) assay in previous

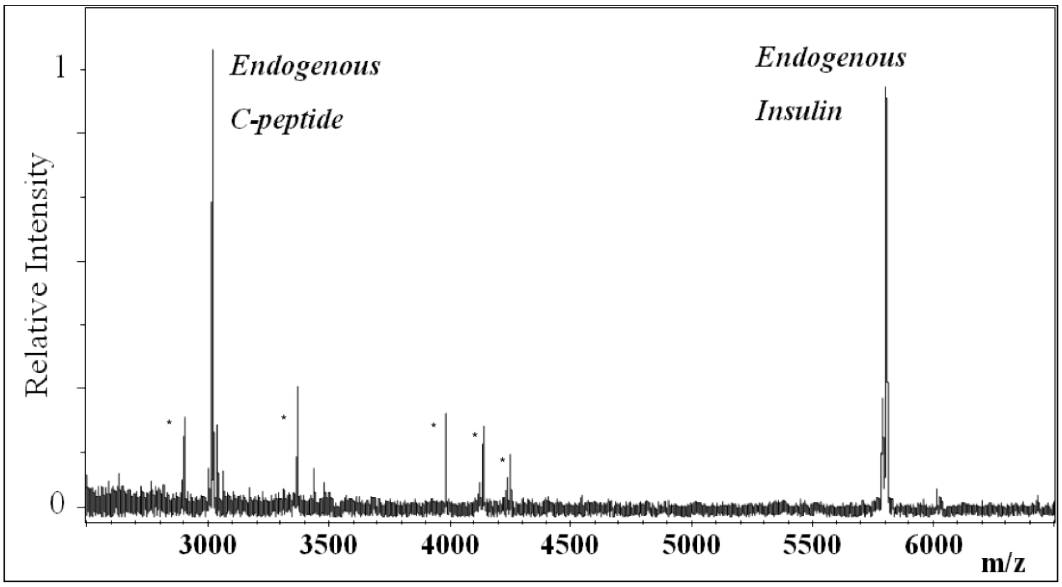

Figure 9: Multiplexed C-peptide and Insulin spectrum. Multiplexed C-peptide (observed 3019.91 m/z, theoretical 3019.521) and insulin (observed 5804.65 m/z, theoretical 5804.65 m/z) MSIA performed in order to evaluate performance when applied to human plasma. * Denotes non-specific binding.

qualitative population screenings (n = 108) (20, 91), a total of nine variants related to C-peptide and insulin were observed [C-peptide (1-31), C-peptide (2-31), C-peptide (3-31), C-peptide (4-31), Intact Insulin, Insulin Des (B30), Lantus, Lantus Des (B32-21), and Novalog]. Other than cataloging variants, this exercise scrutinized the mass ranges surrounding the wild-type species so that internal standards could be judiciously chosen so not to interfere with the quantification of the plasma-borne variants. Notably, C-peptide (3-31) is a particular isoform that we previously discovered and found associated to diabetes (91). This variant likely has implications for diabetic therapeutics, as we hypothesized it is produced via the truncation of intact C-peptide (1-31) via Dipeptidyl Peptidase-4 (DPP-IV), an enzyme responsible for regulating glucose metabolism (40, 67, 92). Insulin (20), C-peptide (1-31), and the newly discovered C-peptide (3-31) were quantified. **Figure 10** shows the results of both C-peptide variants and their respective heavy-isotope internal standards being captured from plasma. Of note, the four C-peptide isoforms identified thus far were found to have an equal binding affinity in limit of detection experiments using purified recombinant standards (data not shown). Consequently, use of multiple internal standards for C-peptide isoform quantification may be superfluous when the assay is run in intact parent-ion quantification mode as apposed to MS/MS quantification mode, as explained below. The six health human samples assayed had insulin and C-peptide average concentrations of 37 ± 18 pM and 1.7 ± 0.56 nM, respectively.

Lower limits of detection of the multiplexed assay ranged from 1 – 12.5 pM, dependent on the variant. Quantitative standard curves for intact insulin and C-peptide (and variants) exhibited good dynamic range and linearity (dynamic range = 1000, average R^2 for three consecutive days of analysis = 0.99). Limits of quantification ranged from 15pM - 15nM. **Figure 11** presents an example working curve for C-peptide (3-31) with actual spectra representing a set of points comprising the working curve.

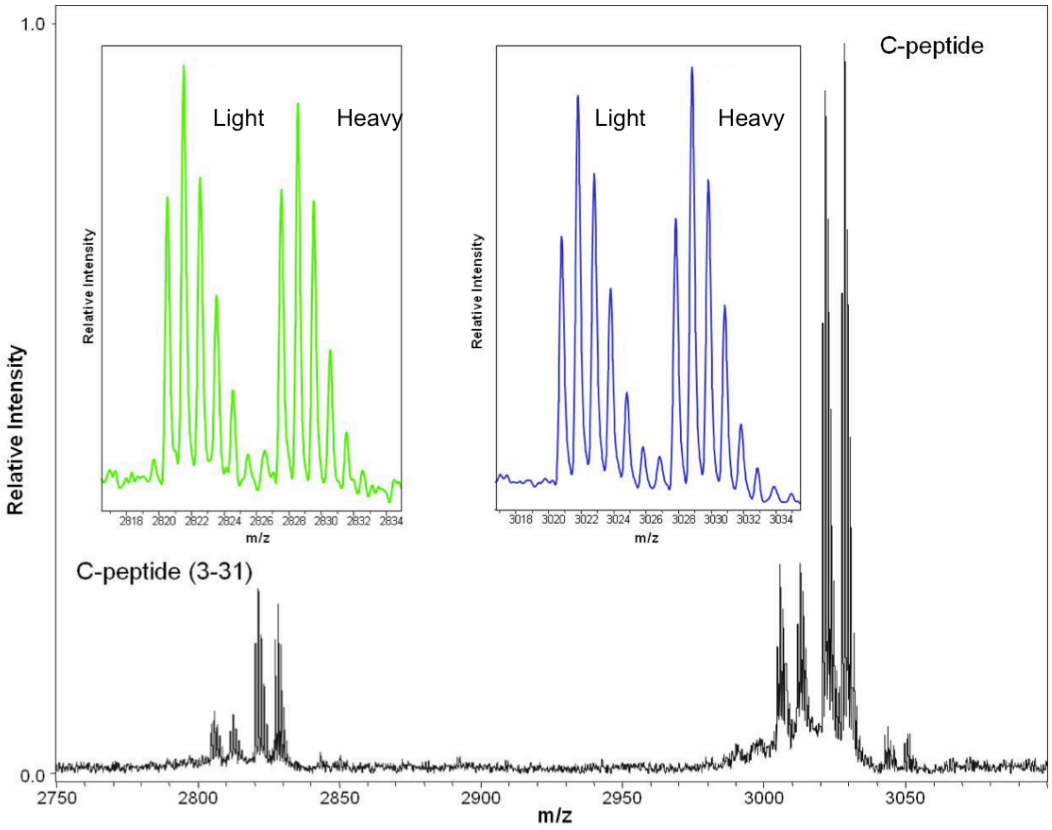

Figure 10: Dual-capture of light and heavy C-peptide variant standards. C-peptide (1-31) (observed 3017.51 m/z, theoretical 3017.51 m/z) and C-peptide (3-31) (observed 2817.45 m/z, theoretical 2817.45 m/z) variants and their respective heavy-isotope internal standards captured from plasma (observed 3024.52, theoretical 3024.46 m/z; observed 2824.46, theoretical 2824.40 m/z, respectively) being captured from plasma.

The assay was subsequently applied to two sets of OGTT samples (representing two individuals) in five thirty-minute intervals (**Figure 12**). An OGTT is clinical test whereby an individual ingests 75 grams of glucose with concurrent sample collection across multiple time points (with time point zero representing the moment before ingestion). The intent is to monitor for the clearance of glucose from the blood stream and ultimately for the presence of diabetes (i.e. high basal glucose levels).

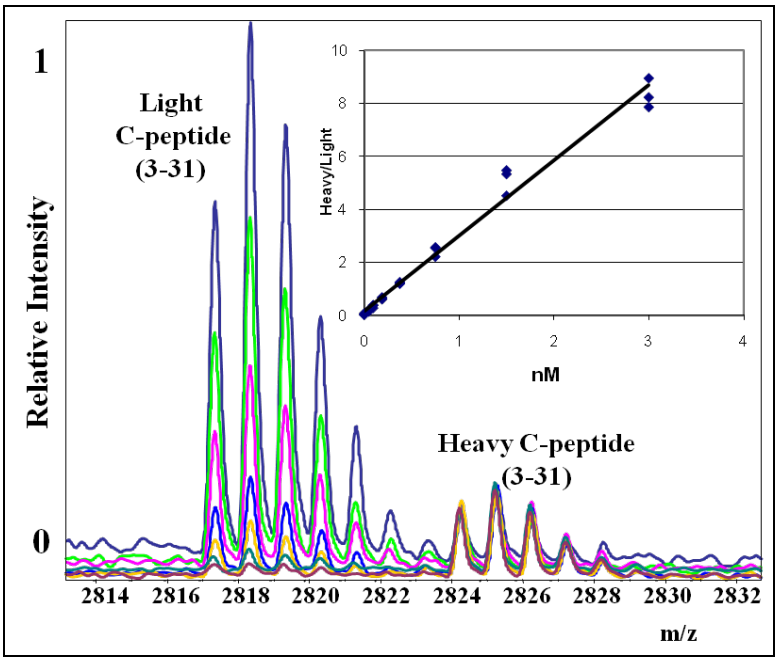

Figure 11. C-peptide (3-31) quantitation. The working curve for truncated c-peptide (c-peptide (3-31) and overlaid MALDI spectra for each point on the line ($R^2 = 0.99$).

As one might expect, certain variations of this test also include monitoring for insulin and C-peptide (93). We thought it would be of clinical relevance to

monitor insulin and C-peptide and any respective isoforms. Of note, the samples were captured using Bd P800 collection tubes (94) which contain a proprietary inhibitor cocktail. These tubes are used to prevent the degradation of endocrine hormones responsible for glucose metabolism (of note, DPP-IV is a key enzyme targeted). The two subjects were healthy males of Asian ancestry between the ages of 25-60. Both subjects displayed ordinarily observed OGTT trends, which include an insulin and C-peptide spike in response to the ingested glucose followed by a steady decrease. However, subject 2 displayed a delayed response with substantial increases in insulin and C-peptide release, with still-heightened levels towards the conclusion of the test. Previous studies have shown age influences the results of this test (93), and as such, we hypothesize subject 2 was older and than subject 1. Likely due as a result of the inhibitor cocktail, C-peptide (3-31) was not observed in any samples, which again, we suspect is an enzymatic product generated by DPP-IV. Interestingly, C-peptide (4-41) was detected in both samples and demonstrated a similar trend as observed with C-peptide and insulin.

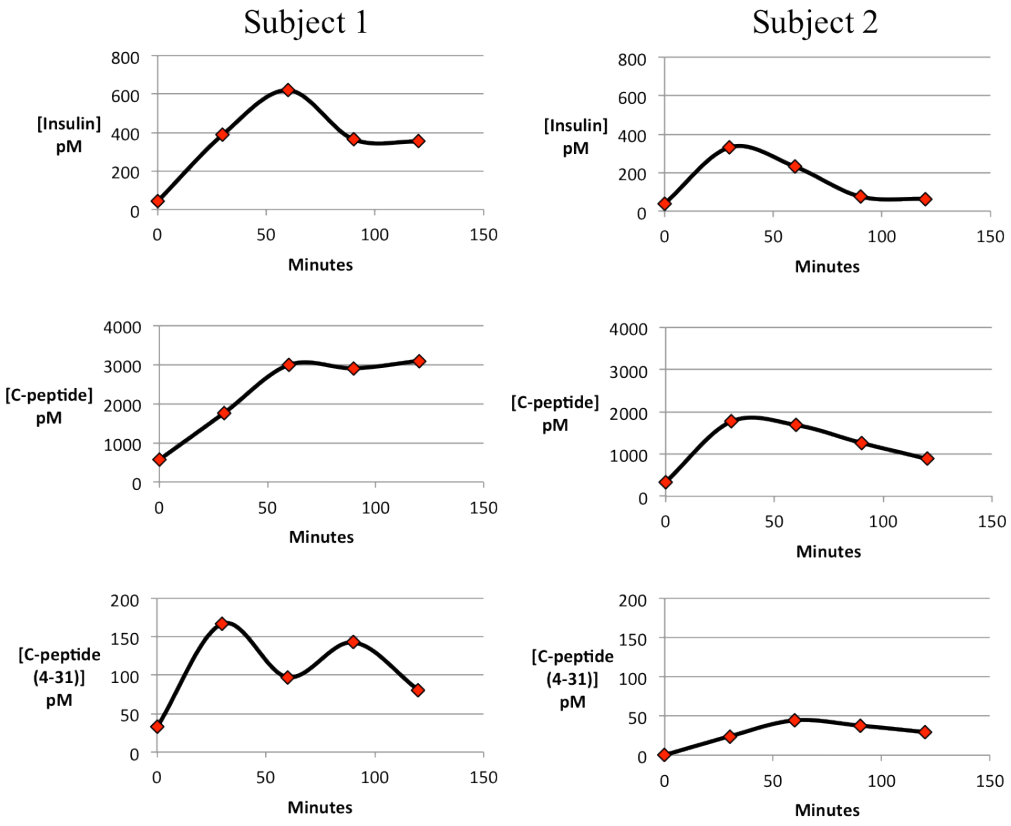

Figure 12: Oral glucose tolerance test results for two healthy individuals. Intact insulin, C-peptide (1-31), C-peptide (4-31) were quantified at five time points over a timespan of 120 minutes.

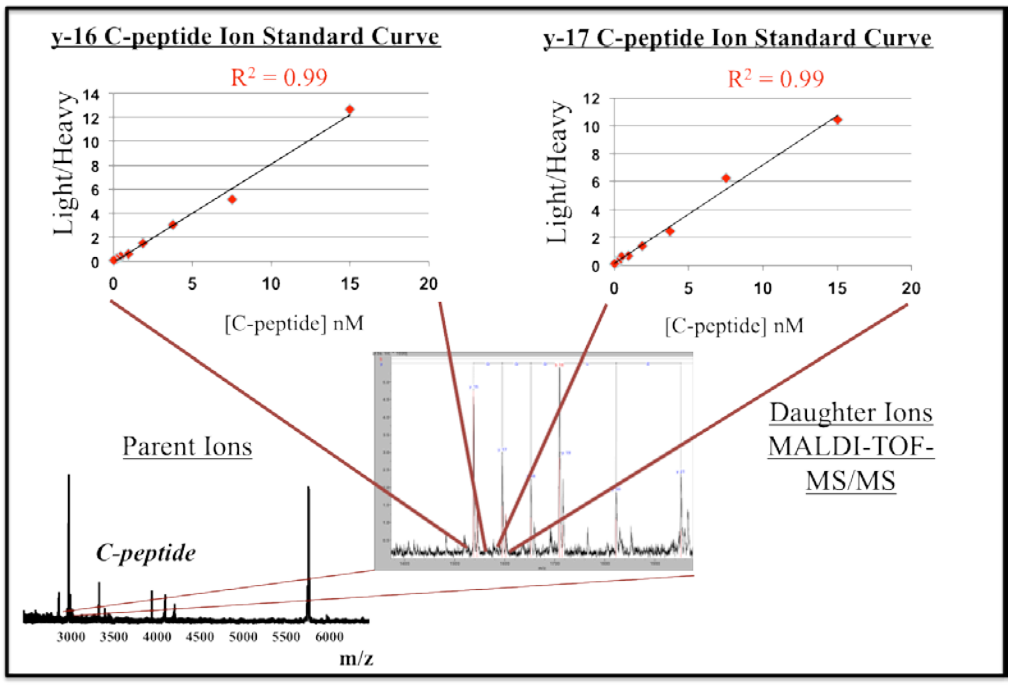

Figure 13: MALDI-TOF/TOF (MS/MS) quantitative working curves. In this figure the y-16 and y-17 working curves are presented with $R^2 = 0.99$ for both curves. Notably, these y-ions shift for discovered C-peptide variants (e.g. C-peptide 3-31). The sequence of human C-peptide is H_2N-EAEDLQVGQVELGGGPGAGSLQPLALEGSLQ-CO_2H.

Figure 13 introduces preliminary data on a novel way to quantify proteins and peptides using MALDI-TOF/TOF (MS/MS). This approach is akin to the Multiple Reaction Monitoring (MRM) mass spectrometric technique whereby a protonated peptide undergoes multiple stages of separation within a triple quadruple mass spectrometer, ultimately becoming fragmented and detected via the unique daughter-ions signatures. As presented here, the MALDI-TOF/TOF (MS/MS) precursor selection window is set wide enough to allow the native protein and/or peptide and the corresponding internal standard to enter the flight-

tube and become fragmented simultaneously. In the illustrated example, C-peptide is quantified at physiological concentrations via two separate working curves: the y-16 C-peptide ion and the y-17 C-peptide ion. Both ions exhibited good linearity (R^2 = 99). To the best of our knowledge, this form of quantification using MALDI has not been presented in the literature. Although this approach to MALD quantification may be viewed as extraneous if one acknowledges the specificity imparted by the antibody, the relatively high resolution (e.g. 15,000 for insulin; m/Δm; FWHM), and the lack of interference shown by control experiments, it's conceivable that certain clinical applications may require higher degree of assay specificity as a precautionary measure (e.g. 1 out of 500 patients have a blood-borne a non-specific protein that interferes with the assay). For example, if an interfering signal registering at 3017.50 m/z (the mono-isotopic molecular weight of C-peptide (1-31) in negative-ion mode) was proven to be non-specific, this could be bypassed by quantifying via C-peptide daughter-ions (notably, we have found no evidence of assay inference for insulin or C-peptide). As an added benefit to using this approach, suppression effects should to be substantially diminished which allow for increased sensitivity. Although only one protein or peptide can be quantified per laser shot fired, future iterations of MALDI-TOF are suspected to be capable of monitoring many proteins simultaneous, akin to a triple-quadruple but with full-scan and high m/z proficiencies inherent with MALDI-TOF.

Future studies will be focused on establishing the physiological quantification range of endogenous insulin and C-peptide metabolites with the use of thousands of samples within the context of diabetes and related diseases.

Chapter 6

INTRAPERSONAL AND POPULATIONAL HETEROGENEITY OF THE CHEMOKINE RANTES

Chemokines are essential to the initiation and maintenance of inflammation. They perform their duty via the mechanisms of chemotaxis whereby leukocytes are attracted to higher gradients of chemokines. More than forty chemokines and twenty chemokine receptors have been identified. The chemokine superfamily is broken up into four main groups (C, CC, CXC, and CX3C); this is based upon the position of the first two cysteine residues in a conserved four-cysteine motif found pervasively among chemokines (RANTES is a CC chemokine, hence its alternative name: *CC*L5) (95). The receptors are G-protein coupled, seven-transmembrane receptors named accordingly to the class of chemokine they bind (e.g. RANTES/CCL5 binds to the CCRX receptor subset) (96). Proinflammatory chemokine receptors tend to have less discriminative ligand binding specificities whereas receptors involved in normal leukocyte trafficking have higher specificities (96-98). RANTES (which stands for Regulated on Activation, Normal T cell Expressed and Secreted) binds to CCR1, CCR3, CCR5, and DARC receptors and correspondingly has an integral role in inflammation, cell recruitment, and T cell activation. RANTES can be released from multiple sources, including activated T lymphocytes and monocytes/macrophages, epithelial cells, bronchial epithelium, and dermal fibroblast and renal tubular epithelium (99). The native-wild type is composed of 68 amino acids and has a

molecular weight of 7847 Da with both disulfide bonds intact (notably, the signal-containing protein is 91 a.a. in size). To date, there are two well-established RANTES variants: truncated versions comprised of residues [3-68] and [4-68]. These variants are the products of two separate regulatory enzymes (Dipeptidyl Peptidase IV and Cathepsin G, respectively) and have modified chemotactic and antiviral functionality compared to that of intact RANTES (100, 101). Furthermore, there is evidence that an O-linked glycosylated RANTES variant may exist (102). Consequently, research concerned with RANTES, which was discovered in 1988 via a cDNA study of T-cells (103), has in a short amount of time begun to unravel a molecule of depth that appears to be connected to an array of pathophysiological conditions that arise in humans.

The clinical significance of RANTES is considerable as it has been associated with many diseases including kidney related complications (e.g. renal failure and renal cancer), autoimmune diseases (e.g. arthritis, diabetes, and glomerulonephritis), sepsis-induced disseminated intravascular coagulation in infants, and several forms of carcinoma including breast and cervical cancer (99, 104-106). Indeed, plasma RANTES concentrations have been found increased in order of cancer stage (I, II, III, or IV) (99). Furthermore, a large population study found RANTES in higher plasma concentrations in subjects with Type 2 diabetes and impaired glucose tolerance (IGT) relative to healthy controls (107). Concerning its role in viral disease, RANTES was discovered to be an effective antiviral agent that restricts the entry of CCR5-tropic HIV-1 strains by means of

the CCR5 receptor (100). The 3-68 variant form of RANTES was subsequently found to also inhibit HIV to the same degree but lacked the same binding affinity to the CCR1 receptor. Thus, the impact of RANTES microheterogeneity in biological systems stands to be as important as its quantitative fluctuation.

Commercially available RANTES assays exist widely as enzyme-linked immunosorbent assays (ELISAs) and appear to be the primary tool for non-variant-specific quantification of plasma RANTES in disease-related studies (99, 108, 109). For reference, one such assay has a sensitivity of 2 ng/L, a measuring range of 31.2-2000 ng/L, and intra-assay and inter-assay coefficient of variations (CV) of 3.6% and 10.3%, respectively (109). Healthy circulating plasma concentrations appear to be around 3 μg/L (99). The ELISA approach lacks the intrinsic ability to differentiate between wild-type and variant forms of RANTES. The consideration of microheterogeneity, however, may help to explain potential measurement discrepancies found between assays. This additional element of multiplexed variant detectability enables a view of the genetic and posttranslational variants of proteins, which may have significant diagnostic value in personalized medicine. Indeed, McIntosh writes “Researchers should be encouraged to evaluate and report as a secondary or even primary analysis the natural variation of the proteome in the clinical biosamples they analyze ” (110).

Thus, future quantitative studies of RANTES stand to benefit from a more complete survey of qualitatively different variants of RANTES as they exist in healthy and diseased populations. Toward this end, this report focuses on

mapping the structural differences of RANTES found in a variety of diseases. As a result it provides an alternative qualitative and semi-quantitative method for high throughput population-based analysis of RANTES and may assist in the expanding our understanding of this molecule's complex nature in biological systems.

EXPERIMENTAL

STUDY SUBJECTS, SAMPLE COLLECTION AND PREPARATION

CDI (1,1'-Carbonyldiimidazole)-activated affinity pipette tips were prepared and derivatized with mouse monoclonal anti-human RANTES antibody (R&D Systems), as previously described for other antibodies (23). For the development of the assay, bulk healthy human female plasma from a healthy donor was used. Two hundred and thirty nine additional human samples were acquired under IRB approval and grouped into non-overlapping cohorts as follows: 37 healthy individuals (plasma), 29 healthy individuals (serum), 50 type 2 diabetics (T2D) (plasma), 25 individuals with congestive heart failure (CHF) and T2D (plasma), 17 individuals with CHF, a history of myocardial infarction (hMI), and T2D (plasma), 25 individuals with CHF and hMI (plasma), 29 individuals with only CHF (plasma), and 27 individuals with cancer (prostate, breast, and colon cancer; plasma). In all plasma samples EDTA was used as the anticoagulant. Cohorts were age and sex matched. Two hundred and thirty microliters of human plasma was pre-treated with 115 µL of a detergent solution containing: 4.5 % Tween 20,

150mM Octyl-β-glucopyranoside, 1.5M Ammonium Acetate, and concentrated PBS (0.67M sodium phosphate, 1M sodium chloride), for a total analytical volume of 345 µL. Negative control MSIA tips were immobilized with monoclonal anti-human C-peptide and Insulin antibody (AbD Serotec).

PLASMA MASS SPECTROMETRIC IMMUNOASSAYS

RANTES was extracted with the aid of a Beckman Multimek 96 pipetting robot by repeatedly (500 repetitions) drawing and expelling (back into the analytical volume) 125 µL aliquots of the analytical volume through an anti-RANTES affinity pipette. After extraction, the pipettes were rinsed using HBS-P (0.01M HEPES, 0.15M NaCl, 0.05% v/v Surfactant P20, pH 7.4), H_2O, 100mM Tris(hydroxymethyl)aminomethane hydrochloride (pH 4.6), and H_2O (in this order, each rinse = 10 repetitions of 150 µL), after which RANTES was eluted and prepared for MALDI-TOF MS by drawing 4 µL of MALDI matrix solution (saturated aqueous solution of sinapic acid, 33% (v/v) acetonitrile, 0.45% (v/v) trifluoroacetic acid, TFA) into the pipette and depositing onto a MALDI target.

MASS SPECTROMETRY

MALDI-TOF MS was performed using a Bruker Ultraflex III MALDI-TOF instrument operating in the positive ion, delayed-extraction mode; linear mode with ‘ion source 1’ at 25.00 kV, ‘ion source 2’ at 23.50 kV, lens at 6.00 kV, 50 ns delayed extraction, deflection signal suppression up to *m/z* 3000, and 1 GS/s sample rate. Single measurements were acquired, per individual, using twenty

thousand laser-shots signal averaged to ensure good ion counting statistics. Spectra were externally calibrated with a mixture of 4 proteins, supplied by Bruker (Cat. No. 208241), ranging from *m/z* 5734.52 (Insulin $[M+H]^+$) to *m/z* 12,360.97 (Cytochrome C $[M+H]^+$).

DATA PROCESSING

Individual mass spectra were baseline subtracted (Tophat algorithm) and smoothed (SavitzkyGolay algorithm; width = 0.2 m/z; cycles = 1) prior to peak integration using Bruker Daltonics flexAnalysis 3.0. Peaks representing intact RANTES and RANTES variants were integrated (using Intrinsic Bioprobes Inc. Zebra 1.0) and tabulated in a spreadsheet for determination of relative percent abundances.

DUAL EXTRACTION

RANTES was extracted as described above followed by elution into a new sample reservoir. This new reservoir was then extracted as if it were a plasma sample itself, generating a high purity sample with minimal non-specific protein binding and an exceptionally clean MALDI-TOF-MS spectrum of RANTES. The dual extraction was performed by extracting 20 tips using the normal sample preparation (with the exception of using 1 mL plasma and 500 µL detergent solution per sample) followed by MSIA tip elution with 7 µL of 33% (v/v) acetonitrile and 0.45% (v/v) TFA into an eppendorf tube containing 1 mL HBS-N (0.01M HEPES and 0.15M NaCl) and 10 µL of 3.9 g/L prealbumin antibody

(DAKO). The antibody was used as a carrier protein. This enriched sample was subsequently extracted using a new anti-RANTES affinity pipette and eluted using the same methodology as previously described. The process was repeated exactly using anti-human insulin antibody immobilized tips to serve as a negative control.

RESULTS AND DISCUSSION

Figure 14 shows a MSIA spectrum that is qualitatively representative of those obtained for the individuals investigated in this study (note: spectrum is a resized version of that seen in Panel B of **Figure 15**). Along with intact RANTES, the following variants were identified: two N-terminally truncated forms (maroon; II and III), one C-terminally truncated form (pink; V), seven C- and N-terminally truncated forms (blue; IV, VI, VIII, and X-XIII), glycated forms representing intact and [3-68] (purple; VIII and XIV), oxidized forms (+16 m/z, unlabeled), and four glycosylated forms (green; XVI-XIX) (see **Figure 14** and **Table 4**), for a total of at least 19 variants. After fine-tuning to ensure that all MS signals were specific to RANTES via a dual extraction (described below), the ions represented in Fig. 14 were tentatively mass mapped. Most of these peaks were found in the majority of the samples. With regards to specificity of peak assignments, this type of technique may be viewed as analogous to an ultra-high resolution western blot that is performed hundreds of times with consistent results. Notably, peaks I-XIX were not observed in control experiments using blank tips (no antibody

immobilized), anti-human C-peptide MSIA tips (single extraction), and anti-human Insulin MSIA tips (single and dual extraction).

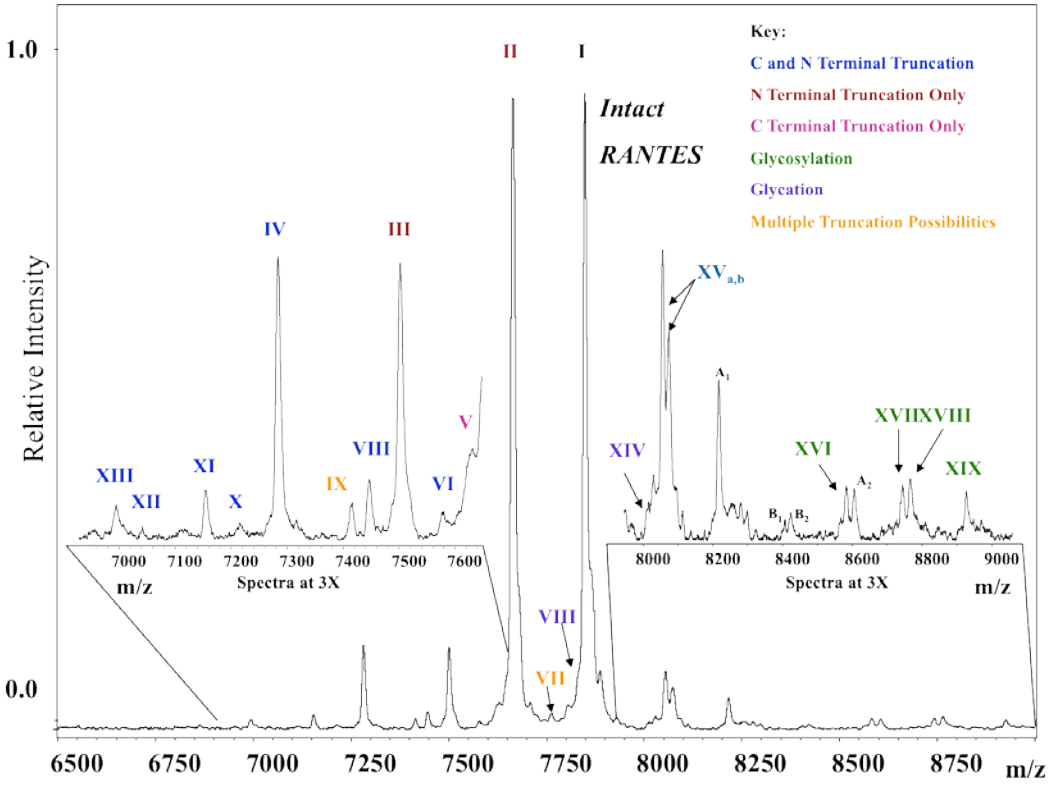

Figure 14: Mass spectrum resulting from the targeted top-down analysis of RANTES. Indicated are signals from the ~19 major protein isoforms. Isoforms fall into six categories: C- and N-terminal truncation, N-terminal truncation only, C-terminal truncation only, multiple truncation possibilities (due to identical masses), glycosylation, and glycation. Table 1 lists the identities of each variant. A_1 and A_2 denote signals that appeared in negative control experiments and therefore may not be related to RANTES (8215.4 m/z and 8603.5 m/z). B_1 and B_2 denote signals that may be related to RANTES but are unknown (8404.28 m/z and 8421.33 m/z).

Table 4 RANTES variants evident in human plasma[a]			
Isoforms	**Observed $[M+H]^+$**	**Theoretical $[M+H]^+$**	**Identity**
Intact			
I	7848.0	7848.0	[1-68]
C and N Terminal Truncation			
VI	7576.3	7576.7	[3-67]
VIII	7445.1	7445.5	[3-66]
IV	7282.2	7282.3	[4-66]
X	7213.4	7213.3	[2-63]
XI	7153.0	7153.2	[4-65]
XII	7039.9	7040.1	[4-64]
XIII	6992.9	6993.1	[7-66]
N Terminal Truncation Only			
II	7663.8	7663.8	[3-68]
III	7500.6	7500.6	[4-68]
C Terminal Truncation Only			
V	7629.4	7629.7	[1-66]
Multiple Truncation Possibilities			
IX	7413.3	7413.5	[2-65], [4-67], or [5-68]
VII	7761.6	7760.9	[1-67] or [2-68]
Glycation			
VII	7826.4	7825.9	[3-68] + Hex
XIV	8010.6	8010.1	[1-68] + Hex
Glycosylation			
XVI	8580.6	8581.7	[3-68] + $(Hex)_1(HexNAc)_3(Deoxyhex)_1$
XVII	8741.8	8743.8	[3-68] + $(Hex)_2(HexNAc)_3(Deoxyhex)_1$
XVIII	8764.5	8765.9	[1-68] + $(Hex)_1(HexNAc)_3(Deoxyhex)_1$
XIX	8925.2	8928.0	[1-68] + $(Hex)_2(HexNAc)_3(Deoxyhex)_1$
Oxidation			
Unlabeled	7679.4	7679.8	[3-68] + oxidation
Unlabeled	7863.8	7864.0	[1-68] + oxidation
Matrix Adducts			
XV_a	8054.1	8054.2	[1-68] + Sinapic acid
XV_b	8071.9	8072.2	[1-68] + Sinapic acid
[a] Roman numerals correspond to labeled peaks in Fig. 14.			

To ensure accurate mass mapping assignments, the development of a secondary extraction process (*dual extraction*) was designed to support the removal of nonspecifically bound proteins and to create an exemplar full-scan spectral view of endogenous RANTES microheterogeneity in humans. Typically, one MSIA affinity pipette is used to extract a protein from a single plasma sample, which is then rinsed and immediately eluted. Here we eluted many affinity pipettes from pooled human plasma into a single buffered solution to create a sample with much lower non-specific protein concentrations and

significantly higher RANTES concentration. This consequently created a vastly cleaner MSIA MALDI-TOF-MS spectrum with amplified signals corresponding to the weakest endogenous RANTES species present within humans (see **Figure 15**).

Relative percent abundance (RPA) values of isoforms can be obtained after integrating all mass spectral peak areas (previously determined by a verified protein variant map, e.g. **Figure 14**), followed by dividing the peak area of each isoform by the summed areas of all isoforms and finally multiplying by one hundred. To test the reproducibility of this form of semi-quantification, a single sample was run 96 times (i.e. 96 MSIA tips extracted RANTES from same individual from 96 samples). In this test, RANTES variants [1-68], [3-68], [4-68], and [4-66] had RPA values ± standard deviations of 77.82 ± 0.53, 20.3 ± 0.49, 1.26 ± 0.07, and 0.62 ± 0.05. The range for these variants were observed to be 77.08 – 79.60 %, 18.67 – 20.97%, 1.08 – 1.43 %, and 0.51 – 0.76% respectively. After establishing a map of RANTES heterogeneity, individual classes of posttranslational modifications were scrutinized in more detail as follows.

TRUNCATION

RANTES was found consistently in a multitude of N- and C- terminally truncated forms (ten individual truncated isoforms were identified). The two previously known truncated variants, [3-68] (II) and [4-68] (III), are generated by two separate regulatory enzymes: DPP-IV and Cathepsin G (100, 101).

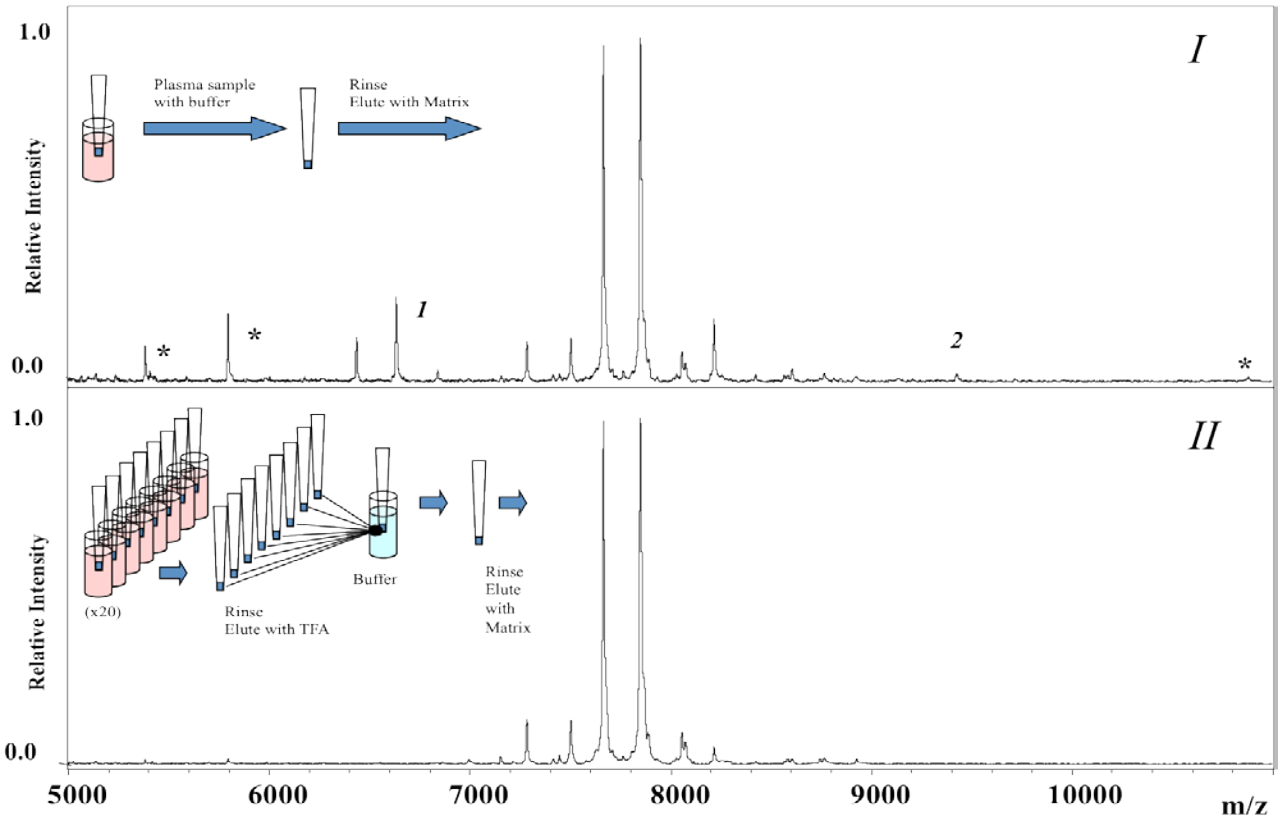

Figure 15: Dual extraction methodology. Mass spectra resulting from the targeted top-down analysis of RANTES from a healthy pooled plasma sample using a standard single MSIA extraction (I) and also after a dual MSIA extraction (II). Indicated are signals from the major nonspecific binding proteins (Apolipoprotein C1[1], Apolipoprotein C3[2], and unknown[*]).

RANTES, as with most chemokines, contains its receptor binding motif at the N-terminus, thus if truncation proceeds, modified chemotactic activity ensues. Therefore, the information content is twofold within such a multiplexed assay: indirectly, the enzymatic activity/expression *and* directly, the relative abundance of inactive and active protein variants. In this context, this is in the form of DPP-IV and Cathespsin G activity from the abundance of [3-68] and [4-68] *and* each individual's relative ability to induce and/or block signal transduction on target receptors (e.g. full length RANTES versus DPP-IV cleaved RANTES). As for the other eight alternate truncated forms of RANTES found here, the enzymatic activity they indirectly represent remains unknown. A decade ago, Proost et al reported on two related C-C chemokines, MCP-1 and MCP-2, and the discovery that they exist in several N- and/or C-terminally truncated forms with corresponding modified activity (111). Notably, they observed that N- truncated forms were almost completely devoid of activity but C-terminus-only truncated forms retained full activity. Furthermore, they observed a particular N- truncated form of MCP-2 to act as a natural inhibitor for MCP-2, MCP-1, and RANTES in regards to chemotactic activity. Proost also found an analogous case with RANTES [3-68] whereby they observed the variant to also act as a natural inhibitor against full length RANTES and as an effective antagonist of HIV entry into mononuclear cells (112). We expect these N-terminal truncated variants to be devoid of activity with increasing lack of receptor specificity the further the variant is truncated inward. Conversely, we expect the C-terminal truncations to

have little effect on biological activity. This may be superfluous in this case, however, because most of the C-truncated variants are also N-truncated. A case-in-point example regarding the imperative of acknowledging all truncated isoforms of a protein comes from the calcium regulatory protein Parathyroid Hormone (PTH). PTH exists in several embodiments including N- and/or C-truncations. PTH binds to two separate receptors, the classical receptor is specific for the amino terminus and an as-of-yet uncloned receptor on the carboxyl terminus, the two exerting opposite biological effects in modulating calcium concentrations (113, 114). Interestingly, PTH microheterogeneity had been studied for almost half a century but the possibility of a C-terminal receptor binding domain was assumed to not exist until very recently. We recently produced a multiplexed assay than can simultaneously distinguish between these active forms (26). Thus, it seems logical that additional assays stand to profit from the ability to unambiguously identify, in a multiplexed manner, an entire full length protein form. Conversely, as with most "biased" quantification proteomic approaches whereby only one or two surrogate peptides (resulting from a tryptic digest) are monitored to represent an entire set of protein variants as they exist endogenously, the degree of protein heterogeneity presented here would have been disguised and unacknowledged. This would have been true for *all* truncated forms if the surrogate peptide were chosen from a mid-region. Even if a surrogate peptide were chosen from a terminal region (e.g. to represent 3-68), the assay would still be blind to C-terminal truncation and the possibility of discovering

more variants. The MSIA analytical approach allows for the continual analysis of all of these variants.

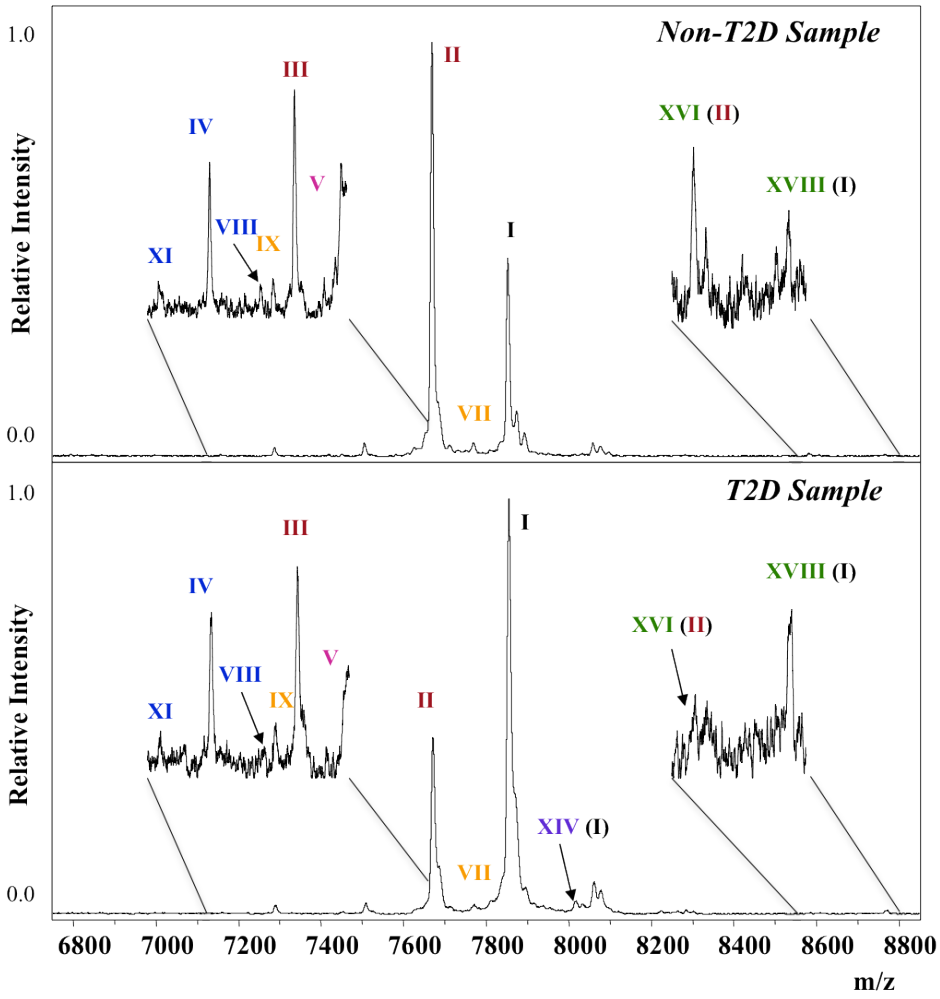

Figure 16: Mass spectra from a T2D individual and a non-T2D individual. Table 1 lists the identities of the individual variants. Note the correlation between the ratio of [1-68] (I) and [3-68] (II) to the ratio of XXII (I) to XIX (II) (both glycosylated with $Deoxyhex_1HexNAc_3Hex_1$). Also note the increase in glycation observed in the T2D sample.

GLYCOSYLATION AND GLYCATION

We mass mapped the presence of at least four putative O-linked glycosylated variants that appear to exist on both intact and truncated forms of RANTES (observable only on [1-68] and [3-68]; more were not detected corresponding to the other variants likely due to their already low relative abundance). A ladder like structure was observed reaching its largest potential at a mass of 8926.9 Da representing intact RANTES with $Deoxyhex_1HexNAc_3Hex_2$ (see **Figure 14** and **Table 4).** Importantly, the ratio of O-glycosylated ($Deoxyhex_1HexNAc_3Hex_1$) intact (XVIII) to O-glycosylated ($Deoxyhex_1HexNAc_3Hex_1$) [3-68] (XVI) was found to be conserved relative to the ratio of intact (I) and [3-68] (II) among essentially all samples in the population study, providing further verification of the mass mapping assignments (**Figure 16**). About two decades ago, Kameyoshi et al discovered a putative RANTES variant that possessed the same N-terminal sequence as intact RANTES yet had an increase in mass of approximately 500 mass units (full length intact protein was detected at 8355 ± 10 m/z). It was assumed to be an O-glycosylated variant due to the absence of edman degradation sequence information at a hypothesized dual serine O-glycosylation site (at residues 4 and 5). Interestingly, they observed that this variant retained similar eosinophil (Eo) chemotactic activity relative to the native form (102). This putative variant was not detected in this study. A few years later, Proost et al (in the same study mentioned previously (111)) found O-linked glycosylated variants of MCP-1 which had a 2-3 fold decrease in chemotactic function on monocytes

and human acute monocytic leukemia cell lines (THP-1) relative to intact MCP-1. Because of the structural relatedness between RANTES and MCP-1, it remains quite possible for RANTES O-linked glycosylation variants to have modified activity as well. Regardless, it is essential to be aware of RANTES in all of its structural embodiments.

The glycated signatures of [1-68] and [3-68] were detected in the majority of samples. Glycation is common among plasma proteins. To date, however, there do not appear to be any previous reports of RANTES glycation. As we previously demonstrated with Vitamin D binding protein (DBP) (21), significant population differences in DBP glycation levels between healthy, T2D, CVD, and Cancer were found to be common. Predictably, there is a markedly high increase in glycation in the Diabetic and Cancer samples studied here. **Figure 16** displays the RANTES spectrum of a non-T2D (CVD) patient compared to that of a T2D patient. A glycation peak is observed in the T2D spectrum labeled XIV (I) but this peak is absent in the non-T2D spectrum. Several population trends such as this were encountered (**Figures 17-20**).

POPULATION STUDY

Figures 17-20 represent a population of ~250 individuals in different states of health and the diversity of RANTES found therein. The relative abundance for several distinct categories of RANTES heterogeneity is presented. Significant RPA differences were observed between all disease cohorts. The subsequent figures compare the relative abundance of [1-68] and [3-68] (**Figure 17**),

Oxidation (**Figure 18**), Glycation (**Figure 19**), and [4-66], [3-66], [3-67], and [1-66] (**Figure 20**) across all of the disease states. Obvious variation in RANTES profiles begin to emerge in this larger context .

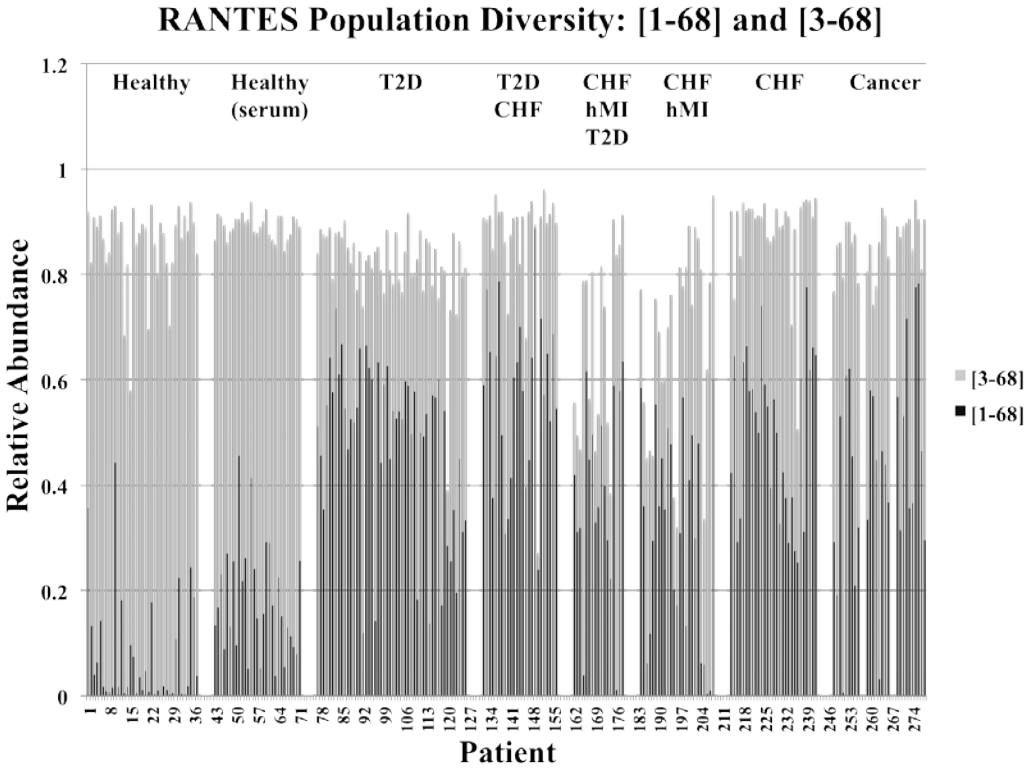

Figure 17: Stacked bar plot population data for mixed cohort of about 250 individuals: [1-68] and [3-68]. Healthy, T2D, CHF (with or without T2D and/or MI), and Cancer [1-68] averages were 7.54%, 48.31%, 44.99%, and 43.12%. T2D, CHF (with or without T2D and/or MI), and Cancer [1-68] statistically significant from the healthy cohort at $P < 0.001$. Healthy, T2D, CHF (with or without T2D and/or hMI), and Cancer [3-68] averages were 78.15%, 33.66%, 44.99%, and 43.12%. Healthy [3-68] statistically significant from the T2D, CHF (with or without T2D and/or hMI), and Cancer cohort at $P < 0.001$.

For example, in **Figure 17** a large increase in the RPA of [1-68] and a large decrease in RPA of [3-68] is observed in the majority of the diseased individuals relative to the healthy controls. In **Figure 19** glycation increases significantly in the diseased cohorts with the T2D indivduals unsurprinsgly exhibiting the highest

relative abundace with a average value and range of 1.84 ± 0.84% and 0.68 – 4.06% compared to the healthy cohort value of 0.43 ± 0.35% and range of 0.05 – 2.55% (note: the glycation calcuation comes from adding the glycated [1-68] and [3-68] together).

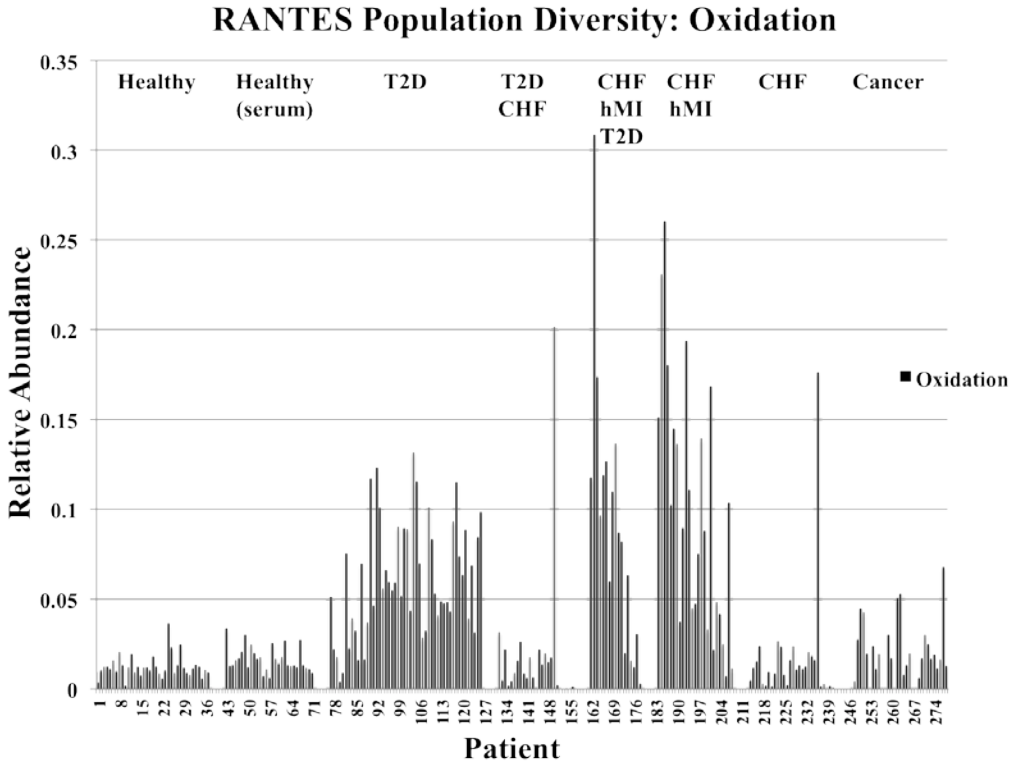

Figure 18: Population data for mixed cohort of about 250 individuals: oxidized RANTES. Averages of oxidized RANTES in healthy, T2D, CHF and MI, and Cancer were 1.23%, 6.12%, 9.65%, and 2.24%. Healthy oxidized RANTES was statistically significant from the T2D and hMI cohorts at $P < 0.001$ and statistically significant from the cancer cohort at $P = 0.0013$.

In **Figure 18** a markedly higher RPA of oxidized RANTES is observed in the diseased individuals, with the highest increase observed in those with a history of myocardial infarction (average value and range of 9.65 ± 7.16% and 0.27 – 30.86% compared to the healthy cohort value of 1.42 ± 0.69% and 0.17 – 3.63%).

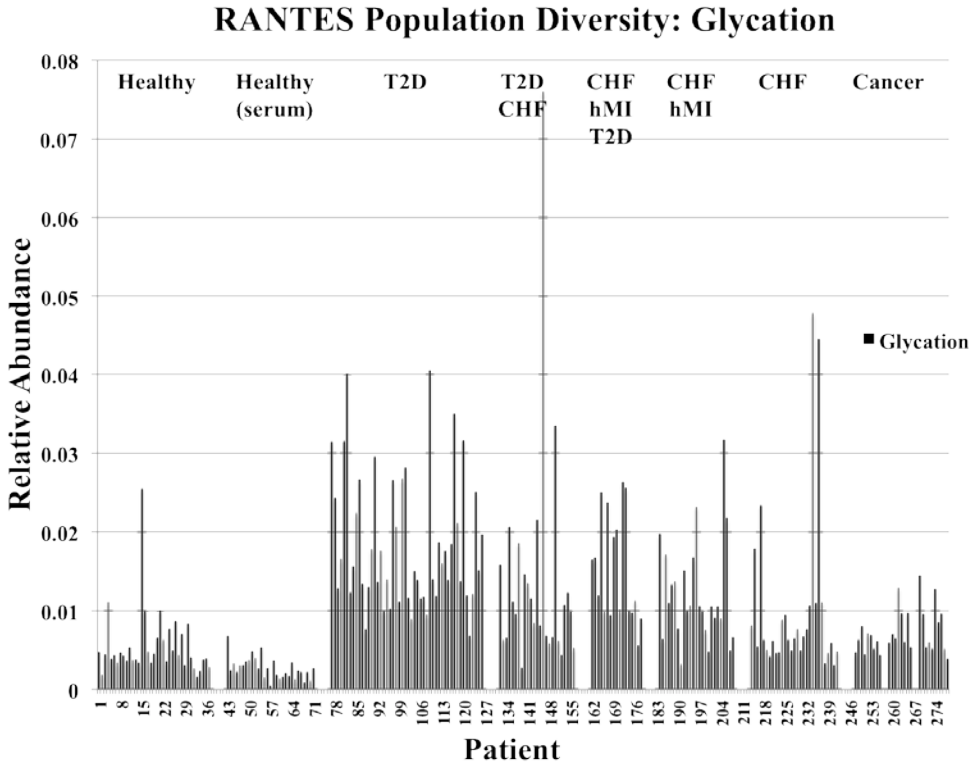

Figure 19: Population data for mixed cohort of about 250 individuals: glycated RANTES. Averages of glycated RANTES in healthy, T2D, and CHF (with or without T2D and MI) were 0.55%, 1.84%, and 1.36%. Healthy glycated RANTES was statistically significant from the T2D and CHF (with or without T2D and MI) cohort at $P < 0.001$.

Finally, the differences in the relative percent adundances of the lowest level truncated variants is presented in **Figure 20** with micro differences observed between most disease states including the abnormal higher relative adundance of [1-66] in the CHF and hMI individuals with an average value and range of 3.05 ± 7.54% and 0.02 – 36.67% compared to the healthy cohort value of 1.07 ± 0.58% and 0.10 – 4.26%.

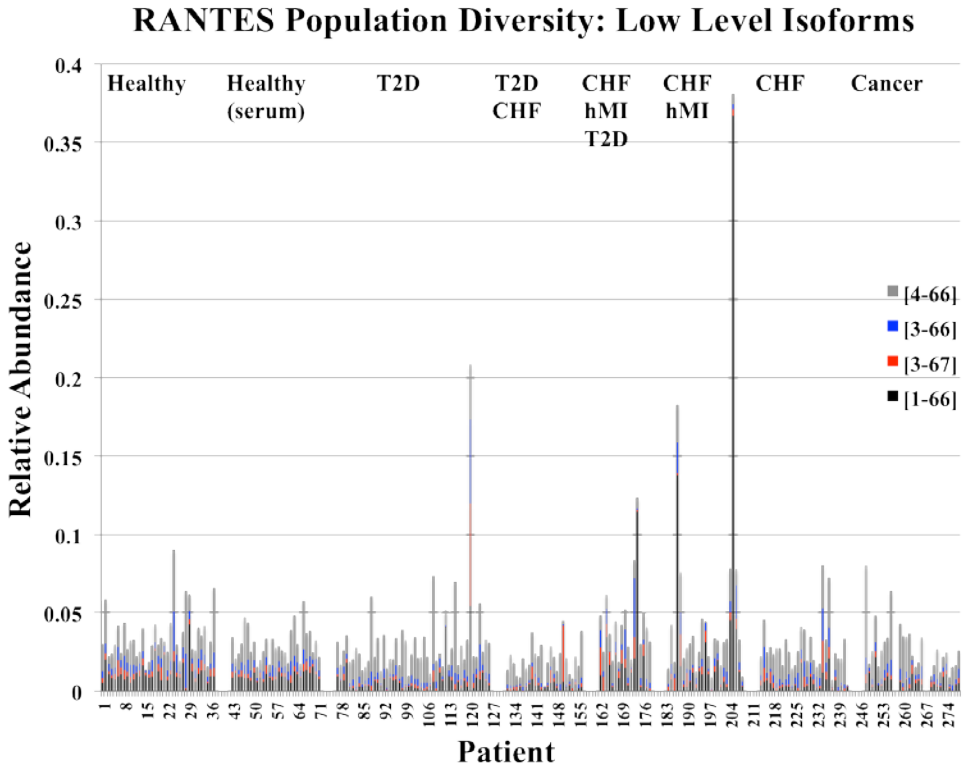

Figure 20: Stacked bar plot population data for mixed cohort of about 250 individuals: low level isoforms. Relative abundance of some of the lowest level RANTES isoforms: [4-66], [3-66], [3-67], and [1-66] are shown.

Recognizing heterogeneity in this context of multiple diseases presents a unique prospect for diagnosing more than one disease, using independent variant markers, from a single protein analysis. It is only after looking at protein phenotypes (e.g. concentration and posttranslational modifications) in the context of populations when deviations in protein multiplicity, including changes in population frequency and relative abundance, become clear and thus biomedically applicable (21, 31).

Notably, due to the *ex vivo* activity of enzymes in plasma (confirmed from our laboratory by observing intact to be processed into [3-68]) future population studies may be designed with the use of collection tubes containing enzyme inhibitors. This will guarantee an accurate readout of bioactive (and inactive) RANTES isoforms at the time of collection, which will also be beneficial to establishing inter-laboratory standardizations. Regardless, the results illustrate the necessity to acknowledge RANTES diversity and optimistically suggest it may hold multipurpose clinical utility.

In the span of two decades studies have quickly taken the comprehension of RANTES from a single gene product found in T-cells to a molecule that appears to be related with several diseases, expressed in a range of tissues, and acutely regulated via truncation by specific enzymes. This report adds to this the body of work by introducing over sixteen new forms of the molecule apparent in human plasma in the context of disease populations. The structural variety RANTES exhibits in different disease states should influence the design of future quantitative clinical assays (choice of variant to monitor, internal standard, etc). The population diversity explored here strongly suggests RANTES variants should be monitored, independent from one another, to assess RANTES chemokine function and regulation accurately in the context of disease.

Chapter 7

A MASS SPECTROMETRIC IMMUNOASSAY FOR KIDNEY DISEASE AND RELATED DISORDERS

It is estimated that 11.5% of adults 20 years and older in the United States (approximately 23 million individuals) have physiological indications of having chronic kidney disease (CKD) (115). Alarmingly, there were 87,812 deaths in 2007 for all patients undergoing treatment for end state renal disease (ESRD) (116). Furthermore, ESRD resulted in $35.32 billion dollars in public and private spending in the United States in the year 2007 (116). Due to its widespread prevalence in the population and the corresponding economic burden, new targeted proteomic solutions that help detect, monitor, and assist in treating kidney disease may have substantial clinical utility.

Chronic kidney disease and related complications arise from abnormalities in the metabolism of calcium, phosphorous, and magnesium (117). Regulation of these minerals is accomplished principally through interactions between three major organs: the intestine, bone, and kidney. These organs communicate via two chief hormones: parathyroid hormone (PTH) and vitamin D. PTH is secreted from the chief cells of the parathyroid gland and is activated via a negative feedback loop when plasma Ca^{2+} levels drop. PTH restores calcium homeostasis in healthy individuals by increasing bone mineral dissolution (which releases stored calcium and magnesium from the bone), increasing calcium and magnesium renal reabsorption, and indirectly by triggering $1,25(OH)_2D$ (calcitriol) synthesis, the

active form of Vitamin D, which augments gastrointestinal absorption of calcium and phosphorous (117, 118).

PTH is synthesized in the parathyroid glands via a two-step conversion of prepro-PTH (115 amino acids) to pro-PTH (90 amino acids), and finally to the native 84 amino acid form: PTH (1-84). Individuals with CKD typically have elevated PTH plasmatic concentrations due to several factors including phosphate retention, hypocalcemia, and calcitriol deficiency, with prolonged periods of PTH secretion leading to the condition known as secondary hyperparathyroidism (119, 120). As a consequence of extended periods of elevated bioactive PTH levels and disrupted mineral metabolism, individuals are threatened with bone abnormalities, calcification of the cardiovascular system, and increased mortality. PTH has a half-life of approximately 4 minutes (121) and is quickly degraded via uptake and proteolytic processing within the Hepatic Kupffer cells, followed by release back into circulation (122). This action produces an abundance of shortened, C-terminal PTH variants, which themselves have considerably longer half-lives due to their clearance exclusively by glomerular filtration (i.e. kidney clearance). It is therefore of paramount importance for assays to accurately measure the bioactive form of PTH distinct from C-terminal PTH variants for effective detection and management of PTH related diseases (e.g. CKD, hyperparathyroidism, etc).

Indeed, clinicians for the past 50 years have been determined to realize the objective of unambiguous bioactive PTH detection. Three generations of PTH assays have served clinicians in interpreting bioactive PTH levels, with varying

degrees of success. The motivation for subsequent generations of PTH assays has been due to two principle discoveries: PTH exerts its effects if its N-terminus is intact (i.e. the first 34 amino acids (123)) and 80-95% of circulating PTH is N-terminally truncated (114, 124). This "paradox" has motivated researchers to uncover the truth behind PTH. First generation PTH assays (circa 1971) were radioimmunoassays with antibody epitopes located towards the c-terminus of the molecule (125, 126). As PTH exists largely as N-terminally truncated variants and is thus inactive, these assays were supplanted by later generation assays due to the large degree of cross-reactivity. Second generation assays were developed as a reaction to interference and are called Intact (I)-PTH assays. These sandwich assays were built with capture antibodies specific for PTH (39-84) and detection antibodies specific for PTH (1-34), with the later having epitopes typically between 13-34 (127). Although these assays had a substantial impact on the community and are still widely used, these assays were later found to cross-react with the highly potent, opposite acting forms deemed non-(1-84) PTH fragments (e.g. PTH (7-84)). These fragments can comprise up to 45% of immunoreactive PTH in renal failure individuals and 20% in health individuals (128). As such, at the turn of the century third generation assays began to emerge that had detection epitopes in the 1-4 region (129). Despite these assays yielding a solution that provides a high-degree of certainty in detecting intact N-terminus PTH, these assays were found to cross-react with PTH molecules containing a theoretical phosphate group (114), and, if PTH exists in other unanticipated forms such as C-

terminal truncated forms, cross-reactivity caused by such forms and the implications remain questionable. As a result, innovative diagnostic approaches that provide a “fourth generation PTH assay” solution may engender clinical utility if able to solve the unmet needs of previous generations of assays. Such an assay might provide unambiguous detection of bioactive PTH (i.e. intact N-terminus PTH) as well as multiplexed detection capabilities of additional modified forms of PTH within the framework of the recently acknowledged *dual nature* of the PTH molecule (114). Indeed, this emerging biological model views PTH as a molecule that depending upon its proteolytical processing within the parathyroid glands and/or peripheral tissues, can exert opposing effects on calcemic homeostasis via two distinct antagonistic receptors which bind to the opposite ends of the molecule -- the N-terminus and C-terminus (114, 130-132). As such, assays that can accurately detect and monitor PTH in the context of the newfound dual nature of PTH may have clinical utility.

PARATHYROID HORMONE MICROHETEROGENEITY IN RENAL FAILURE POPULATIONS

Parathyroid hormone (PTH) has remained an elusive protein despite decades of research aimed at uncovering structural variants that exist within individuals. An emerging paradigm regarding PTH has begun to reconcile the complexity surrounding PTH microheterogeneity by acknowledging that PTH binds to two separate receptors (114). The PTH/PTHrP type I receptor exerts the classical biological effects of PTH by binding to the intact n-terminal domain of PTH (intact PTH can account for as little as 5% total circulating PTH). The second receptor binds C-PTH fragments, which correspondingly binds to the intact c-terminal domain (e.g. PTH34-84 binds to this receptor). These receptors exert opposing biological effects in regulating Ca^{2+} concentration. Regarding the origin of C-PTH fragments, C-PTH is released from the parathyroid glands in a Ca^{2+} dependent manner and may also be produced in the liver Kuppfer cells via the conversion of circulating PTH (1-84) in C-PTH (133). The general consensus is that circulating PTH largely exists as numerous structural forms but the precise structural compositions are unknown and likely vary from individual to individual.

A limitation of previous generations of PTH assays that are built using ELISAs and related technologies is that they rely on detection based solely on antibody-PTH interactions. In this mode, the detected species cannot be directly known with 100% certainty. The detection is “interpreted” via a chemical reaction

or fluoresce signal rather than an unambiguous “molecule specific” method such as that may be yielded with a mass spectrometer. Nonetheless, third generations assays such as the CAP (cyclase-activating PTH) assay from Scantibodies Laboratory and the Bio-Intact PTH assay from Nichols Institute Diagnostics have excellent interday CVs ranging from 3.4-8.3% (8.3% at 31ng/L) and 2.7-3.7% (2.7% at 20.8ng/L), respectively, and have detection capabilities at relevant physiological concentrations (134). Given that PTH is a molecule that is correlated to several conditions such hyper/hypoparathyroidism, hyper/hypocalcemia, CKD, and parathyroid adenoma, and exists largely as distinct isoforms in circulation, identification of disease specific profiles of PTH presentation in blood may have impact in the clinical community. To this end, this study focuses on the use of mass spectrometric immunoassay (MSIA) (25) to map structural differences of PTH found in ESRD relative to healthy individuals as a beginning point in establishing distinct PTH disease profiles. Such profiles will help facilitate the successful translation to a clinically applied mass-spectrometric PTH platform.

Of note, besides offering an introduction to the PTH work I personally conducted, this chapter is intended to describe which unique attributes and insights I provided for the subsequent chapter (previously published (26)) wherein I was a co-author and had a significant contribution.

EXPERIMENTAL

This experimental section closely follows the protocol employed in the subsequent chapter (26).

REAGENTS

Goat polyclonal Anti PTH39-84 antibody was purchased from Immutopics International (San Clemente, CA). Recombinant human PTH (rhPTH) was obtained from Bachem (Torrance, CA). Premixed MES-buffered saline powder packets were from Pierce (Rockford, IL). Extraction of PTH from plasma was carried out with proprietary MSIA pipette tips (MSIA-Tips) from Intrinsic Bioprobes (Tempe, AZ) derivatized with the PTH antibodies via 1,1' Carbonyldiimidazole (CDI) chemistry as described below. Premade 10X 0.1M Hepes-buffered saline buffer (HBS-N) with 30 mM EDTA and 0.2% (v/v) surfactant P20 (HBS-EP) were purchased from BIACORE (Piscataway, NJ). Synthetic heavy labeled peptides were obtained from Thermofisher (Ulm, Germany). All other chemicals were obtained from Sigma-Aldrich (St. Louis, MO).

SAMPLES

All samples used in this study were acquired under an Institutional Review Board (IRB) approved protocol and Informed Consent. Twenty four serum samples representing twelve individuals diagnosed with either sever renal impairment or end-stage renal disease (10 males and 2 females; mean age 66.7) and twelve

healthy individuals (10 males and 2 females; mean age 65) were used in the study. The renal failure samples represented 3 Hispanics, 2 Asians, 2 African Americans, and 6 Caucasians. Information on the ethnicities of the healthy samples was not available.

SAMPLE PREPARATION AND IMMUNOCAPTURE

MSIA-Tips were prepared by Intrinsic Bioprobes as previously described (22, 23, 25, 135). Prior to analysis samples were thawed to 25 ^{o}C using a water bath and one mL of plasma was diluted with 750 µL HBS-EP buffer to result in a total analytical volume of 1.75 mL. PTH was then extracted with the aid of a Beckman Multimek 96 pipetting robot by repeatedly (1,500 repetitions) drawing and expelling (back into the analytical volume) 125 µL aliquots of the analytical volume through the antibody prelinked MSIA-Tip. After extraction, the pipettes were rinsed using HBS-EP, H_2O, 3:1 ratio of ammonium acetate/acetonitrile, and again with H_2O (in this order, each rinse = 15 repetitions of 150 µL), after which PTH was immediately eluted for detection with MALDI-TOF-MS.

MALDI-TOF MASS SPECTROMETRY

Samples were prepared for MALDI-TOF MS by drawing 4 µL of MALDI matrix solution (saturated aqueous solution of sinapic acid, in 33% (v/v) acetonitrile, 0.4% (v/v) trifluoroacetic acid, TFA) into the pipette and depositing onto a MALDI-TOF-MS target (136). MALDI-TOF-MS was performed using a Bruker

Ultraflex MALDI-TOF instrument operating in the positive ion, delayed-extraction mode; reflector engaged with 'ion source 1' at 25.00 kV, 'ion source 2' at 21.90 kV, lens at 9.50 kV, 'reflector' at 26.30 kV, 'reflector 2' at 13.80, 340 ns delayed extraction, deflection signal suppression up to *m/z* 4000, and 2 GS/s sample rate. Ten thousand laser-shots were signal averaged for each mass spectrum using a laser repetition rate of 100 Hz. Spectra were externally calibrated with a mixture of 4 proteins supplied by Bruker (Cat. No. 208241) ranging in average *m/z* from 5734.52 (Insulin $[M+H]^+$) to 12,360.97 (Cytochrome C $[M+H]^+$).

RESULTS AND DISCUSSION

Figure 21 (bottom panel), shows two qualitatively representative mass spectra overlaid to depict the healthy and renal failure individuals in this study. The top panel displays the "PTH variant map" created from the PTH diversity encountered within this study (variants correspond to signals observed in the bottom panel). PTH was found to exist in multiple variations within all of the samples. These modified forms may be conceptually grouped into three categories: positive acting forms (i.e. classical biological effects of intact PTH), negative acting forms (i.e. opposing effects relative to intact; i.e. C-PTH fragments), and assumed inactive forms. The only form of PTH that acts as a classically active form, at least detected by this assay, is intact PTH. However, it's possible there may be endogenous PTH fragments that have an intact N-terminal

domain. PTH exerts its function on bone and kidney by binding to the PTH/PTHrP receptor and by likewise initiating the protein kinase A and C pathways in respective tissues (114, 137). Intact PTH was observed in all of the renal failure samples and in only two of the twelve healthy samples. These results are consistent with the pathophysiology of kidney disease whereby due to the decreased levels of calcium in serum, excess PTH is secreted by the parathyroid glands in attempt to increase the calcium levels. C-PTH fragments were also observed in higher S/N and in much higher frequencies relative to the healthy controls. This is also consistent with other studies finding that C-PTH fragments (albeit the C-PTH identities were unknown) represented more than 95% of the total hormone in circulation compared to just 80% in healthy individuals (via a two-site immunometric assay) (114, 128). Signals were considered relevant if S/N > 3. C-PTH fragments observed in populations included: PTH (28-84), PTH (34-84), PTH (37-84), PTH (38-84), PTH (45-84), and PTH (48-84) (PTH 28-84 and PTH 48-84 were previously unreported). The frequencies of these fragments in the renal failure population were consistently found in at least in 8 out of 12 individuals. In the healthy cohort, these frequencies were decreased and were consistently found in less than 8 of out 12 individuals. The third groups of PTH molecules detected were previously unreported C-terminally truncated C-PTH fragments, which are assumed to be inactive (although this remains to be proven).

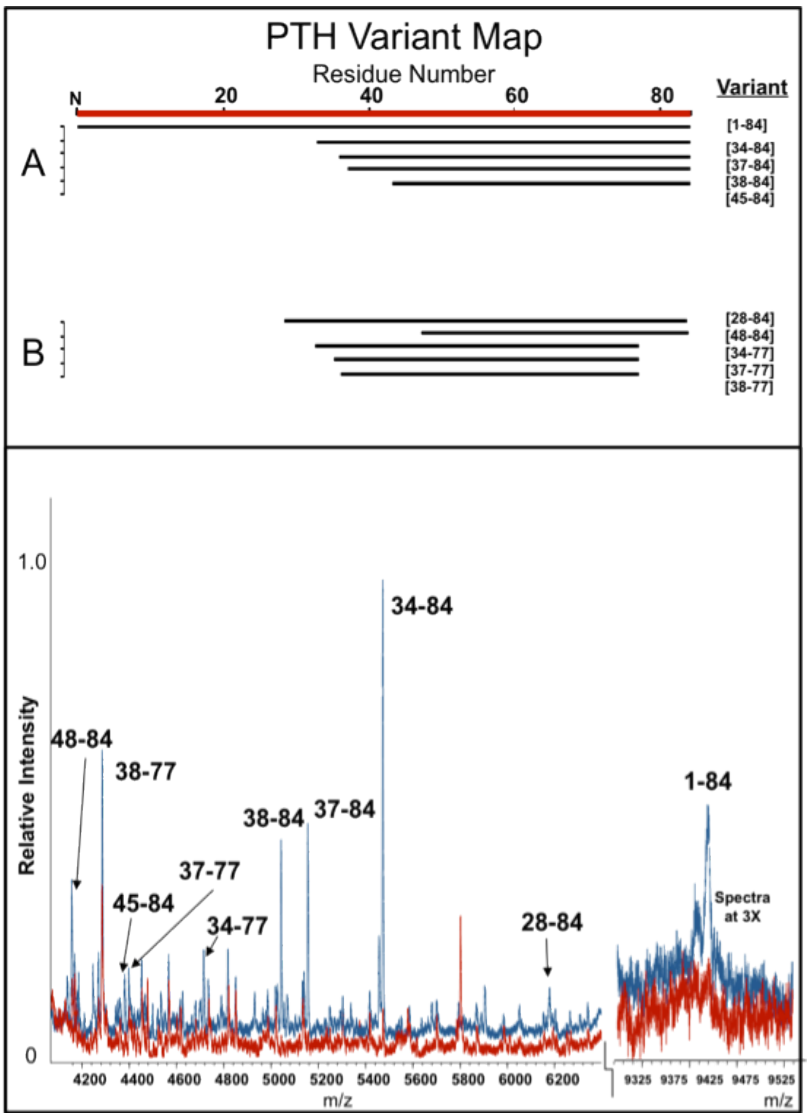

Figure 21: PTH variant map. Top panel: A. list of all the N-terminally truncated PTH variants identified previously by others that were detected in this study B. Variants discovered and added to the map during this study using full-scan MSIA (MALDI-TOF-MS). All variants depicted in (A) and (B) were observed in the majority of clinical samples under investigation. (MALDI-TOF-MS) spectra representative of the 12 renal failure samples (blue) and the 12 healthy controls (red). The following species, as seen labeled in the figure, were consistently found at higher frequency relative abundance in the renal failure cohort (m/z observed; calculated): PTH1-84 (9426.03; 9425.71), PTH28-84 (6179.61; 6179.91), PTH34-84 (5472.91; 5473.16), PTH37-84 (5155.71; 5155.77), PTH38-84 (5051.92; 5051.61), PTH34-77 (4715.98; 4716.26), PTH37-77 (4397.71; 4398.87), PTH45-84 (4379.65; 4379.82), PTH38-77 (4285.57; 4285.71) and PTH48-84 (4136.42; 4136.60).

Others had already shown that C-truncated PTH molecules exist but their specific identities were not known (113); this data thus serves to begin establishing the identities of these molecules. A conserved truncation site at residue 77 was also observed in the molecules. These fragments included: PTH (34-77), PTH (37-77), and PTH (38-77). These findings are intriguing because they may represent the aftermath of a secondary regulatory mechanism in inactivating negatively acting C-PTH fragments. These were found in the renal failure samples at a frequency of ≥ 8 out of 12 individuals and ≤ 5 out of 12 individuals within the healthy cohort. Notably, many more truncated forms of PTH were mass mapped to PTH isoforms, but due to their relative low population frequencies, they have been omitted from Figure 21.

Table 5 shows the populational frequencies of all signals that have been mass mapped to PTH variants. This addresses the question of the number of samples (of the total) in which a particular protein variant was observed. When these three classes of PTH variants are taken into consideration regarding the new dual receptor paradigm (PTH/PTHrP type 1 receptor and the C-PTH receptor), an insight into an individual's unique Ca^{2+} metabolism and (indirectly) bone turnover profile is presented from within a single PTH MSIA MALDI-TOF-MS spectrum respective to the parathyroid gland's response.

Table 5: PTH variant frequencies as measured by MALDI-TOF-MS.

Variant	Molecular mass, amu[a]	PTH variant frequencies											
		Renal failure samples											
		1	2	3	4	5	6	7	8	9	10	11	12
48–84	4135.596	x	x	x	x	x	x	x	x	x	x	x	x
45–84	4378.815		x	x	x		x	x			x	x	x
38–84	5041.603	x	x	x	x	x	x	x	x	x	x	x	x
37–84	5154.762	x	x	x	x	x	x	x	x	x	x	x	x
34–84	5472.149	x	x	x	x	x	x	x	x	x	x	x	x
28–84	6178.904		x	x	x	x	x	x	x	x	x	x	x
Intact PTH	9424.716			x		x		x	x	x	x	x	x
34–77	4715.25		x	x	x	x		x	x		x	x	x
37–77	4397.863		x	x	x				x	x	x	x	x
38–77	4284.704		x	x	x	x	x		x	x	x	x	x
		Normal samples											
		1	2	3	4	5	6	7	8	9	10	11	12
48–84	4135.596	x		x		x	x	x	x	x	x	x	x
45–84	4378.815			x									
38–84	5041.603						x						
37–84	5154.762												
34–84	5472.149	x	x				x		x	x			x
28–84	6178.904												
Intact PTH	9424.716											x	x
34–77	4715.25												
37–77	4397.863	x		x			x	x		x			
38–77	4284.704	x								x			

[a] amu, atomic mass unit.

ROC (receiver operating characteristic) curve analysis can be a useful tool in diagnostics to display the efficacy of a particular test in discriminating diseased individuals from healthy individuals (138). Many of the PTH isoforms explored here produced very high ROC_{AUC} values via an analysis of variant signal intensity (area under the ROC curve; this indicates the true positive rate and true negative rate with a value of 1 equaling perfect discrimination). For the most abundant ions (PTH (34-84), PTH (37-84), and PTH (38-84)) ROC_{AUC} values were ≥ 0.98, indicating the variants were capable in differentiating renal failure samples from healthy samples (e.g. **Figure 22**). This is encouraging due to renal failure being

linked to stage 5 of chronic kidney disease. Likewise, a spectrum in the form of elevating PTH isoforms is ultimately desired if one wants to monitor (and predict) the progression of CKD from stages 1-5. A second type of discrimination emerged from comparing the ratio of C-PTH to inactive forms (the two specific variants used here are PTH 34-84 / PTH 38-77). The population ratio average for the renal failure cohort was found to be 1.54 ± 0.9 compared to a very narrow distribution of just 0.31 ± 0.16 for the healthy cohort. These results are interesting because they suggest inactive fragments may also be regulated differently between disease states (along with C-PTH fragments). **Figure 22** presents a ROC curve demonstrating the diagnostic efficacy of PTH (34-84).

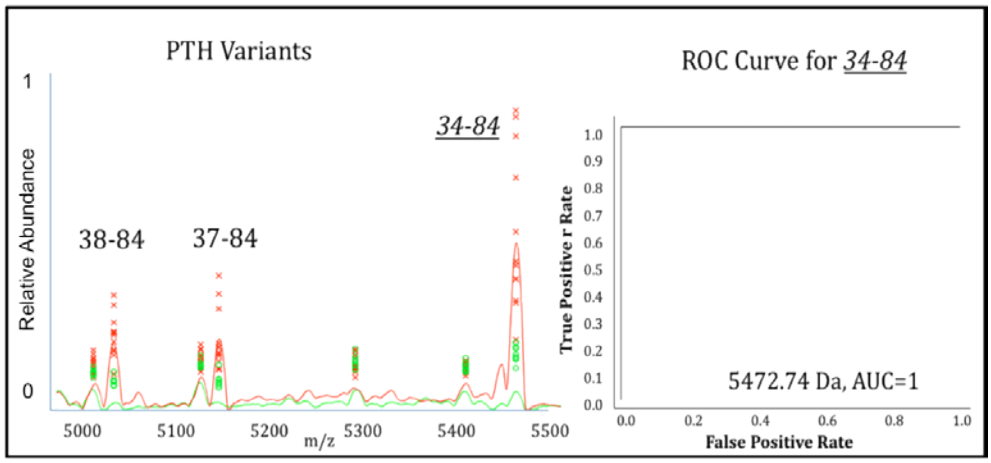

Figure 22: ROC curve for PTH (34-84). On the left: averaged spectra of the two cohorts for three PTH variants (each red x represents a renal failure individual and their respective signal intensity; each green o represents a healthy individual and their respective signal intensity). PTH variants PTH34-84 (5472.91; 5473.16), PTH37-84 (5155.71; 5155.77), PTH38-84 (5051.92; 5051.61) are shown (observered, theoretical m/z). On the right: an ROC curve for the PTH variant 34-84. This ROC curve yeilds 100% sensitivity (no false negatives) and 100% specificity (no false positives), and thus it's ROC(AUC) value of 1.0.

Described here is a high throughput, multiplexed mass spectrometric immunoassay (MSIA) that in a single analysis detects PTH1-84 (wild-type), C-PTH variants (e.g. PTH (34-84)), and previously unreported C-terminally truncated variants (e.g. PTH (38-77)) using MALDI-TOF-MS. In application, the assay was successful in stratifying renal failure from matched healthy controls (with $ROC_{AUC} > 0.90$ for individual variants and in multiplexed mode). The protein diversity explored here adds to the growing awareness and interest in studying protein heterogeneity in the general population. This information in turn serves two functions, it can help explain heterogeneity that may have interfered with conventional PTH assays (i.e. *biological noise*) and it may also, as demonstrated here, include determinant data linked to specific diseases (e.g. chronic kidney disease). Accordingly, from a single PTH MSIA spectrum it may be possible to observe an individual's unique calcium metabolism and bone turnover profile. Future large scale population studies devoted towards more comprehensive screenings of PTH variants specific for disease will have important clinical utility in the understanding and diagnosis of endocrine and bone diseases. Lastly, the work presented here serves as a starting template to create a next-generation PTH quantitative assay that simultaneously detects bioactive PTH as well as disease-specific PTH isoforms.

Chapter 8

SELECTED REACTION MONITORING–MASS SPECTROMETRIC IMMUNOASSAY RESPONSIVE TO PARATHYROID HORMONE AND RELATED VARIANTS

Parathyroid hormone is produced in the parathyroid glands through the 2-step conversion of prepro-PTH (115 amino acids) to pro-PTH (90 amino acids) to the 84 amino acid peptide (PTH1-84). The hormone is secreted into the circulatory system to produce basal (healthy) concentrations of approximately 15–65 ng/L *(139),* and is assayed to assist in the diagnosis of hypo/hyperparathyroidism and hypercalcemia and in monitoring for renal osteodystrophy in patients with end-stage renal failure *(139-141).* Conventional PTH assays typically rely on 2-antibody recognition systems coupled to a variety of detection modalities *(142-144).* Notably, the most specific assays are able to differentiate between different truncated forms of PTH and are referred to as second- and third-generation PTH assays (145, 146).

Key to the application of these later-generation assays is the ability to selectively monitor various PTH forms of known biological consequence. In particular, 2 variants, full-length PTH1– 84 and PTH missing the 6 N-terminal amino acids (PTH7– 84), are the subject of increased clinical investigation and potential diagnostic capability. Because of the inability of existing assays to detect microheterogeneity (21), these variants were historically considered as a single PTH value (i.e., the first-generation assays) (145). The classification of each

variant as its own molecular entity and the analysis and study of each independently suggest an antagonistic relationship between the 2 different forms in regard to calcium homeostasis (147). In fact, there is mounting clinical evidence that the ratio between PTH1– 84 and PTH7– 84 may be used to differentiate between hyper- parathyroid bone turnover and adynamic bone disease (148-150).

The PTH (1-84) to PTH (7-84) paradigm is a recent example of the biological and clinical utility of microheterogeneity within the PTH protein. Indeed, other PTH variants were defined as far back as approximately 40 years ago. Perhaps the most mature of these, PTH (1-34), has been identified as an in vivo variant that exhibits biochemical activity comparable to the full-length protein. Consequently, PTH (1-34) is a classic example of a peptide-based bioactive variant that has transitioned through drug development to the point of US Food and Drug Administration clearance for the treatment of osteoporosis [rPTH1–34 (teriparatide)] (151-153). Collectively the routine monitoring of these clinically relevant PTH variants – PTH (1-84), PTH (7-84), and PTH (1-34) -- is achieved through 3 separate, highly specific immunometric assays. However, there are indications that even greater microheterogeneity exists within PTH, which has yet to be fully characterized to determine clinical utility and/or confounding effects on present-day assays. The accurate examination of known PTH variants and the simultaneous evaluation of other possible variants requires a degree of analytical freedom that universally escapes conventional assays. Here we describe mass

spectrometric immunoassays (MSIA) that, although specifically designed for the detection of PTH (1- 84) and PTH (7-84), also facilitate the simultaneous discovery and evaluation of further microheterogeneity in PTH.

EXPERIMENTAL

APPROACH

As a starting point for the development of selected reaction monitoring (SRM)-based assays for PTH, we surveyed the literature to define molecular variants already identified. In addition to the well-characterized truncated variants (e.g., PTH (1-84) and PTH (7-84), 4 other molecular versions have been reported in the literature as present in human biofluids (primarily plasma or serum). Aligning these fragments to the sequence of PTH (1-84) produced a variant map revealing forms stemming predominantly from N-terminal truncations (**Fig. 23A**). A conserved region (among several variants) was evident between residues 48 to 84. This region was suitable for immmunoaffinity targeting to capture ragged N-terminal variants (e.g., PTH (1-84) and PTH (7-84). We used a full-scan MSIA (MALDI-TOF MS) (15, 25, 154-157) akin to the assay reported by Zhang et al. (158) to capture these variants and to discover other variants that were immunoreactive with the antibody **(Fig. 23B**). Postcapture digestion of retained PTH (and variants) created the basis for SRM- MSIA (19, 159-162), for which surrogate peptides representative of the different PTH variants were selected for analysis (**Fig. 23C**).

REAGENTS

Goat polyclonal anti-PTH (39-84) antibody was purchased from Immutopics International. Recombinant human PTH (rhPTH) was obtained from Bachem. Pre-mixed 2-[morpholino]ethanesulfonic acid-buffered saline powder packets were from Pierce. Extraction of PTH from plasma was carried out with proprietary MSIA pipette tips (MSIA-Tips) from Intrinsic Bioprobes derivatized with the PTH antibodies via 1,1'-carbonyldiimidazole chemistry as described below. Premade 0.01 mol/L HEPES-buffered saline with 3 mmol/L EDTA and 0.05% (vol/vol) surfactant P20 (HBS-EP) was purchased from Biacore. Synthetic heavy-labeled peptides were obtained from ThermoFisher. All other chemicals were obtained from Sigma-Aldrich.

SAMPLES

All samples used in this study were acquired under an Institutional Review Board approved protocol, and informed consent was obtained from all study participants. A total of 24 serum samples, from 12 individuals with a diagnosis of severe renal impairment or end stage renal disease (10 males and 2 females; mean age 66.7 years) and 12 healthy individuals (10 males and 2 females; mean age 65 years) were used in the study. Of the patients with renal failure who donated samples, 3 were Hispanic, 2 were Asian, 2 were African American, and 6 were white. The ethnicity information for the healthy sample donors was not available. Calibration curves were prepared from pooled human plasma by step-wise, 2-fold serial dilution of an initial sample containing rhPTH at a concentration of 1000 ng/L (8

steps, range 1000–7.8 ng/L). Samples were frozen at -80 °C until use.

SAMPLE PREPARATION AND IMMUNOCAPTURE

MSIA-Tips were prepared by Intrinsic Bioprobes as previously described (17-22). Before analysis, samples were thawed to 25 °C in a water bath, and 1 mL of serum (or plasma) was diluted with 750 μL HBS-EP buffer to a total analytical volume of 1.75 mL. PTH was then extracted with the aid of a Beckman Multimek 96 pipetting robot by repeatedly (1500 repetitions) drawing and expelling (back into the analytical volume) 125-μL aliquots of the analytical volume through the antibody-prelinked MSIA-Tip. After extraction, the pipettes were rinsed with HBS-EP and H2O (in this order; each rinse = 15 repetitions of 150 μL), after which PTH was either immediately eluted for detection with MALDI-TOF MS or digested and analyzed with high-resolution liquid chromatography–tandem MS (LC-MS/MS) or SRM as described below.

MALDI-TOF MASS SPECTROMETRY

Samples were prepared for MALDI-TOF MS by drawing 4 μL of MALDI matrix solution [saturated aqueous solution of sinapic acid, in 33% (vol/vol) acetonitrile, 0.4% (vol/vol) trifluoroacetic acid] into the pipette and depositing it onto a MALDI-TOF MS target (136). We performed MALDI-TOF MS using a Bruker Ultraflex MALDI-TOF instrument operating in the positive ion, delayed-extraction mode; reflector engaged with ion source 1 at 25.00 kV, ion source 2 at 21.90 kV, lens at 9.50 kV, reflector at 26.30 kV, reflector 2 at 13.80, 340 ns delayed extraction, deflection signal suppression up to *m/z* 4000, and 2 GS/s

sample rate. We signal averaged 10 000 laser shots for each mass spectrum using a laser repetition rate of 100 Hz. Isotopically average spectra were externally calibrated with a mixture of bovine insulin ($[M+H]^+$ = 5734.52), cytochrome c ($[M+2H]^{2+}$ = 6181.05), ubiquitin ($[M+H]^+$ = 8565.76), and cytochrome c ($[M+H]^+$ = 12360.97) (all 4 from Bruker).

SAMPLE ELUTION AND TRYPSIN DIGESTION

Bound proteins were eluted from the tips into a 96-well plate (AB-1300, Abgene) by pipetting 100 μL of 30% acetonitrile/0.5% formic acid up and down for a total of 15 cycles. Samples were lyophilized to dryness and then resuspended in 30 μL of 30% n-propanol/100 mmol/L ammonium bicarbonate, pH 8.0, diluted with 100 μL of 25 mmol/L acetic acid containing 100 ng of trypsin. Samples were allowed to digest for 4 h at 37 °C. After digestion, samples were lyophilized and resuspended in 30 μL of 3% (vol/vol) acetonitrile/0.2% (vol/ vol) formic acid/glucagon/PTH heavy peptides.

HIGH-RESOLUTION LC-MS/MS

High-resolution LC-MS/MS analysis was carried out on an LTQ-Orbitrap XL mass spectrometer (ThermoFisher Scientific). Samples in 5% (vol/vol) acetonitrile/0.1% (vol/vol) formic acid were injected onto a 75-μm x 25-cm fused silica capillary column packed with Hypersil Gold C18AQ 5-μm media (ThermoFisher Scientific), in a 250 μL/min gradient of 5% acetonitrile/0.1% formic acid to 30% acetonitrile/0.1% formic acid over the course of 180 min, with a total run length of 240 min and a flow rate of 285 nL/min. The LTQ-Orbitrap

was run in a top 5 configuration at 60-K resolution for a full scan, with monoisotopic precursor selection enabled, and +1 and unassigned charge state rejected. The analysis was carried out with collision induced dissociation and higher collision energy dissociation fragmentation modes.

SRM ASSAYS

SRM assays were developed on a TSQ Vantage triple-quadrupole mass spectrometer, an Accela pump, a CTC PAL Autosampler, and an IonMax Source equipped with a high-flow metal needle (ThermoFisher Scientific). A mass window of full width at half maximum of 0.7 (unit resolution) was used in the SRM assays because immunoenriched samples had a very high signal-to-noise. Narrower windows were necessary when the matrix background was significant and caused interferences in the SRM channels that re- duced signal-to-noise. Reversed-phase separations were carried out on a 1-mm x 100-mm Hypersil Gold 1.9-μm C18 particle (ThermoFisher Scientific) with a flow rate of 160 μL/min. Solvent A was 0.2% formic acid in LC-MS grade water, and solvent B was 0.2% formic acid in LC-MS grade acetonitrile (Optima grade reagents, ThermoFisher Scientific). Pinpoint software (ThermoFisher Scientific) was used for targeted protein quantification. The recently developed software algorithm automated the prediction of candidate peptides and the choice of multiple fragment ions for SRM assay design, as well as automating peptide identity confirmation and quantitative data processing. For the workflow described herein, the intact PTH sequence was imported into Pinpoint and digested with trypsin in silico, and then

transitions for each peptide were predicted by use of the batch option in the software. This initial list of peptides and transitions was tested with recombinant PTH digest to determine those peptides and transitions delivering optimal signal. After several iterations, a subset of 6 peptides with multiple transitions was chosen. Further assays were conducted with this optimized method. Once the target peptides were identified, heavy arginine or lysine versions were synthesized (ThermoFisher) to be used as internal quantitative standards. Target peptides were subsequently identified and quantified by coeluting light- and heavy-labeled transitions in the chromatographic separation. Time alignment and relative quantification of the transitions was performed with Pinpoint. All samples were assayed in triplicate.

RESULTS AND DISCUSSION

TOP-DOWN ANALYSIS AND DISCOVERY OF NOVEL VARIANTS

The approach described herein coupled targeting a common region of PTH by use of a polyclonal antibody (raised to the C-terminal end of the protein) with subsequent detection by use of MS (either MALDI-TOF MS or SRM). Using a top-down approach (MALDI- TOF MS), we discovered novel truncated PTH variants in clinical samples (**Figure 23**). The lower panel of Fig. 23 shows 2 MSIA (MALDI-TOF MS) spectra representative of those obtained from plasma samples of 12 individuals with renal failure and 12 healthy controls.

Signals corresponding to the previously reported N-terminally truncated variants are indicated, as well as additional signals aligning with other novel variants.

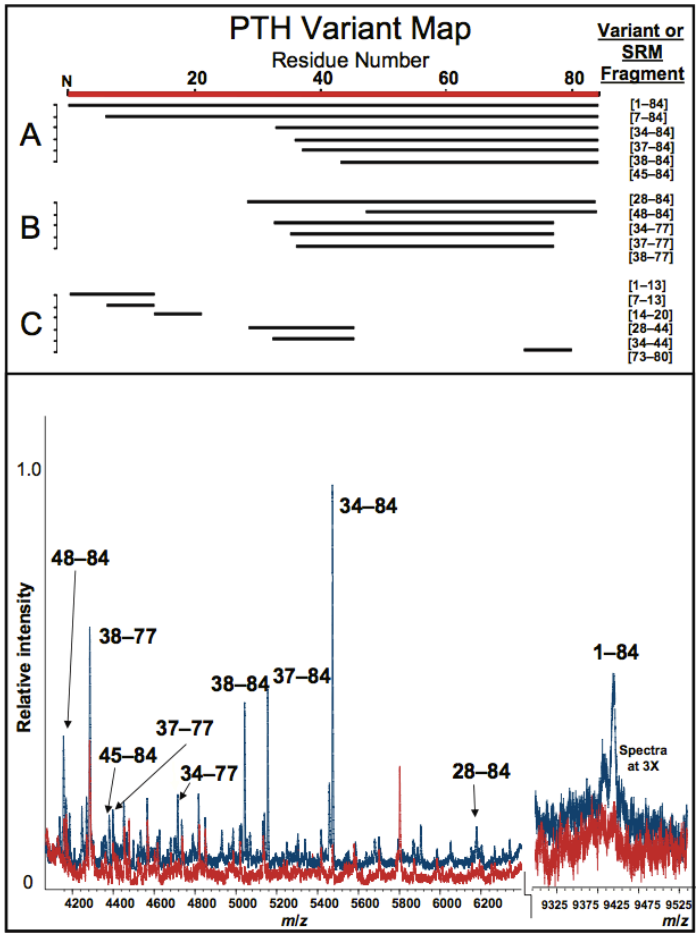

Figure 23: PTH variant map with SRM fragments. (A), N-terminally truncated PTH variants identified previously [D'Amour (11), Zhang et al. (23)]. (B), Variants added to map during this study by use of full-scan MSIA (MALDI-TOF MS) (see Fig. 2). (C), Conserved and truncated tryptic fragments chosen for SRM-MSIA. Bottom panel: MSIA (MALDI-TOF MS) spectra representative of the 12 samples from patients with renal failure (blue) and the 12 from healthy controls (red). The following species were consistently found at higher frequency relative abundance in the renal failure cohort (m/z observed; calculated): PTH (1–84) (9426.03; 9425.71), PTH (28–84) (6179.61; 6179.91), PTH (34–84) (5472.91; 5473.16), PTH (37–84) (5155.71; 5155.77), PTH (38–84) (5051.92; 5051.61), PTH (34–77) (4715.98; 4716.26), PTH (37–77) (4397.71; 4398.87), PTH (45–84) (4379.65; 4379.82), PTH (38–77) (4285.57; 4285.71) and PTH (48–84) (4136.42; 4136.60).

Notably, a conserved cleavage site (residue 77) was observed in several of these new variants (**Figure 23B**). With the exception of PTH (7-84), the variants depicted in **Figure 23, A and B**, were detected in the majority of clinical samples and were not readily evident in the control samples (**Table 6**).

Table 6: PTH variant frequencies as measured by MALDI-TOF-MS.

		PTH variant frequencies											
		Renal failure samples											
Variant	Molecular mass, amu[a]	1	2	3	4	5	6	7	8	9	10	11	12
48–84	4135.596	x	x	x	x	x	x	x	x	x	x	x	x
45–84	4378.815		x	x	x		x	x			x	x	x
38–84	5041.603	x	x	x	x	x	x	x	x	x	x	x	x
37–84	5154.762	x	x	x	x	x	x	x	x	x	x	x	x
34–84	5472.149	x	x	x	x	x	x	x	x	x	x	x	x
28–84	6178.904		x	x	x	x	x	x	x	x	x	x	x
Intact PTH	9424.716			x		x		x	x	x	x	x	x
34–77	4715.25		x	x	x	x		x	x		x	x	x
37–77	4397.863		x	x	x				x	x	x	x	x
38–77	4284.704		x	x	x	x	x		x	x	x	x	x
		Normal samples											
		1	2	3	4	5	6	7	8	9	10	11	12
48–84	4135.596	x		x		x	x	x	x	x	x	x	x
45–84	4378.815			x									
38–84	5041.603						x						
37–84	5154.762												
34–84	5472.149	x	x				x		x	x			x
28–84	6178.904												
Intact PTH	9424.716											x	x
34–77	4715.25												
37–77	4397.863	x		x			x	x		x			
38–77	4284.704	x								x			

[a] amu, atomic mass unit.

As demonstrated in the top-down analysis described above, we were able to simultaneously extract numerous PTH variants with a single, high-affinity polyclonal antibody, and the selection of the epitope was directed by the desired assay target (i.e., intact and N-terminal variants). Our primary goal was to differentiate between intact PTH (1-84) and N-terminal variant PTH (7-84), while

simultaneously identifying any additional N-terminal heterogeneity throughout the molecule. The results of these top-down experiments allowed the development of an initial standard profile for PTH. Clearly, this profile is not finite, and may be expanded to include additional variants found through literature search and/or complementary full-length studies. However, this standard profile provided an initial determination of target sequences for developing specific SRM assays.

SELECTION OF TRANSITIONS FOR SRM

During LC-MS/MS analysis, multiple charge states and fragmentation ions are generated from each fragment, resulting in upward of 1000 different precursor/product transitions possible for PTH digested with trypsin. Owing to time and cost restrictions, the empirical investigation of each transition was not efficient; therefore, a workflow incorporating predictive algorithms with iterative optimization was used to predict the optimal transitions for routine monitoring of tryptic fragments. The workflow we developed using Pinpoint for development of multiplexed SRM assays is shown in **Figure 24**. The strategy facilitated the translation of empirically obtained peptide intensity and fragmentation behavior from high-resolution LC-MS/MS to triple-quadrupole MS SRM assays. Inherent to the success of the workflow was the similarity of peptide ion frag- mentation behavior in trap and triple-quadrupole instruments (163). Empirical data from such LC-MS/MS experiments were used in conjunction with computational methods (e.g., in silico tryptic digestions and prediction of SRM transitions) to enhance the design of effective SRM assays for selected PTH peptides.

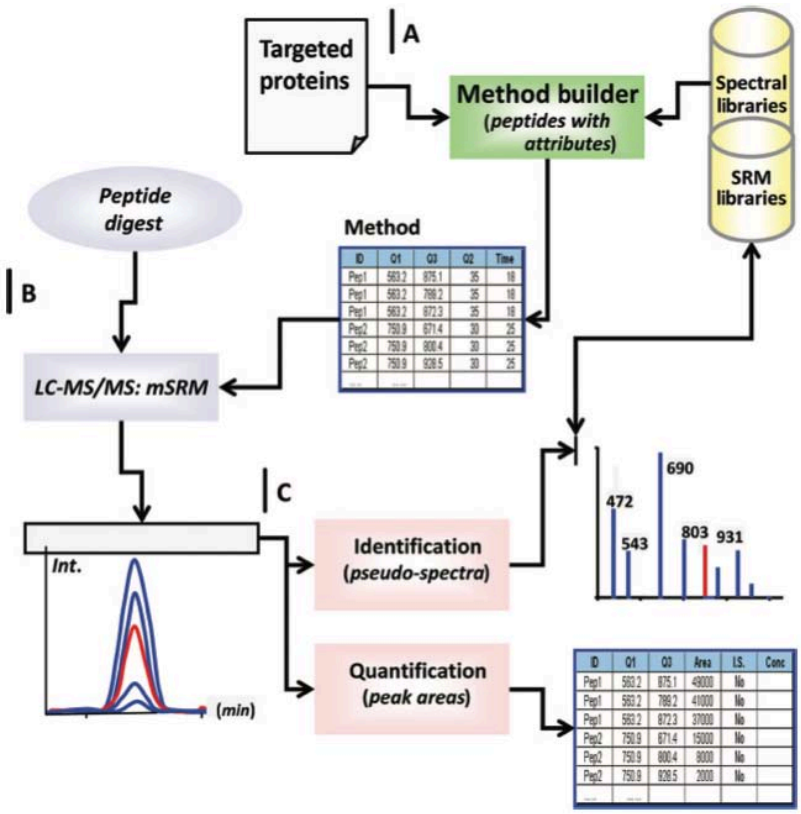

Figure 24: Pinpoint workflow for development of multiplexed SRM assays.Q, quadrupole; mSRM, multiple SRM; Int., intensity; I.S., internal standard; Conc, concentration. Time measurements are in minutes (min).

Using this approach, we generated an initial list of transitions (data not shown) queried empirically to produce an LC-MS/MS profile initially based on 4 tryptic peptides that collectively spanned >50% of the full-length PTH sequence (45 of 84 amino acids). Of these, SVSEIQLMHNLGK [amino acid (aa)1–13] was monitored to represent PTH species with an intact N-terminus—i.e., PTH (1-84). Other tryptic peptides, HLNSMER (aa14-20), LDQVHN FVALGAPLAPR (aa28-44), and ADVNVLTK (aa73-80) were included for monitoring across the PTH sequence. In addition, transitions for 2 truncated tryptic peptides, LMHNLGK (aa7–13) and FVALGAPLAPR (aa34 – 44), were added to the

profile to monitor for truncated variants PTH (7-84) and PTH (34-84), respectively. In summary, 32 SRM transitions tuned to these 6 peptides were used to monitor intact and variant forms of PTH (Fig. 23C presents the intact peptide identities).

GENERATION OF STANDARD CURVES AND LIMITS OF DETECTION AND QUANTIFICATION

We used rhPTH spiked into stock human blood plasma to create calibration curves for all target tryptic peptides through serial dilution. As illustrated in **Figure 25** for peptides LQDVHNFVALGAPLAPR (aa28-44) and SVSEIQLMHNLGK (aa1-13) respectively, SRM transitions for the 4 wild-type tryptic fragments exhibited linear responses ($R2 = 0.90 – 0.99$) relative to rhPTH concentration, with limits of detection for intact PTH of 8 ng/L and limits of quantification for these peptides calculated at 31 and 16 ng/L, respectively. Standard error of analysis for all triplicate measurements in the curves ranged from 3% to 12% for all peptides with <5% chromatographic drift between replicates. In addition, all experimental peptide measurements were calculated relative to heavy-labeled internal standards, and the CVs of integrated areas under the curve for 54 separate measurements (for each heavy peptide) ranged from 5% to 9%. Monitoring of variant SRM transitions showed no inflections relative to rhPTH concentration, as may be expected owing to the absence of truncated variants in the stock rhPTH.

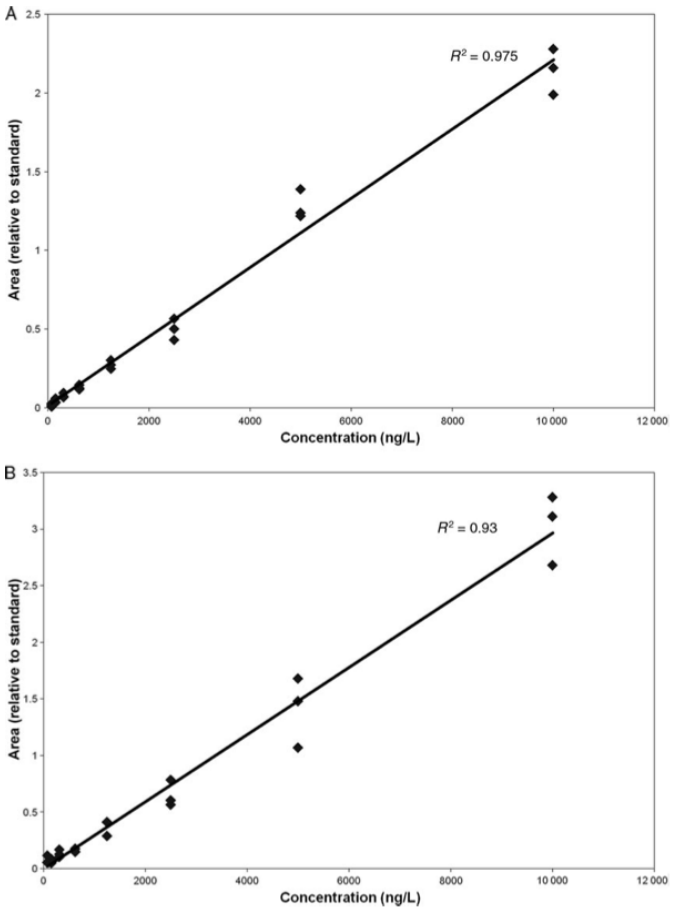

Figure 25: SRM calibration curves for PTH peptides. A) Peptide LQDVHNFVALGAPL-APR aa28–44. B) Peptide SVSEIQLMHNLGK aa1–13.

EVALUATION OF CLINICAL SAMPLES

Initial SRM data were acquired from replicate plasma samples. Chromatograms for peptides SVSEIQLM HNLGK (aa1–13), LQDVHNFVALGAPLAPR (aa28 – 44), and LMHNLGK (aa7–13) are shown in **Figure 26**. Peak integration area and individual fragment transitions for both light and heavy peptides are illustrated. The light and heavy peptides coeluted precisely in all samples. Further SRM experiments were then carried out on the cohort of renal failure (n = 12) and

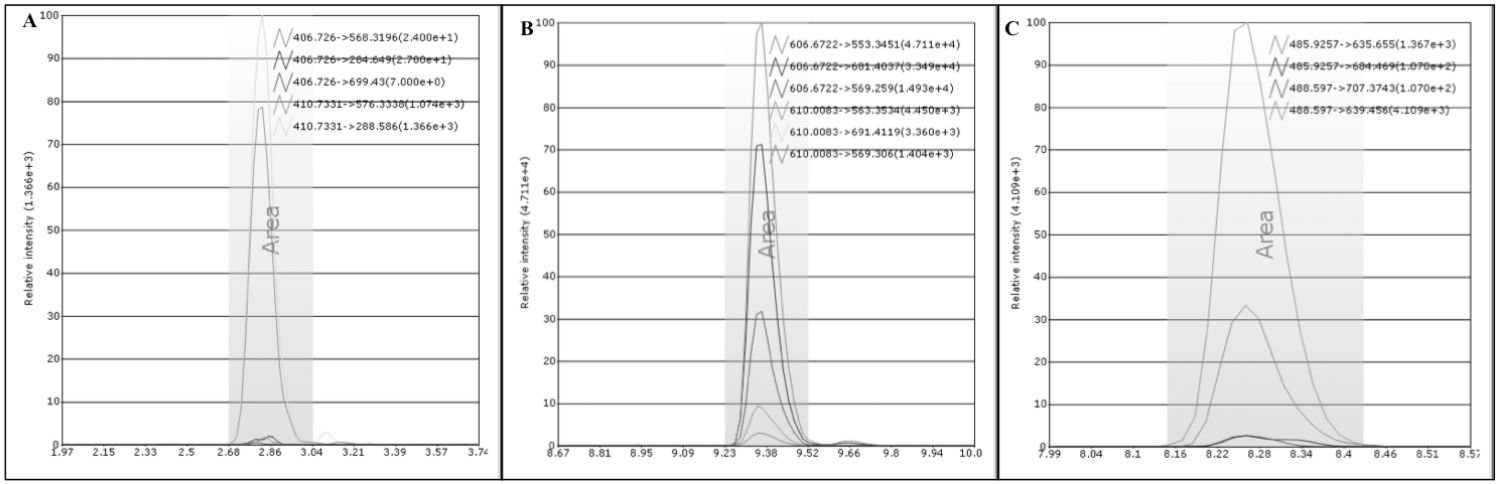

Figure 26: Chromatograms for peptides SVSEIQLM HNLGK (aa1–13), LQDVHNFVALGAPLAPR (aa28 – 44), and LMHNLGK (aa7–13) for A, B, and C, respectively. Peak integration area and individual fragment transitions for both light and heavy peptides are illustrated.

normal (n = 12) clinical samples. Based on the MALDI-TOF MS data presented in **Figure 23**, bottom panel, and **Table 6**, the most prominent PTH variant in the renal failure samples was PTH (34-84). To quantify this observation with SRM, we interrogated all samples to determine the expression ratios of renal failure to normal for the various target peptides, including FVALGAPLAPR (aa34-84), which should be specific to the 34-84 variant. Chromatographic data from single renal failure samples for peptides FVALGAPLAPR (aa34-84) and SVSEIQLM HNLGK (aa1-13) are shown in **Figure 27**.

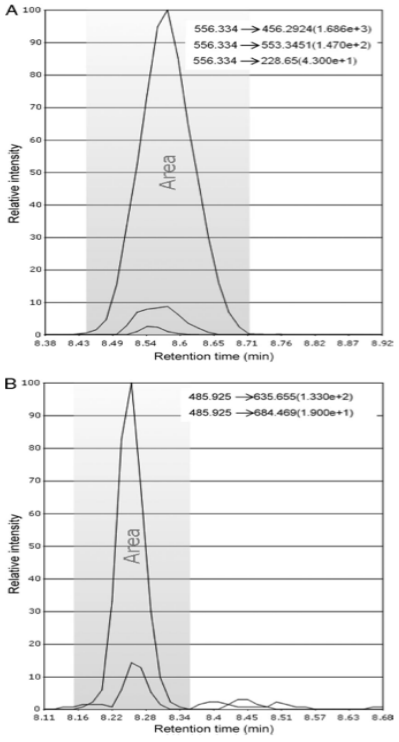

Figure 27. Pinpoint SRM data from clinical samples of normal and renal failure patients. Chromatographic data illustrate peak integration area and individual fragment transitions for peptides from single renal failure samples. (A), Semitryptic peptide FVALGAPLAPR (aa34–44), specific to the 34–84 variant (see Fig. 1). (B), Tryptic peptide SVSEIQLMHNLGK (aa1–13).

The peak integration area and individual coeluting fragment transitions for each peptide are illustrated. Similar chromatograms were obtained for peptides LQDVH NFVALGAPLAPR (aa28-44), HLNSMER (aa14-20), and ADVNVLTK (aa73-80) (data not shown). The sample variances and expression ratios of renal failure to normal clinical samples for each peptide are shown in **Figure 28**. The expression ratios for the peptides ranged from 4.4 for FVALGAPLAPR (aa34-84) to 12.3 for SVSEIQLMHNLGK (aa1-13).

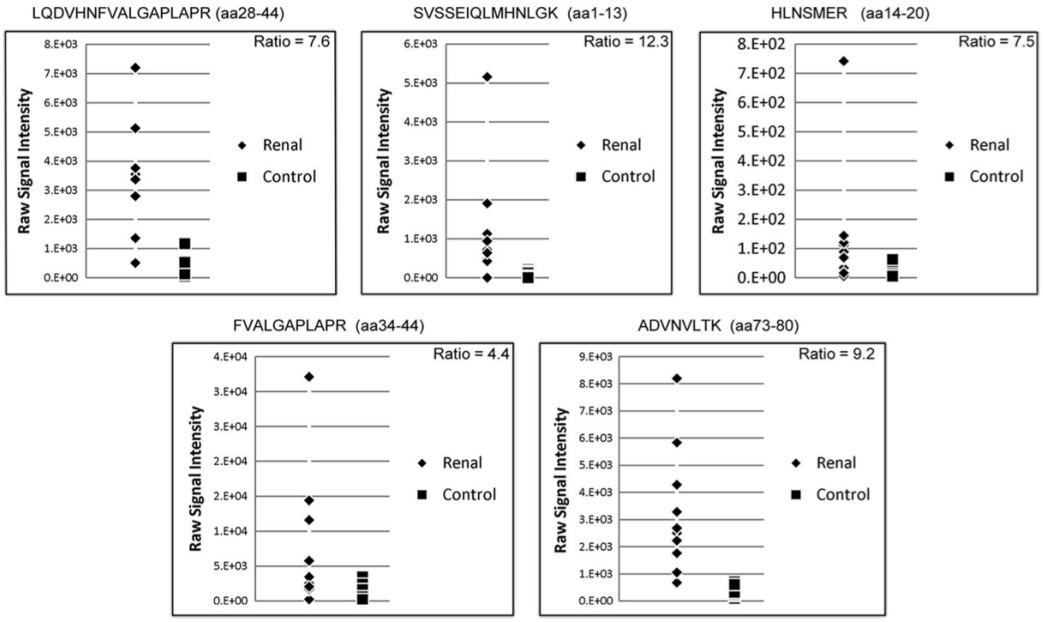

Figure 28. SRM quantitative ratios and sample variances of PTH peptides in samples from renal failure patients (Renal) and healthy controls. Ratios refer to the average value of the renal cohort divided by the average value of the healthy control cohort.

We did not detect notable quantities of peptide LMHNLGK (aa 7–13) in these samples. Sample variances illustrated in the scatter plots in Fig. 5 demonstrate that the renal failure and normal samples groups were clearly segregated by the 5 target peptides.

Many current clinical assays are based on the quantification of an analyte (protein) bound to an immobilized antibody and detected with another antibody labeled with a fluorophore, radioisotope, or reporter enzyme. For proteins of clinical interest, these techniques are limited by the ability of the antibodies to discriminate microheterogeneity in the target analytes, i.e., different molecular species that are very similar in structure. This limitation means that current assays do not capture the full information content of a target analyte (and its variants), which often results in ambiguities in the exact molecular species under investigation. Because upstream causes and downstream effects of disease are often due to such structural modifications, these limitations represent significant problems during the routine analysis of clinically significant analytes. A solution to this problem is to use mass spectrometry to accurately detect, identify, and quantify heterogeneous ligands captured by antibodies.

We developed an SRM-MSIA capable of simultaneously monitoring full-length PTH and truncated variants with analytical metrics suitable for clinical research use. The primary object of our investigations was the design of assays able to capture data on 2 of these species — PTH (1-84) (intact) and PTH (7-84) (an N-terminal variant). Through judicious choice of antibody, we eliminated

potentially confounding data from PTH (1-34) (because it was not captured and did not enter into the analysis). Using a workflow incorporating postcapture tryptic digestion, surrogate peptides representative of these 2 species were generated and monitored by using SRM. In addition, tryptic fragments spanning other regions of PTH were incorporated into the analysis. Relative ion signals for these species confirmed that the assay was functional and created the basis for a standard PTH profile. This standard profile was expanded to include a peptide representative of a novel clinical variant PTH (34-84), clipped at the N-terminus. In its present form, 32 SRM transitions are analyzed in a multiplexed assay to monitor nonvariant PTH sequences with >50% sequence coverage, as well as the 2 truncated variants. In further work, a systematic workflow allowed for the construction of an expandable variant map that presently contains an additional 8 molecular forms of PTH, including variants exhibiting conserved C-terminal truncations (i.e., truncations at PTH77). These newfound variants can be regarded in only 2 ways—as novel molecular forms of potential clinical value, or analytical nuisances that stand to confound PTH analysis. In either case, construction of assays responsive to such possibilities is critical to achieving the most accurate qualitative and quantitative definitions of PTH and its related variants. Given that such differentiation is now warranted in clinical research applications, rationally designed MSIAs and associated integrated workflows, as presented here, will facilitate this goal.

Chapter 9

PERFORMANCE CHARACTERISTICS OF INTACT (I)-PTH ASSAYS RELATIVE TO A MASS SPECTROMETRIC IMMUNOASSAY FOR PARATHYROID HORMONE

In the present study, a mass spectrometric immunoassay specific for parathyroid hormone is evaluated relative to two Intact (I)-PTH assays: the Roche *Cobas* assay and the Beckman Coulter *Access 2* assay. Recent studies have shown significant variability among PTH assays, with one study reporting PTH levels ranging from 60 – 152%, on average, relative to a third generation PTH assay (164, 165). This is of significance due to (I)-PTH assays routine use in the management of end stage renal disease. Thus, variability among commercial PTH assays could, conceivably, present adverse patient outcomes. Although much work has been done on establishing the variability among conventional immunoassays, there exists a need to establish a gold-standard reference method that is *molecule specifi*c and not *immunereactive specific*. This may be accomplished via the use of a mass spectrometric immunoassay whereby the analyte is captured using an antibody (or multiple antibodies) with an epitope intelligently selected within the context of a protein's established circulating presentation (which may be determined from mass spectrometric population studies population studies (21)), followed by unambiguous mass spectrometric detection. Therefore, determining the extent to which (I)-PTH assays report parathyroid hormone levels relative to unequivocal mass spectrometric detection

of *intact N-terminal PTH*, the portion of the molecule responsible for exerting the classical effects of maintaining calcium homeostasis, may provide a definitive reference assay. This would not only aid in determine the relative degree of PTH heterogeneity interference within commercial assays, but ensure that commercial assays provide adequate levels of performance for the diagnosis and treatment of end-stage renal disease.

EXPERIMENTAL

SAMPLES

For the *Cobas* study, a collection of 129 human samples comprised of a mix of plasma (K2 EDTA collection tubes) and serum (silicone-coated interior collection tubes) samples were collected under an Institutional Review Board approved protocol. All samples were collected with informed consent. Samples were assayed blind and are assumed to vary in clinical severity. For the *Access 2* study, eighty-nine serum samples (silicone-coated interior collection tubes) were collected under an Institutional Review Board approved protocol. All samples were collected with informed consent. Samples were assayed blind and are assumed to vary in clinical severity. Samples were frozen at -80 °C until use.

ASSAYS

(I)-PTH assays (*Cobas* assay; Roche Diagnostics, Indianapolis, and *Access 2* assay; Beckman Coulter, Fullerton, CA) were run according to the manufactures protocol.

The mass spectrometric immunoassay for parathyroid hormone was run in SRM-mode as previously described (26).

STATISTICAL ANALYSIS

Patient data was processed using Microsoft Excel 2007. Linear regression analysis was performed between (I)-PTH assays relative to the mass spectrometric method.

RESULTS AND DISCUSSION

ROCHE COBAS PTH ASSAY VS. MSIA FOR PTH

One hundred and twenty nine human samples were assayed over a period of three days. The tryptic/SRM PTH peptides (1-13), (14-20), (28-44), (34-44), and (73-80) were quantified, as previously described (26). Duplicate samples were run in parallel on an automated second-generation PTH assay (i.e. an Intact (I)-PTH Assay; the *Cobas* platform from Roche Diagnostics) (166, 167). The *Cobas* assay, which utilizes electrochemiluminescence detection, incorporates a capture antibody specific for the C-terminal portion of the molecule, PTH (38-84), and a reporter antibody specific for the N-terminal PTH (1-37) region of the molecule. **Figure 29A** shows a side-by-side comparison of PTH (1-13) quantification relative to the *Cobas* assay. Regression analysis produced and equation of $y = 0.83x - 15.76$ with $R^2 = 0.84$. Despite the slope ($m = 0.83$) and R^2 value indicating a relatively strong assay correlation, thus supporting the relative efficacy of the PTH MSIA, the < 1 slope and negative y-intercept is suggestive that the *Cobas*

assay is likely cross-reacting with N-terminally truncated PTH variants and that there is a back-ground level assay interference, hence the assays tendency to presumably overestimate intact PTH levels. **Figure 29B** presents a similar analysis but uses quantification of PTH (73-80) as the comparison. Regression analysis produced the equation of $y = 3.38x + 62.21$ with $R^2 = 0.53$. The > 1 slope and positive y-intercept may be interpreted in the context of PTH presentation in serum largely existing as N-terminally truncated forms, and due to the MSIA's ability to distinguish between intact N-terminal PTH (1-13) and the C-terminal region of the molecule (73-80) via the use of signature SRM tryptic peptides, the assay provides a higher-degree of information content regarding the true presentation PTH as it exists in circulation. **Table 7** presents sample data from the first 10 patients assayed on day 1. Indeed, 10 out of 10 samples report higher PTH levels on the *Cobas* assay relative to quantification of PTH (1-13) via MSIA quantification, with signature peptides from the mid to C-terminal region of PTH showing substantial elevated levels of PTH degradation. For example, *patient #8* had a PTH (1-13) concentration of 321 pg/mL (*Cobas* PTH concentration of 372 pg/mL) and a PTH (73-80) concentrations of 2373 pg/mL. Interestingly, quantification of PTH (14-20) is lower than PTH (1-13) in most samples (it might be assumed that PTH (14-20) would be at least be equal in concentration, if not elevated). This seemingly irregular result might be explained by a few recent studies. One study presented data from third generation PTH assays (e.g. Scantibodies PTH assay) coupled with HPLC separation of PTH isoforms.

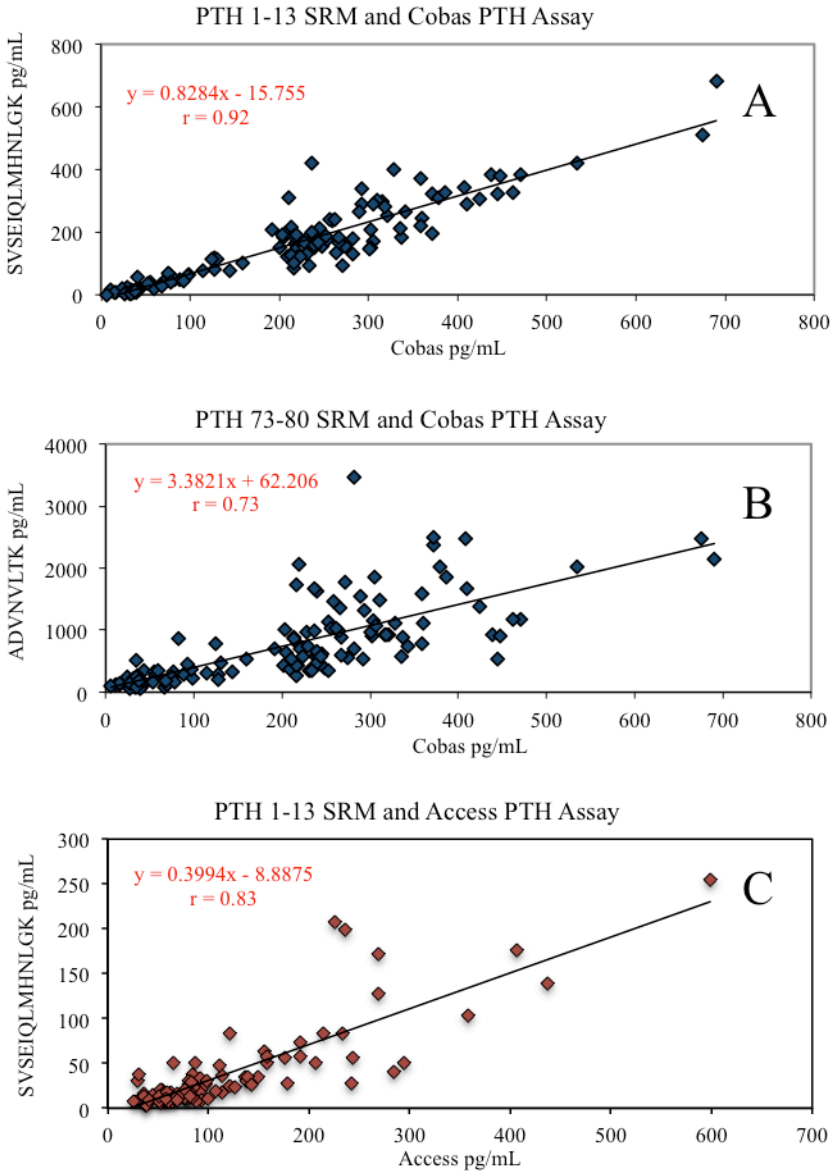

Figure 29: Commercial (I)-PTH assays vs PTH MSIA assay. A and B: (I)-PTH values for 129 patient samples measured with the commercial cobas (I)-PTH assay (x-axis) plotted against PTH 1-13 (A) and PTH 73-80 (B) obtained with the PTH MSIA (y-axis). C: (I)-PTH values for 89 (separate cohort) patient samples measured with the commercial access (I)-PTH assay (x-axis) plotted against PTH 1-13 (C) obtained with the PTH MSIA (y-axis). Linear regression analysis was performed.

This type of separation yielded a novel immunoreactive variant of PTH that was slightly more hydrophilic, but as-of-yet, structurally unconfirmed isoform of PTH (114, 168). Repeat HPLC separation of this novel PTH isoform coupled with second-generation PTH assays with epitopes in the 12-18 and 12-24 region resulted in poor immunoreactivity. Conversely, this variant reacts normally in second generation assays that have 26-32 epitopes, suggesting some type of modification around residues 12-18 (114). Although unconfirmed, residue 17, a serine, is hypothesized to exist as a phosphorylated variant. Subsequent PTH SRM MSIA studies will be specific for this putative variant as well. SRM quantification data representing PTH (1-13), (14-20), (28-44), (34-44), and (73-80) is not shown.

BECKMAN ACCESS PTH ASSAY VS. MSIA FOR PTH (AND COBAS ASSAY)

Eighty-nine samples were assayed using both on an electrochemiluminescence detection-based Beckman Coulter *Access 2* PTH platform (167) and a MSIA for PTH (in SRM mode) (26). The *Access 2* PTH assay is an automated second-generation PTH assay (aka an Intact (I)-PTH Assay). Of note, capture and reporter antibodies epitopes are proprietary information and thus unknown but are assumed to be fairly similar to the Cobas assay. As seen in **Figure 29C,** a direct comparison of quantification of PTH (1-13) to "Intact" PTH levels on the Beckman assay yields a linear regression equation of $y = 0.3994x - 8.8875$ and an R^2 of 0.68. These results indicate the Beckman assay may be significantly over-

estimating bioactive PTH levels. SRM quantification data representing PTH (1-13), PTH (14-20), PTH (28-44), PTH (34-44), and PTH (73-80) is not shown.

Table 8 presents an overview of the two studies within the context of bioactive PTH quantification. Due to samples from the *Cobas* study containing an excess of clinical samples with relatively high levels of PTH, all samples with PTH > 300pg/mL were removed from this dataset with the intent to provide a more balanced side-by-side comparison (nonetheless, the two cohorts are assumed to be clinically distinct from on another). For comparison purposes, SRM PTH (1-13) quantification is considered the reference assay and is presumed to completely accurate in representing bioactive intact PTH due to antibody specificity and unequivocal, *molecule specific*, mass spectrometric detection of the intact N-terminus. The *percent detected* is equivalent to the average ((I)-PTH / MSIA) multiplied by 100. The *Cobas* and *Access 2* assays exhibited large disparities relative to the reference assay: 202% and 452%, respectively (statistically significant from the SRM PTH [1-13] quantification at $p < 0.001$ for both assays). This is striking when one considers the ramifications in regards to the personalized treatment of parathyroid disorders which include administration of specific dosage quantities of Vitamin D sterols based upon specific PTH levels and whether or not to prescribe a parathyroidectomy (i.e. removal of one or both of the parathyroid glands), also determined by circulating PTH levels (169). In other words, a patient could conceivably receive an entirely different diagnosis and treatment depending entirely upon the specific assay the physician happens to

be using (e.g. the *Cobas* or *Access 2*). Due to the blind nature of this study (sample identify information was not available at time of publication), the large discrepancy between the mean of [1-13] MSIA in the *Cobas* study relative to the *Access 2* is assumed to be due to disparate clinical cohorts.

Due the increased presence of C-PTH fragments in certain ailments such as with end stage renal disease (e.g. PTH (34-84) (26)), this side-by-side comparison of two second-generation PTH platforms with a PTH mass spectrometric immunoassay supports the idea that there exists a clinical need for a *total* PTH quantification (intact N-terminal PTH and variants). At the very least, a better understanding of the relative degree of PTH variant interference across the spectrum of the parathyroid hormone molecule (e.g. PTH (1-13), (14-20), (28-44), (34-44), and (73-80)) with regards to commercially available assays is clinically beneficial.

Table 7: Cobas and PTH MSIA Quantification Values for the First Ten Patients Assayed						
Clinical Samples	Cobas assay: pg/mL	PTH MSIA: SVSEIQLMHNLGK PTH (1-13) pg/mL	PTH MSIA: HLNSMER PTH (14-20) pg/mL	PTH MSIA: LQDVHNFVAL-GAPLAPR PTH (28 to 44) pg/mL	PTH MSIA: ADVNVLTK PTH (73 to 80) pg/mL	PTH MSIA: FVALGAPLAPR PTH (34-44) pg/mL
Day 1 - Patient 1	292	291	224	318	534	187
Day 1 - Patient 2	33	10	ND	27	86	ND
Day 1 - Patient 3	127	118	67	125	292	60
Day 1 - Patient 4	218	162	91	162	435	48
Day 1 - Patient 5	67	33	ND	54	87	39
Day 1 - Patient 6	534	421	359	805	2017	550
Day 1 - Patient 7	410	290	257	560	1660	458
Day 1 - Patient 8	372	321	119	555	2373	545
Day 1 - Patient 9	43	22	N/D	32	355	20
Day 1 - Patient 10	305	172	88	480	1852	357
*ND (not detected) signifies signal below the LOQ.						

Table 8: An overview of the two studies within the context of bioactive PTH quantification

	[1-13] MSIA	Roche Cobas	[1-13] MSIA	Beckman Coulter Access 2
	n = 92; < 300 pg/mL		n = 86; < 300 pg/mL	
Mean PTH pg/mL	109.0	153.0	33.8	105.0
Standard Deviation pg/mL	85.0	97.0	38.0	68.0
Difference pg/mL	~0	44.0	~0	73.0
Standard Deviation pg/mL	~0	44.0	~0	49.0
Percent Detected pg/mL	100%	202%	100%	452%
Standard Deviation pg/mL	~0%	142%	~0%	254%
Slope	1	0.80	1	0.39
Y-Intercept	~0	-10.73	~0	-8.15
r	1.0	0.92	1.0	0.83
T-test	P < 0.001		P < 0.001	

The *percent detected* is equivalent to the average ((I)-PTH / MSIA) x 100. The *difference* is equivalent to average ((I)-PTH) – (MSIA).

Chapter 10

CONCLUSION

As proteomics hinges on moving into widespread use in clinical diagnostics, there is an opportunity at hand. Through targeted proteomics efforts focused on full-length characterization of human proteins, studies such as those described herein have the potential to begin documenting the enigmatic landscape of protein diversity across human populations. Beyond the exciting prospects this has in supporting the expansion and revision of currently held assumptions in protein biology (e.g. parathyroid hormone), the notion of reporting the natural variation of protein heterogeneity may have long-term implications for diagnostics. Indeed, the RANTES MSIA study presented herein describes nineteen variant forms comprised of truncated, glycated, glycosylated, and oxidized RANTES that collectively discriminated between healthy, T2D, congestive heart failure, myocardial infarction, and various combinations thereof -- in a single multiplexed assay (**Figures 17-20**). This exemplar of variant efficacy towards diagnosis may be just the beginning and the prognosis value remains to be seen.

However, a more pertinent consideration is the implication protein diversity has for candidate biomarkers discovered using “peptide fingerprints” (170). As candidate biomarkers transition down the “biomarker pipeline” towards verification and validation, quantification approaches based on surrogate peptide detection modalities (e.g. SRM based-assays) should be thoughtful of protein diversity in the context of interference as well as diagnostic usefulness. This holds

true for classical markers that have remained relatively accepted since their implementation into mainstream diagnostics prior to MALDI and ESI (e.g. insulin and C-peptide). Indeed, Duncan et al. cautions that "quantification of any modified or potentially modified protein, *e.g.*, oxidized, nitrated, alternatively spliced, truncated forms, *etc.* presents a dilemma. Whether measurement is based on an unmodified or modified peptide, no qualitative or quantitative insights into any of the other forms are available…Under these circumstances the "verification" study may cloud rather than clarify."(170). As such, next-generation assays employed to quantify insulin, C-peptide, RANTES, and/or parathyroid hormone within the context of diabetes, kidney disease, and related comorbidities stand to benefit from the work presented here.

REFERENCES

1. Aebersold RH, Leavitt J, Saavedra RA, Hood LE, Kent SB. Internal amino acid sequence analysis of proteins separated by one- or two-dimensional gel electrophoresis after in situ protease digestion on nitrocellulose. Proc Natl Acad Sci U S A 1987;84:6970-4.

2. Tarroux P, Vincens P, Rabilloud T. Hermes: A second generation approach to the automatic analysis of two dimensional electrophoresis gels. Part v: Data analysis. Electrophoresis 1987;8:187-99.

3. Patterson SD, Aebersold RH. Proteomics: The first decade and beyond. Nat Genet 2003;33 Suppl:311-23.

4. Anderson NG, Anderson L. The human protein index. Clin Chem 1982;28:739-48.

5. Fenn JB, Mann M, Meng CK, Wong SF, Whitehouse CM. Electrospray ionization for mass spectrometry of large biomolecules. Science 1989;246:64-71.

6. Karas M, Hillenkamp F. Laser desorption ionization of proteins with molecular masses exceeding 10,000 daltons. Anal Chem 1988;60:2299-301.

7. Gygi SP, Corthals GL, Zhang Y, Rochon Y, Aebersold R. Evaluation of two-dimensional gel electrophoresis-based proteome analysis technology. Proceedings of the National Academy of Sciences 2000;97:9390.

8. Mauri P, Scigelova M. Multidimensional protein identification technology for clinical proteomic analysis. Clin Chem Lab Med 2009;47:636-46.

9. Wilkins MR, Sanchez JC, Gooley AA, Appel RD, Humphery-Smith I, Hochstrasser DF, Williams KL. Progress with proteome projects: Why all proteins expressed by a genome should be identified and how to do it. Biotechnol Genet Eng Rev 1996;13:19-50.

10. Parker CE, Pearson TW, Anderson NL, Borchers CH. Mass-spectrometry-based clinical proteomics--a review and prospective. Analyst 2010;135:1830-8.

11. Anderson NL. The clinical plasma proteome: A survey of clinical assays for proteins in plasma and serum. Clin Chem 2010;56:177-85.

12. Anderson L. Candidate-based proteomics in the search for biomarkers of cardiovascular disease. J Physiol 2005;563:23-60.

13. Anderson NL, Anderson NG. The human plasma proteome: History, character, and diagnostic prospects. Mol Cell Proteomics 2002;1:845-67.

14. Whiteaker JR, Zhao L, Anderson L, Paulovich AG. An automated and multiplexed method for high throughput peptide immunoaffinity enrichment and multiple reaction monitoring mass spectrometry-based quantification of protein biomarkers. Mol Cell Proteomics 2010;9:184-96.

15. Niederkofler EE, Kiernan UA, O'Rear J, Menon S, Saghir S, Protter AA, et al. Detection of endogenous b-type natriuretic peptide at very low concentrations in patients with heart failure. Circ Heart Fail 2008;1:258-64.

16. Oran PE, Jarvis JW, Borges CR, Nelson RW. C-peptide microheterogeneity in type 2 diabetes populations. PROTEOMICS - CLINICAL APPLICATIONS 2010;4:106-11.

17. Oran PE, Sherma ND, Borges CR, Jarvis JW, Nelson RW. Intrapersonal and populational heterogeneity of the chemokine rantes. Clinical chemistry 2010;56:1432.

18. Tubbs KA, Nedelkov D, Nelson RW. Detection and quantification of beta-2-microglobulin using mass spectrometric immunoassay. Anal Biochem 2001;289:26-35.

19. Anderson NL, Anderson NG, Haines LR, Hardie DB, Olafson RW, Pearson TW. Mass spectrometric quantitation of peptides and proteins using stable isotope standards and capture by anti-peptide antibodies (siscapa). J Proteome Res 2004;3:235-44.

20. Oran PE, Jarvis JW, Borges CR, Sherma ND, Nelson RW. Mass spectrometric immunoassay of intact insulin and related variants for population proteomics studies. PROTEOMICS – Clinical Applications 2011;5:454-9.

21. Borges CR, Rehder DS, Jarvis JW, Schaab MR, Oran PE, Nelson RW. Full-length characterization of proteins in human populations. Clin Chem 2010;56:202-11.

22. Niederkofler EE, Tubbs KA, Gruber K, Nedelkov D, Kiernan UA, Williams P, Nelson RW. Determination of beta-2 microglobulin levels in plasma using a high-throughput mass spectrometric immunoassay system. Anal Chem 2001;73:3294-9.

23. Niederkofler EE, Tubbs KA, Kiernan UA, Nedelkov D, Nelson RW. Novel mass spectrometric immunoassays for the rapid structural characterization of plasma apolipoproteins. J Lipid Res 2003;44:630-9.

24. Oran PE, Sherma ND, Borges CR, Jarvis JW, Nelson RW. Intrapersonal and populational heterogeneity of the chemokine rantes. Clin Chem 2010;56:1432-41.

25. Nelson RW, Krone JR, Bieber AL, Williams P. Mass spectrometric immunoassay. Anal Chem 1995;67:1153-8.

26. Lopez MF, Rezai T, Sarracino DA, Prakash A, Krastins B, Athanas M, et al. Selected reaction monitoring-mass spectrometric immunoassay responsive to parathyroid hormone and related variants. Clin Chem 2010;56:281-90.

27. Borges CR, Jarvis JW, Oran PE, Rogers SP, Nelson RW. Population studies of intact vitamin d binding protein by affinity capture esi-tof-ms. J Biomol Tech 2008;19:167-76.

28. Tubbs KA, Nedelkov D, Nelson RW. Detection and quantification of [beta]-2-microglobulin using mass spectrometric immunoassay. Analytical Biochemistry 2001;289:26-35.

29. Nelson RW, Borges CR. Mass spectrometric immunoassay revisited. Journal of The American Society for Mass Spectrometry:1-9.

30. Nelson RW, Nedelkov D, Tubbs KA, Kiernan UA. Quantitative mass spectrometric immunoassay of insulin like growth factor 1. Journal of Proteome Research 2004;3:851-5.

31. Nedelkov D, Phillips DA, Tubbs KA, Nelson RW. Investigation of human protein variants and their frequency in the general population. Mol Cell Proteomics 2007;6:1183-7.

32. Oran PE, Jarvis JW, Borges CR, Sherma ND, Nelson RW. Mass spectrometric immunoassay of intact insulin and related variants for population proteomics studies. PROTEOMICSñClinical Applications.

33. Pertea M, Salzberg SL. Between a chicken and a grape: Estimating the number of human genes. Genome biology 2010;11:206.

34. Wild S, Roglic G, Green A, Sicree R, King H. Global prevalence of diabetes: Estimates for the year 2000 and projections for 2030. Diabetes Care 2004;27:1047-53.

35. Narayan KM, Boyle JP, Thompson TJ, Sorensen SW, Williamson DF. Lifetime risk for diabetes mellitus in the united states. JAMA 2003;290:1884-90.

36. Hogan P, Dall T, Nikolov P. Economic costs of diabetes in the us in 2002. Diabetes Care 2003;26:917-32.

37. Diagnosis and classification of diabetes mellitus. Diabetes Care 2011;34 Suppl 1:S62-9.

38. Alberti KG, Zimmet PZ. Definition, diagnosis and classification of diabetes mellitus and its complications. Part 1: Diagnosis and classification of diabetes mellitus provisional report of a who consultation. Diabet Med 1998;15:539-53.

39. Turk Z, Mesic R, Benko B. Comparison of advanced glycation endproducts on haemoglobin (hb-age) and haemoglobin a1c for the assessment of diabetic control. Clin Chim Acta 1998;277:159-70.

40. Miller S, St Onge EL. Sitagliptin: A dipeptidyl peptidase iv inhibitor for the treatment of type 2 diabetes. Ann Pharmacother 2006;40:1336-43.

41. Steiner DF, Clark JL, Nolan C, Rubenstein AH, Margoliash E, Aten B, Oyer PE. Proinsulin and the biosynthesis of insulin. Recent Prog Horm Res 1969;25:207-82.

42. Marques RG, Fontaine MJ, Rogers J. C-peptide: Much more than a byproduct of insulin biosynthesis. Pancreas 2004;29:231-8.

43. Chevenne D, Trivin F, Porquet D. Insulin assays and reference values. Diabetes Metab 1999;25:459-76.

44. Torn C. C-peptide and autoimmune markers in diabetes. Clin Lab 2003;49:1-10.

45. Polonsky KS, Licinio-Paixao J, Given BD, Pugh W, Rue P, Galloway J, et al. Use of biosynthetic human c-peptide in the measurement of insulin

secretion rates in normal volunteers and type i diabetic patients. J Clin Invest 1986;77:98-105.

46. Polonsky KS, Given BD, Hirsch L, Shapiro ET, Tillil H, Beebe C, et al. Quantitative study of insulin secretion and clearance in normal and obese subjects. J Clin Invest 1988;81:435-41.

47. Steiner DF, Rubenstein AH. Proinsulin c-peptide--biological activity? Science 1997;277:531-2.

48. Ohtomo Y, Aperia A, Sahlgren B, Johansson BL, Wahren J. C-peptide stimulates rat renal tubular na+, k(+)-atpase activity in synergism with neuropeptide y. Diabetologia 1996;39:199-205.

49. Zhang W, Yorek M, Pierson CR, Murakawa Y, Breidenbach A, Sima AA. Human c-peptide dose dependently prevents early neuropathy in the bb/wor-rat. Int J Exp Diabetes Res 2001;2:187-93.

50. Henriksson M, Shafqat J, Liepinsh E, Tally M, Wahren J, Jornvall H, Johansson J. Unordered structured of proinsulin c-peptide in aqueous solution and in the presence of lipid vesicles. Cell Mol Life Sci 2000;57:337-42.

51. Johansson J, Ekberg K, Shafqat J, Henriksson M, Chibalin A, Wahren J, Jornvall H. Molecular effects of proinsulin c-peptide. Biochemical and Biophysical Research Communications 2002;295:1035-40.

52. Borg H, Arnqvist HJ, Bjork E, Bolinder J, Eriksson JW, Nystrom L, et al. Evaluation of the new ada and who criteria for classification of diabetes mellitus in young adult people (15-34 yrs) in the diabetes incidence study in sweden (diss). Diabetologia 2003;46:173-81.

53. Wright-Pascoe R, Mills J, Choo-Kang E, Morrison EY. The role of c-peptide in the classification of diabetes mellitus. West Indian Med J 2000;49:138-42.

54. Ahn CW, Kim HS, Nam JH, Song YD, Lim SK, Kim KR, et al. Clinical characteristics, gad antibody (gada) and change of c-peptide in korean young age of onset diabetic patients. Diabet Med 2002;19:227-33.

55. Ashby JP, Frier BM. Circulating c peptide: Measurement and clinical application. Annals of clinical biochemistry 1981;18:125-30.

56. Rendell M. The expanding clinical use of c-peptide radioimmunoassay. Acta Diabetol Lat 1983;20:105-13.

57. Little RR, Rohlfing CL, Tennill AL, Madsen RW, Polonsky KS, Myers GL, et al. Standardization of c-peptide measurements. Clin Chem 2008;54:1023-6.

58. Kohek M, Leme C, Nakamura IT, De Oliveira SA, Lando V, Mendonca BB. Effects of edta and sodium citrate on hormone measurements by fluorometric (fia) and immunofluorometric (ifma) methods. BMC clinical pathology 2002;2:2.

59. Rogatsky E, Balent B, Goswami G, Tomuta V, Jayatillake H, Cruikshank G, et al. Sensitive quantitative analysis of c-peptide in human plasma by 2-dimensional liquid chromatography-mass spectrometry isotope-dilution assay. Clin Chem 2006;52:872-9.

60. Cabaleiro DR, Stockl D, Kaufman JM, Fiers T, Thienpont LM. Feasibility of standardization of serum c-peptide immunoassays with isotope-dilution liquid chromatography-tandem mass spectrometry. Clinical chemistry 2006;52:1193-6.

61. Fierens C, Thienpont LM, Stockl D, Willekens E, De Leenheer AP. Quantitative analysis of urinary c-peptide by liquid chromatography-tandem mass spectrometry with a stable isotopically labelled internal standard. J Chromatogr A 2000;896:275-8.

62. Fierens C, Stockl D, Baetens D, De Leenheer AP, Thienpont LM. Application of a c-peptide electrospray ionization-isotope dilution-liquid chromatography-tandem mass spectrometry measurement procedure for the evaluation of five c-peptide immunoassays for urine. J Chromatogr B Analyt Technol Biomed Life Sci 2003;792:249-59.

63. Fierens C, Stockl D, Baetens D, De Leenheer AP, Thienpont LM. Standardization of c-peptide measurements in urine by method comparison with isotope-dilution mass spectrometry. Clin Chem 2003;49:992-4.

64. Rodriguez-Cabaleiro D, Stockl D, Thienpont LM. Improvement of sample pretreatment prior to analysis of c-peptide in serum by isotope-dilution liquid chromatography/tandem mass spectrometry. Rapid Commun Mass Spectrom 2005;19:3600-2.

65. Stockl D, Cabaleiro DR, Thienpont LM. Collision-induced dissociation of the [m-2h]2- ion of c-peptide. Rapid Commun Mass Spectrom 2004;18:3140-1.

66. Meier JJ, Nauck MA. Glucagon-like peptide 1(glp-1) in biology and pathology. Diabetes Metab Res Rev 2005;21:91-117.

67. Mannucci E, Pala L, Ciani S, Bardini G, Pezzatini A, Sposato I, et al. Hyperglycaemia increases dipeptidyl peptidase iv activity in diabetes mellitus. Diabetologia 2005;48:1168-72.

68. Verchere CB, Paoletta M, Neerman-Arbez M, Rose K, Irminger JC, Gingerich RL, et al. Des-(27-31)c-peptide. A novel secretory product of the rat pancreatic beta cell produced by truncation of proinsulin connecting peptide in secretory granules. J Biol Chem 1996;271:27475-81.

69. Paoletta M, Kahn SE, Halban PA. Truncated (des-[27-31]) c-peptide is not a major secretory product of human islets. Diabetologia 2002;45:1523-7.

70. Rasmussen HB, Branner S, Wiberg FC, Wagtmann N. Crystal structure of human dipeptidyl peptidase iv/cd26 in complex with a substrate analog. Nat Struct Biol 2003;10:19-25.

71. McIntosh CHS, Demuth H-U, Kim S-J, Pospisilik JA, Pederson RA. Applications of dipeptidyl peptidase iv inhibitors in diabetes mellitus. The International Journal of Biochemistry & Cell Biology 2006;38:860-72.

72. Pauly RP, Demuth HU, Rosche F, Schmidt J, White HA, Lynn F, et al. Improved glucose tolerance in rats treated with the dipeptidyl peptidase iv (cd26) inhibitor ile-thiazolidide. Metabolism 1999;48:385-9.

73. Deacon CF, Hughes TE, Holst JJ. Dipeptidyl peptidase iv inhibition potentiates the insulinotropic effect of glucagon-like peptide 1 in the anesthetized pig. Diabetes 1998;47:764-9.

74. Chan SJ, Seino S, Gruppuso PA, Schwartz R, Steiner DF. A mutation in the b chain coding region is associated with impaired proinsulin conversion in a family with hyperproinsulinemia. Proc Natl Acad Sci U S A 1987;84:2194-7.

75. Yano H, Kitano N, Morimoto M, Polonsky KS, Imura H, Seino Y. A novel point mutation in the human insulin gene giving rise to hyperproinsulinemia (proinsulin kyoto). J Clin Invest 1992;89:1902-7.

76. Minn AH, Kayton M, Lorang D, Hoffmann SC, Harlan DM, Libutti SK, Shalev A. Insulinomas and expression of an insulin splice variant. Lancet 2004;363:363-7.

77. Sakura H, Iwamoto Y, Sakamoto Y, Kuzuya T, Hirata H. Structurally abnormal insulin in a diabetic patient. Characterization of the mutant insulin a3 (val----leu) isolated from the pancreas. J Clin Invest 1986;78:1666-72.

78. Temple RC, Carrington CA, Luzio SD, Owens DR, Schneider AE, Sobey WJ, Hales CN. Insulin deficiency in non-insulin-dependent diabetes. Lancet 1989;1:293-5.

79. Niederkofler EE, Kiernan UA, O'Rear J, Menon S, Saghir S, Protter AA, et al. Detection of endogenous b-type natriuretic peptide at very low concentrations in patients with heart failure. Circulation: Heart Failure 2008;1:258-64.

80. Manley SE, Stratton IM, Clark PM, Luzio SD. Comparison of 11 human insulin assays: Implications for clinical investigation and research. Clin Chem 2007;53:922-32.

81. Kippen AD, Cerini F, Vadas L, Stocklin R, Vu L, Offord RE, Rose K. Development of an isotope dilution assay for precise determination of insulin, c-peptide, and proinsulin levels in non-diabetic and type ii diabetic individuals with comparison to immunoassay. J Biol Chem 1997;272:12513-22.

82. Stocklin R, Vu L, Vadas L, Cerini F, Kippen AD, Offord RE, Rose K. A stable isotope dilution assay for the in vivo determination of insulin levels in humans by mass spectrometry. Diabetes 1997;46:44-50.

83. Darby SM, Miller ML, Allen RO, LeBeau M. A mass spectrometric method for quantitation of intact insulin in blood samples. J Anal Toxicol 2001;25:8-14.

84. Van Uytfanghe K, Rodriguez-Cabaleiro D, Stockl D, Thienpont LM. New liquid chromatography/electrospray ionisation tandem mass spectrometry measurement procedure for quantitative analysis of human insulin in serum. Rapid Commun Mass Spectrom 2007;21:819-21.

85. Thevis M, Thomas A, Schanzer W. Mass spectrometric determination of insulins and their degradation products in sports drug testing. Mass Spectrom Rev 2008;27:35-50.

86. Rehder DS, Borges CR. Possibilities and pitfalls in quantifying the extent of cysteine sulfenic acid modification of specific proteins within complex biofluids. BMC biochemistry 2010;11:25.

87. Oran PE, Jarvis JW, Borges CR, Nelson RW. C-peptide microheterogeneity in type 2 diabetes populations. Proteomics Clin Appl 2010;4:1-6.

88. Karam JH. Pancreatic hormones & antidiabetic drugs. In: Katzung BG, ed. Basic & clinical pharmacology, Vol. 7th ed. Stamford, Connecticut: Appleton & Lange, 1998.

89. Thevis M, Schanzer W. Mass spectrometry in sports drug testing: Structure characterization and analytical assays. Mass Spectrom Rev 2007;26:79-107.

90. Korec R. [50th anniversary of discovery and isolation of insulin. Paulesco 1921, banting best and collip 1922]. Cas Lek Cesk 1971;110:416-8.

91. Oran PE, Jarvis JW, Borges CR, Nelson RW. C-peptide microheterogeneity in type 2 diabetes populations. Proteomics Clin Appl 2010;4:106-11.

92. Lambeir AM, Durinx C, Scharpe S, De Meester I. Dipeptidyl-peptidase iv from bench to bedside: An update on structural properties, functions, and clinical aspects of the enzyme dpp iv. Crit Rev Clin Lab Sci 2003;40:209-94.

93. Stevic R, Zivkovic TB, Erceg P, Milosevic D, Despotovic N, Davidovic M. Oral glucose tolerance test in the assessment of glucose-tolerance in the elderly people. Age Ageing 2007;36:459-62.

94. Yi J, Liu Z, Gelfand CA, Craft D. Investigation of peptide biomarker stability in plasma sample using time-course ms analysis. Vol.: Springer, 2010.

95. Nelson PJ, Krensky AM. Chemokines, chemokine receptors, and allograft rejection. Immunity 2001;14:377-86.

96. Rossi D, Zlotnik A. The biology of chemokines and their receptors. Annu Rev Immunol 2000;18:217-42.

97. Murphy PM, Baggiolini M, Charo IF, Hebert CA, Horuk R, Matsushima K, et al. International union of pharmacology. Xxii. Nomenclature for chemokine receptors. Pharmacol Rev 2000;52:145-76.

98. Segerer S, Nelson PJ, Schlondorff D. Chemokines, chemokine receptors, and renal disease: From basic science to pathophysiologic and therapeutic studies. J Am Soc Nephrol 2000;11:152-76.

99. Niwa Y, Akamatsu H, Niwa H, Sumi H, Ozaki Y, Abe A. Correlation of tissue and plasma rantes levels with disease course in patients with breast or cervical cancer. Clin Cancer Res 2001;7:285-9.

100. Lim JK, Lu W, Hartley O, DeVico AL. N-terminal proteolytic processing by cathepsin g converts rantes/ccl5 and related analogs into a truncated 4-68 variant. J Leukoc Biol 2006;80:1395-404.

101. Oravecz T, Pall M, Roderiquez G, Gorrell MD, Ditto M, Nguyen NY, et al. Regulation of the receptor specificity and function of the chemokine rantes (regulated on activation, normal t cell expressed and secreted) by dipeptidyl peptidase iv (cd26)-mediated cleavage. J Exp Med 1997;186:1865-72.

102. Kameyoshi Y, Dorschner A, Mallet AI, Christophers E, Schroder JM. Cytokine rantes released by thrombin-stimulated platelets is a potent attractant for human eosinophils. J Exp Med 1992;176:587-92.

103. Schall TJ, Jongstra J, Dyer BJ, Jorgensen J, Clayberger C, Davis MM, Krensky AM. A human t cell-specific molecule is a member of a new gene family. J Immunol 1988;141:1018-25.

104. Krensky AM, Ahn YT. Mechanisms of disease: Regulation of rantes (ccl5) in renal disease. Nat Clin Pract Nephrol 2007;3:164-70.

105. Azenshtein E, Luboshits G, Shina S, Neumark E, Shahbazian D, Weil M, et al. The cc chemokine rantes in breast carcinoma progression: Regulation of expression and potential mechanisms of promalignant activity. Cancer Res 2002;62:1093-102.

106. Ng PC, Li K, Leung TF, Wong RP, Li G, Chui KM, et al. Early prediction of sepsis-induced disseminated intravascular coagulation with interleukin-10, interleukin-6, and rantes in preterm infants. Clin Chem 2006;52:1181-9.

107. Herder C, Haastert B, Muller-Scholze S, Koenig W, Thorand B, Holle R, et al. Association of systemic chemokine concentrations with impaired glucose tolerance and type 2 diabetes: Results from the cooperative health research in the region of augsburg survey s4 (kora s4). Diabetes 2005;54 Suppl 2:S11-7.

108. Kaburagi Y, Shimada Y, Nagaoka T, Hasegawa M, Takehara K, Sato S. Enhanced production of cc-chemokines (rantes, mcp-1, mip-1alpha, mip-1beta, and eotaxin) in patients with atopic dermatitis. Arch Dermatol Res 2001;293:350-5.

109. Christodoulakos GE, Lambrinoudaki IV, Economou EV, Papadias C, Vitoratos N, Panoulis CP, et al. Circulating chemoattractants rantes, negatively related to endogenous androgens, and mcp-1 are differentially suppressed by hormone therapy and raloxifene. Atherosclerosis 2007;193:142-50.

110. McIntosh M. The need to characterize and report the normal heterogeneity of proteins in clinical biological samples. J Proteome Res 2007;6:2913.

111. Proost P, Struyf S, Couvreur M, Lenaerts JP, Conings R, Menten P, et al. Posttranslational modifications affect the activity of the human monocyte chemotactic proteins mcp-1 and mcp-2: Identification of mcp-2(6-76) as a natural chemokine inhibitor. J Immunol 1998;160:4034-41.

112. Proost P, De Meester I, Schols D, Struyf S, Lambeir AM, Wuyts A, et al. Amino-terminal truncation of chemokines by cd26/dipeptidyl-peptidase iv. Conversion of rantes into a potent inhibitor of monocyte chemotaxis and hiv-1-infection. J Biol Chem 1998;273:7222-7.

113. D'Amour P, Brossard JH, Rousseau L, Nguyen-Yamamoto L, Nassif E, Lazure C, et al. Structure of non-(1-84) pth fragments secreted by parathyroid glands in primary and secondary hyperparathyroidism. Kidney Int 2005;68:998-1007.

114. D'Amour P. Circulating pth molecular forms: What we know and what we don't. Kidney Int Suppl 2006:S29-33.

115. Levey AS, Stevens LA, Schmid CH, Zhang YL, Castro AF, 3rd, Feldman HI, et al. A new equation to estimate glomerular filtration rate. Ann Intern Med 2009;150:604-12.

116. Usrds 2009 annual data report. http://www.usrds.org/adr.htm (Accessed November, 10 2009).

117. Moe SM. Disorders involving calcium, phosphorus, and magnesium. Prim Care 2008;35:215-37, v-vi.

118. Komaba H, Goto S, Fukagawa M. Critical issues of pth assays in ckd. Bone 2009;44:666-70.

119. Drueke TB. Cell biology of parathyroid gland hyperplasia in chronic renal failure. J Am Soc Nephrol 2000;11:1141-52.

120. Silver J, Kilav R, Naveh-Many T. Mechanisms of secondary hyperparathyroidism. Am J Physiol Renal Physiol 2002;283:F367-76.

121. Segre GV, Niall HD, Habener JF, Potts JT, Jr. Metabolism of parathyroid hormone: Physiologic and clinical significance. Am J Med 1974;56:774-84.

122. Segre GV, Perkins AS, Witters LA, Potts J, Jr. Metabolism of parathyroid hormone by isolated rat kupffer cells and hepatocytes. J Clin Invest 1981;67:449-57.

123. Tregear GW, Van Rietschoten J, Greene E, Keutmann HT, Niall HD, Reit B, et al. Bovine parathyroid hormone: Minimum chain length of synthetic peptide required for biological activity. Endocrinology 1973;93:1349-53.

124. Habener JF, Segre GV, Powell D, Murray TM, Potts JT, Jr. Immunoreactive parathyroid hormone in circulation of man. Nat New Biol 1972;238:152-4.

125. Woodhead JS, Walker DA. Assay of parathyroid hormone in human serum and its uses. Ann Clin Biochem 1976;13:549-54.

126. Arnaud CD, Tsao HS, Littledike T. Radioimmunoassay of human parathyroid hormone in serum. J Clin Invest 1971;50:21-34.

127. Solal ME, Sebert JL, Boudailliez B, Marie A, Moriniere P, Gueris J, et al. Comparison of intact, midregion, and carboxy terminal assays of parathyroid hormone for the diagnosis of bone disease in hemodialyzed patients. J Clin Endocrinol Metab 1991;73:516-24.

128. Brossard JH, Cloutier M, Roy L, Lepage R, Gascon-Barre M, D'Amour P. Accumulation of a non-(1-84) molecular form of parathyroid hormone (pth) detected by intact pth assay in renal failure: Importance in the interpretation of pth values. J Clin Endocrinol Metab 1996;81:3923-9.

129. John MR, Goodman WG, Gao P, Cantor TL, Salusky IB, Juppner H. A novel immunoradiometric assay detects full-length human pth but not amino-terminally truncated fragments: Implications for pth measurements in renal failure. Journal of Clinical Endocrinology & Metabolism 1999;84:4287.

130. McKee MD, Murray TM. Binding of intact parathyroid hormone to chicken renal plasma membranes: Evidence for a second binding site with carboxyl-terminal specificity. Endocrinology 1985;117:1930-9.

131. Kaji H, Sugimoto T, Kanatani M, Miyauchi A, Kimura T, Sakakibara S, et al. Carboxyl-terminal parathyroid hormone fragments stimulate osteoclast-like cell formation and osteoclastic activity. Endocrinology 1994;134:1897-904.

132. Rao LG, Murray TM. Binding of intact parathyroid hormone to rat osteosarcoma cells: Major contribution of binding sites for the carboxyl-terminal region of the hormone. Endocrinology 1985;117:1632-8.

133. Mayer GP, Keaton JA, Hurst JG, Habener JF. Effects of plasma calcium concentration on the relative proportion of hormone and carboxyl fragments in parathyroid venous blood. Endocrinology 1979;104:1778-84.

134. Terry AH, Orrock J, Meikle AW. Comparison of two third-generation parathyroid hormone assays. Clin Chem 2003;49:336-7.

135. Kiernan UA, Tubbs KA, Gruber K, Nedelkov D, Niederkofler EE, Williams P, Nelson RW. High-throughput protein characterization using mass spectrometric immunoassay. Analytical Biochemistry 2002;301:49-56.

136. Nelson RW. The use of bioreactive probes in protein characterization. Mass spectrometry reviews 1997;16:353-76.

137. Abou-Samra AB, Juppner H, Force T, Freeman MW, Kong XF, Schipani E, et al. Expression cloning of a common receptor for parathyroid hormone and parathyroid hormone-related peptide from rat osteoblast-like cells: A single receptor stimulates intracellular accumulation of both camp and inositol trisphosphates and increases intracellular free calcium. Proc Natl Acad Sci U S A 1992;89:2732-6.

138. Griner PF, Mayewski RJ, Mushlin AI, Greenland P. Selection and interpretation of diagnostic tests and procedures. Principles and applications. Ann Intern Med 1981;94:557-92.

139. Aloia JF, Feuerman M, Yeh JK. Reference range for serum parathyroid hormone. Endocr Pract 2006;12:137-44.

140. Soldin SJ, Morales A, Albalos F, Lenherr S, Rifai N. Pediatric reference ranges on the abbott imx for fsh, lh, prolactin, tsh, t4, t3, free t4, free t3, t-uptake, ige, and ferritin. Clin Biochem 1995;28:603-6.

141. Fraser WD. Hyperparathyroidism. Lancet 2009;374:145-58.

142. Brown R, Aston J, St John A, Woodhead J. Comparison of poly-and monoclonal antibodies as labels in a two-site immunochemiluminometric assay for intact parathyroid hormone. Journal of immunological methods 1988;109:139-44.

143. Endres D, Villanueva R, Sharp Jr C, Singer F. Immunochemiluminometric and immunoradiometric determinations of intact and total immunoreactive parathyrin: Performance in the differential diagnosis of hypercalcemia and hypoparathyroidism. Clinical chemistry 1991;37:162.

144. Nussbaum SR, Zahradnik R, Lavigne J, Brennan G, Nozawa-Ung K, Kim L, et al. Highly sensitive two-site immunoradiometric assay of parathyrin, and its clinical utility in evaluating patients with hypercalcemia. Clinical chemistry 1987;33:1364.

145. Boudou P, Ibrahim F, Cormier C, Chabas A, Sarfati E, Souberbielle JC. Third-or second-generation parathyroid hormone assays: A remaining debate in the diagnosis of primary hyperparathyroidism. Journal of Clinical Endocrinology & Metabolism 2005;90:6370.

146. Gao P, D'Amour P. Evolution of the parathyroid hormone (pth) assay--importance of circulating pth immunoheterogeneity and of its regulation. Clinical laboratory 2005;51:21.

147. Langub MC, Monier-Faugere MC, Wang G, Williams JP, Koszewski NJ, Malluche HH. Administration of pth-(7-84) antagonizes the effects of pth-(1-84) on bone in rats with moderate renal failure. Endocrinology 2003;144:1135.

148. d'Amour P. Circulating pth molecular forms: What we know and what we don't. Kidney International 2006;70:S29-S33.

149. John MR, Goodman WG, Gao P, Cantor TL, Salusky IB, J¸ppner H. A novel immunoradiometric assay detects full-length human pth but not amino-terminally truncated fragments: Implications for pth measurements

in renal failure. Journal of Clinical Endocrinology & Metabolism 1999;84:4287.

150. Salusky IB, Goodman WG. Adynamic renal osteodystrophy: Is there a problem? Journal of the American Society of Nephrology 2001;12:1978.

151. Winer KK, Yanovski JA, Cutler GB. Synthetic human parathyroid hormone 1-34 vs calcitriol and calcium in the treatment of hypoparathyroidism. JAMA: The Journal of the American Medical Association 1996;276:631.

152. Neer RM, Arnaud CD, Zanchetta JR, Prince R, Gaich GA, Reginster JY, et al. Effect of parathyroid hormone (1-34) on fractures and bone mineral density in postmenopausal women with osteoporosis. New England Journal of Medicine 2001;344:1434-41.

153. Miller PD, Bilezikian JP, Deal C, Harris ST, ci RP. Clinical use of teriparatide in the real world: Initial insights. Endocrine Practice 2004;10:139-48.

154. Kiernan UA, Nedelkov D, Tubbs KA, Niederkofler EE, Nelson RW. Selected expression profiling of full-length proteins and their variants in human plasma. Clinical Proteomics 2004;1:7-16.

155. Kiernan UA, Tubbs KA, Nedelkov D, Niederkofler EE, Nelson RW. Detection of novel truncated forms of human serum amyloid a protein in human plasma. FEBS letters 2003;537:166-70.

156. Nedelkov D, Kiernan UA, Niederkofler EE, Tubbs KA, Nelson RW. Investigating diversity in human plasma proteins. Proceedings of the National Academy of Sciences of the United States of America 2005;102:10852.

157. Nedelkov D, Phillips DA, Tubbs KA, Nelson RW. Investigation of human protein variants and their frequency in the general population. Molecular & Cellular Proteomics 2007;6:1183.

158. Zhang CX, Weber BV, Thammavong J, Grover TA, Wells DS. Identification of carboxyl-terminal peptide fragments of parathyroid hormone in human plasma at low-picomolar levels by mass spectrometry. Analytical chemistry 2006;78:1636-43.

159. Berna M, Schmalz C, Duffin K, Mitchell P, Chambers M, Ackermann B. Online immunoaffinity liquid chromatography/tandem mass spectrometry

determination of a type ii collagen peptide biomarker in rat urine: Investigation of the impact of collision-induced dissociation fluctuation on peptide quantitation. Analytical Biochemistry 2006;356:235-43.

160. Oe T, Ackermann BL, Inoue K, Berna MJ, Garner CO, Gelfanova V, et al. Quantitative analysis of amyloid peptides in cerebrospinal fluid of alzheimer's disease patients by immunoaffinity purification and stable isotope dilution liquid chromatography/negative electrospray ionization tandem mass spectrometry. Rapid communications in mass spectrometry 2006;20:3723-35.

161. Ackermann BL, Berna MJ. Coupling immunoaffinity techniques with ms for quantitative analysis of low-abundance protein biomarkers. Expert review of proteomics 2007;4:175-86.

162. Berna M, Ackermann B. Increased throughput for low-abundance protein biomarker verification by liquid chromatography/tandem mass spectrometry. Analytical chemistry 2009;81:3950-6.

163. Lopez M, Kuppusamy R, Sarracino D, Prakash A, Athanas M, Krastins B, et al. Discovery and targeted srm assay development of first-trimester peptide biomarker candidates for trisomy 21 in maternal blood. Mol Cell Proteomics Forthcoming 2010.

164. Cantor T, Yang Z, Caraiani N, Ilamathi E. Lack of comparability of intact parathyroid hormone measurements among commercial assays for end-stage renal disease patients: Implication for treatment decisions. Clin Chem 2006;52:1771-6.

165. Cole DE, Webb S, Chan PC. Update on parathyroid hormone: New tests and new challenges for external quality assessment. Clin Biochem 2007;40:585-90.

166. Kumar V, Barnidge DR, Chen LS, Twentyman JM, Cradic KW, Grebe SK, Singh RJ. Quantification of serum 1-84 parathyroid hormone in patients with hyperparathyroidism by immunocapture in situ digestion liquid chromatography-tandem mass spectrometry. Clin Chem 2010;56:306-13.

167. La'ulu SL, Roberts WL. Performance characteristics of six intact parathyroid hormone assays. Am J Clin Pathol 2010;134:930-8.

168. D'Amour P, Brossard JH, Rousseau L, Roy L, Gao P, Cantor T. Amino-terminal form of parathyroid hormone (pth) with immunologic similarities

to hpth(1-84) is overproduced in primary and secondary hyperparathyroidism. Clin Chem 2003;49:2037-44.

169. National Kidney F. K/doqi clinical practice guidelines for bone metabolism and disease in chronic kidney disease. Am J Kidney Dis 2003;42:S1-201.

170. Duncan MW, Yergey AL, Patterson SD. Quantifying proteins by mass spectrometry: The selectivity of srm is only part of the problem. Proteomics 2009;9:1124-7.

APPENDIX A

APROVAL DOCUMENTATION AND LIST OF PUBLICATIONS

USE OF COPYWRITED WORK

For the chapters based on works published in the journal Clinical Chemistry the

following email response authorized use:

Dear Mr. Oran,

Sorry for the delay in responding. There is no problem with your using the articles cited below in your dissertation. Please use this email as your authorization.

Best Wishes,
Mac

Mac Fancher
Publisher, Clinical Chemistry
Director of Publications
AACC
1850 K Street, NW, Suite 625
Washington, DC 20006
Ph - 202-857-0717, Ext. 1714 or
1-800-892-1400, Ext 1714
Fax - 202-833-4568
Email - mfancher@aacc.org

For the chapters based on works published in the journal Proteomics: Clinical

Applications, the following license agreements authorized use:

Copyright Clearance Center RightsLink®

Home | Account Info | Help

Title: Mass spectrometric immunoassay of intact insulin and related variants for population proteomics studies

Author: Paul E. Oran,Jason W. Jarvis,Chad R. Borges,Nisha D. Sherma,Randall W. Nelson

Publication: Proteomics - Clinical Applications

Publisher: John Wiley and Sons

Date: Aug 1, 2011

Logged in as:
Paul Oran

LOGOUT

Order Completed

Thank you very much for your order.

This is a License Agreement between Paul E Oran ("You") and John Wiley and Sons ("John Wiley and Sons"). The license consists of your order details, the terms and conditions provided by John Wiley and Sons, and the payment terms and conditions.

Get the printable license.

License Number	2726190616184
License date	Aug 11, 2011
Licensed content publisher	John Wiley and Sons
Licensed content publication	Proteomics - Clinical Applications
Licensed content title	Mass spectrometric immunoassay of intact insulin and related variants for population proteomics studies
Licensed content author	Paul E. Oran,Jason W. Jarvis,Chad R. Borges,Nisha D. Sherma,Randall W. Nelson
Licensed content date	Aug 1, 2011
Start page	454
End page	459
Type of use	Dissertation/Thesis
Requestor type	Author of this Wiley article
Format	Print
Portion	Full article
Will you be translating?	No
Order reference number	
Total	0.00 USD

ORDER MORE... CLOSE WINDOW

Copyright Clearance Center RightsLink®

Home | Account Info | Help

Title: C-peptide microheterogeneity in type 2 diabetes populations

Author: Paul E. Oran,Jason W. Jarvis,Chad R. Borges,Randall W. Nelson

Publication: Proteomics - Clinical Applications

Publisher: John Wiley and Sons

Date: Jan 1, 2010

Logged in as:
Paul Oran

LOGOUT

Order Completed

Thank you very much for your order.

This is a License Agreement between Paul E Oran ("You") and John Wiley and Sons ("John Wiley and Sons"). The license consists of your order details, the terms and conditions provided by John Wiley and Sons, and the payment terms and conditions.

Get the printable license.

License Number	2726190526248
License date	Aug 11, 2011
Licensed content publisher	John Wiley and Sons
Licensed content publication	Proteomics - Clinical Applications
Licensed content title	C-peptide microheterogeneity in type 2 diabetes populations
Licensed content author	Paul E. Oran,Jason W. Jarvis,Chad R. Borges,Randall W. Nelson
Licensed content date	Jan 1, 2010
Start page	106
End page	111
Type of use	Dissertation/Thesis
Requestor type	Author of this Wiley article
Format	Print
Portion	Full article
Will you be translating?	No
Order reference number	
Total	0.00 USD

ORDER MORE... CLOSE WINDOW

PREVIOUSLY PUBLISHED

Chapter 3 was previously published in 2010 in the journal Proteomics: Clinical Applications. Chapter 4 was previously published in 2011 in the journal Proteomics: Clinical Applications. Chapters 6 and 8 were previously published in 2010 in the journal Clinical Chemistry.

APPROVAL FROM CO-AUTHORS

Co-authors from the studies within have granted me permission to use this work.

IRB APPROVAL

ASU ARIZONA STATE UNIVERSITY

Research Compliance Office
Office for Research & Sponsored Projects Administration
P.O. Box 873503
Tempe, AZ 85287-3503

Phone
(480) 965-6788
Facsimile
(480) 965-7772

To:	Randall Nelson BDB 140C
From:	Mark Roosa, Chair Institutional Review Board
Date:	05/18/2007
Committee Action:	**Exemption Granted**
IRB Action Date:	05/18/2007
IRB Protocol #:	0705001851
Study Title:	Molecular Biosignatures Analysis

The above-referenced protocol is considered exempt after review by the Institutional Review Board pursuant to Federal regulations, 45 CFR Part 46.101(b)(4) .

This part of the federal regulations requires that the information be recorded by investigators in such a manner that subjects cannot be identified, directly or through identifiers linked to the subjects. It is necessary that the information obtained not be such that if disclosed outside the research, it could reasonably place the subjects at risk of criminal or civil liability, or be damaging to the subjects' financial standing, employability, or reputation.

You should retain a copy of this letter for your records.

LIST OF PUBLICATIONS

First-author and Co-authored papers listed.

1) Oran, P. E., J. W. Jarvis, et al. (2010). "C-peptide microheterogeneity in type 2 diabetes populations." PROTEOMICS - CLINICAL APPLICATIONS 4(1): 106-111.

2) Oran, P. E., N. D. Sherma, et al. (2010). "Intrapersonal and populational heterogeneity of the chemokine RANTES." Clinical chemistry **56**(9): 1432.

3) Oran, P. E., J. W. Jarvis, et al. (2011). "Mass spectrometric immunoassay of intact insulin and related variants for population proteomics studies." PROTEOMICS – Clinical Applications **5**(7-8): 454-459.

4) Borges, C. R., P. E. Oran, et al. (2011). "Building multidimensional biomarker views of type 2 diabetes on the basis of protein microheterogeneity." Clin Chem **57**(5): 719-728.

5) Lopez, M. F., T. Rezai, et al. (2010). "Selected reaction monitoring-mass spectrometric immunoassay responsive to parathyroid hormone and related variants." Clin Chem 56(2): 281-290.

6) Borges, C. R., D. S. Rehder, et al. (2009). "Full-Length Characterization of Proteins in Human Populations." Clin Chem.

7) Borges, C. R., J. W. Jarvis, et al. (2008). "Population studies of Vitamin D Binding Protein microheterogeneity by mass spectrometry lead to characterization of its genotype-dependent O-glycosylation patterns." J Proteome Res 7(9): 4143-4153.

8) Borges, C. R., J. W. Jarvis, et al. (2008). "Population studies of intact vitamin D binding protein by affinity capture ESI-TOF-MS." J Biomol Tech 19(3): 167-176.